ALMA MATER STUDIORUM · UNIVERSITÀ DI BOLOGNA

School of Engineering and Architecture
Second Cycle degree in Earth Resources Engineering

Applicability of Uncertainty analysis to groundwater environmental risks through Fault Tree Analysis and Monte Carlo simulations

Supervisor:
Di Federico Vittorio

Defended by:
Glaude Robin

Academic year: 2019-2020

Uncertainty is the fertile ground of pure creativity and freedom.

Deepak Chopra

Applicability of Uncertainty analysis to groundwater environmental risks through Fault Tree Analysis and Monte Carlo simulations

Abstract

The Anthropocene epoch initiated by human influence on its Earth system (biosphere, hydrosphere, ...) leads to an irreversible change: Global warming. Climate change alters all existing natural processes, including the ones related to groundwater.

The present paper aims to study the occurrence's probability of two particular groundwater risks: the generation of thermokarst lakes in permafrost environment and its subsequent thermal consequences in the surroundings as well as seawater intrusion inducing saltwater contamination in pumping wells. These processes are dependent of physical parameters to which is attached uncertainty. Consequently, two uncertainty analysis methods have been applied to determine the probability of occurence of these undesired events: Fault Tree Analysis and Monte Carlo Simulation. Beside the rough approximation performed to evaluate the probability of thermokarst lake occurence (48%) and of talik development under these latter (73%) by means of fault tree analysis, these high failure probabilities translate the urge to slow down global warming due to the irreversible effect on permafrost environment, meaning its thawing and releasing of trapped methane in the atmosphere. On the other hand, Monte Carlo simulations have been performed to compare different scenarii related to seawater intrusion in Akrotiri aquifer in Cyprus. The results once again translate the disastrous effect of climate change regarding the probability of occurence of these unwanted events. Indeed, a failure probability around 6 times greater (43%) is observed in the climate change scenario with respect to the reference scenario (7%).

Uncertainty analysis is good methodology to apply to environmental concerns to quantify the occurence's probability of these undesired events. This would urge public authorities to perform decision making in order to avoid or reduce the failure's probability of these groundwater issues that have irreversible consequences.

Acknowledgement

Perché ho vissuto un anno straordinario in Italia (nonostante la crisi sanitaria che ha colpito il mondo), ho deciso di scrivere questa pagina di ringraziamento in italiano nonostante il mio livello che non sia perfetto.

Prima di tutto, vorrei ringraziare il mio supervisore, *Vittorio Di Federico* che ha gentilmente accettato di supervisionare la mia tesi sin dall'inizio. Era sempre disponibile per rispondere alle mie domande, anche durante la crisi sanitaria per videochiamata. In più, lui prendeva il tempo per chiedermi come mi sentivo durante la crisi sanitaria e cosa pensavo della situazione delle lezione online.
Vorrei anche ringraziare *Alessandro Lenci* che mi ha aiutato all'inizio della scrittura della mia tesi per spiegarmi le basi del FTA e per scegliere sogetti associati al permafrost.
Vorrei anche ringraziare l'università di Bologna in cui ho fatto il mio ultimo anno di studi. In particolare voglio ringraziare *Lisa Borgatti*, la direttrice del corso di laurea ERE (Earth Resources Engineering) che era sempre disponibile per me quando avevo problemi amministrativi o semplicemente per sapire come mi sentivo.

In secondo luogo, desidero ringraziare l'università di Liegi che ha firmato questo contratto di co-diplomazione con l'università di Bologna. Più specificatamente, vorrei ringraziare i professori *Frédéric Nguyen*, il mio professore di geofisica e responsabile della co-diplomazione a Liege, e *Serge Brouyère* con cui lavorerò da settembre.

Vorrei anche ringraziare i miei genitori che mi hanno dato l'opportunità di studiare qui a Bologna e vivere un anno straordinario in Italia. Vorrei ringraziare i miei fratelli con cui ho un buon rapporto e chi mi hanno fatto visita a febbraio.

In fine, vorrei ringraziare tutte le persone senza la quale non avrei potuto vivere un miglio anno: i miei coinquilini e coinquiline (Maria, Marina, Kaltrina, Flavia, Giorgio, Jenny, Vanessa, Leonardo), i miei amici di Belgio che mi hanno visitato, i miei amici internazionale, i miei amici italiani (in particolare Max) e tutti gli altri amici/amiche che studiano come me qui, nella più bella della città, Bologna.

Contents

Chapter 1

Introduction

It has been decades, even centuries if we refer to the First Industrial Revolution, that the number of global evidence related to the impact of human civilization on the Earth system appears and increases. This onset of anthropogenic influence on our planet (atmospheric, geologic, hydrologic, biospheric processes) marks the beginning of a new geological epoch called **Anthropocene**. There is still not a formal agreement on beginning dates of the Anthropocene but 2 particulars alternative synchronous GSSP (Global Stratotype Section and Point which refers to a global marker of an event in stratigraphic material, such as rock, sediment, or glacier ice) might be significant to characterize the initiation of Anthropocene *(Lewis et al. 2015)*. FIGURE 1.1 represents these two GSSP.

1. **Orbis GGSP (1610)**: defined by the pronounced dip in atmospheric CO_2 concentration preceding the continuous increase in carbon dioxide.

2. **Bomb GGSP (1964)**: defined by the peak of atmospheric radiocarbon (C^{14}) induced by the maximal number of nuclear tests.

One particular and most damaging influence of humans on its environment is its impact on climate. Indeed, more and more pieces of evidence have been observed highlighting the terrible impact of global warming on Earth's system, especially in the Arctic environment (Sea ice and albedo reduction, permafrost thawing, Greenland ice sheet melting, weakening of Jet Stream, weakening of AMOC). These consequences in the Arctic have global consequences such as the release of methane trapped in permafrost, sea-level rise due to the melting of the ice sheet, and so on. One particular organization studying deeply climate change is called IPCC and refers to the Intergovernmental Panel on Climate Change. As already mentioned, there are plenty of pieces of evidence highlighting the impact of humans on its environment and the existence of climate change. However, there are uncertainties regarding how the situation will be in the future. IPCC studied consequently different scenarii (from the most optimistic to the most pessimistic) to identify the possible climate paths the Earth could follow. *Steffen et al. 2018* studied the trajectories of the Earth in Anthropocene where they analyzed the risks that the planet Earth moves to a "hothouse Earth" pathway by exceeding a threshold. To simplify, that has been 800,000 years the Earth is following Glacial-Interglacial cycles. However, above $2°C$ of global warming would exit the Earth from these cycles and lead to a non-stable Earth ("hothouse" mood). It is thus extremely important to keep changing the whole system for keeping the Earth in a stable trajectory to avoid

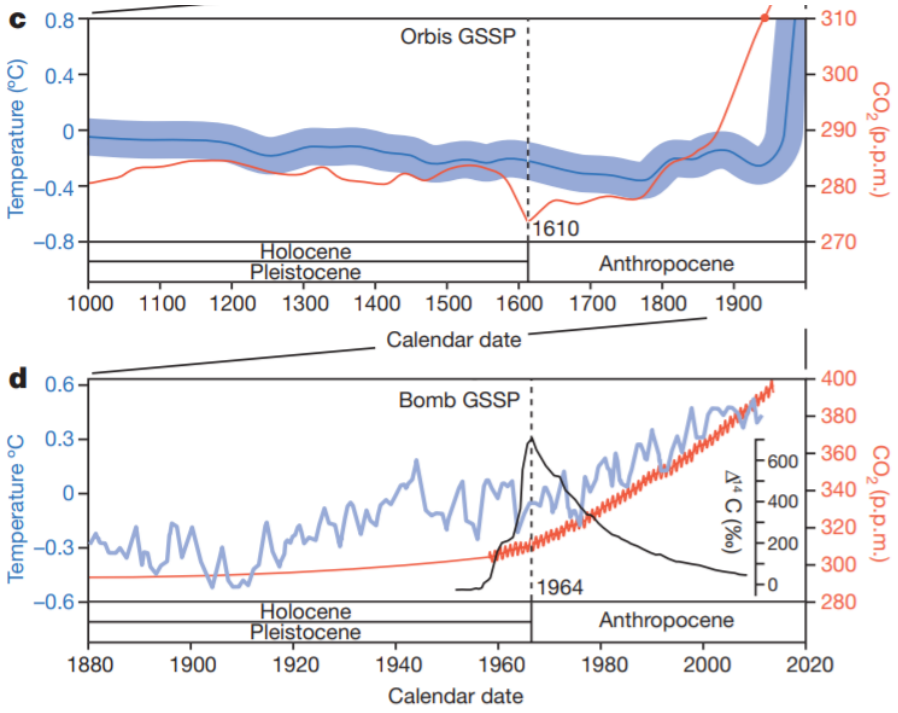

Figure 1.1: The first picture highlights Orbis GSSP with the dip in atmospheric carbon dioxide concentration while the second one highlights the Bomb GSSP with the maximum atmospheric radiocarbon concentration (from *Lewis et al. 2015*)

the collapse of our civilization. FIGURES 1.2 and 1.3 highlight schematically the different pathways took by the planet Earth. It is indeed very important to fight against global warming that would induce a global disequilibrium. Indeed, climate change and non-sustainable management of resources would lead to more socio-political instability, conflicts and so on since the non-stability of one component (climate, environment, development, ...) would have impacts on other components (peace/stability, human rights, ...).

Two particular groundwater environmental issues related to climate change will be studied in the present paper:

1. Thawing of permafrost in cold regions, and more particularly, the generation of thermokarst lakes and its thermal impacts on the surroundings.

2. Seawater intrusion in the coastal area.

Indeed, these both environmental phenomena are particularly related to climate change since:

- Global warming accelerates the thawing process in permafrost and induces more instability of the frozen soil.

- Sea level rise and decrease of replenishment in freshwater in coastal aquifers influence seawater intrusion.

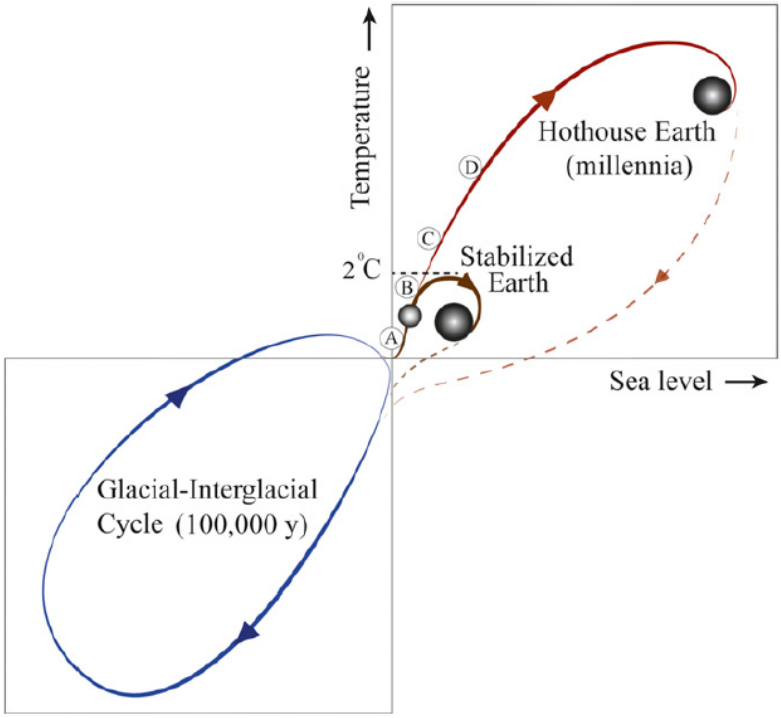

Figure 1.2: Climate paths of planet Earth (from *Steffen et al. 2018*)

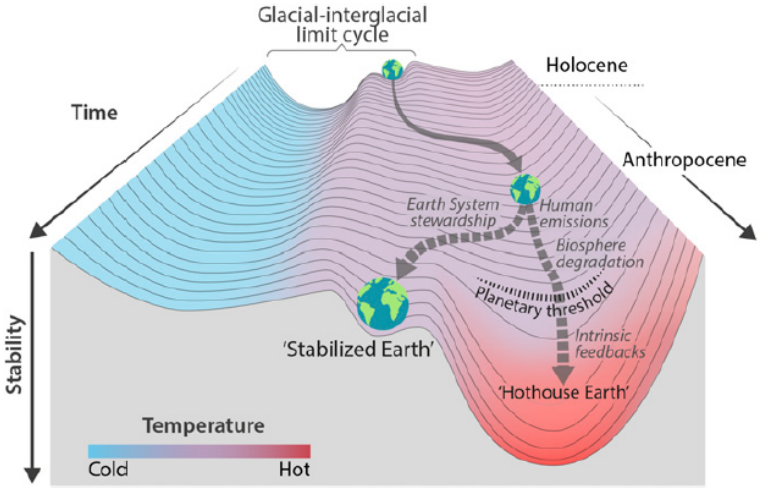

Figure 1.3: Stability landscape of planet Earth (from *Steffen et al. 2018*)

However, uncertainty is attached to these physical phenomena. Indeed, even if the occurrence's probability of these groundwater issues is increasing due to climate change, it doesn't necessarily mean it will occur with certitude. As a consequence, it is fundamental to perform risk analysis methods to evaluate the probability these environmental concerns occur. More particularly, two methods will be applied:

- Fault Tree Analysis (FTA) will be applied to the permafrost environment. This methodology is a failure oriented risk assessment method, meaning that the failure's probability of the studied system is a function of the failure's probability of its components. FTA consists in associating to an undesired event (named Top Event) a combination of basic events by the use of logic gates to which a simultaneous failure would lead to the failure of the whole system.

- Monte-Carlo simulations will be applied to seawater intrusion. This method consists in running several simulations to evaluate the value of a physical parameter which is dependant on other physical random variables. Consequently, for each simulation, values are attributed to the relevant random variables based on their associated probabilistic distribution which allows calculating the physical studied parameter. The set of obtained outcomes is then compared to a threshold value to evaluate the probability of failure of a given system

Finally, the current master thesis will be organized as followed. The first CHAPTER being the current one introduced the problems related to climate change and which particular groundwater environmental issues will be treated. The second CHAPTER aims to describe in detail risk assessment methods by focusing on Fault Tree Analysis and by describing briefly Monte Carlo simulation. The third CHAPTER will be the application of Fault Tree analysis to particular permafrost related issues. More specifically, the first part of this chapter gives an overview of the permafrost environment, the second part is the application of FTA on the generation of thermokarst lakes and the last part of the chapter is the application of FTA to the talik development under thermokarst lakes. Then, the fourth CHAPTER consists in studying seawater intrusion by the use of Monte Carlo simulations. The first part of the chapter will be a description of the problems related to seawater intrusion while the second one will be the application of Monte Carlo to saltwater intrusion after describing analytically the mathematical equations governing this physical phenomenon. Finally, the last CHAPTER is the conclusion of this master thesis, which resumes the most significant observations and results of each chapter with their physical interpretation.

Chapter 2

FTA and Monte-Carlo simulations

The concept of risk is extremely important in any engineering field. Indeed, it is necessary to ensure that any system works properly and achieves what it was created for. Different methods exist to evaluate and assess risk probability. The main method that will be discussed through the following chapter is a useful approach called **Fault Tree analysis**.
While this technique was widely used in the second half of the 20^{th} century as a system safety analysis tool such as in nuclear plants, the design of planes, and so on, this approach can be extended to the analysis of environmental problems. Indeed, some environmental issues induced by anthropogenic activities can be assessed through this method to evaluate its probability of occurrence and its main causal factors. Indeed, any environmental field can be considered as a system on its own with different components composing it.
This section aims thus to introduce this method by explaining basic concepts behind it and how the fault tree is conceived. Furthermore, qualitative and quantitative analysis methods will be explained to get more relevant information about the tree. This basic knowledge about FTA will then be applied in CHAPTER 3.

Another wildly used technique for risk analysis is called **Monte Carlo simulations**. This method by its own doesn't show visually the interconnection between cause factors. However, it provides a rigorous way to evaluate the unwanted event occurrence given the uncertainties related to parameters governing the studied environmental issue. The second part of this chapter aims thus to describe briefly the principles of this method.

2.1 Fault Tree Analysis (FTA)

2.1.1 Overview

2.1.1.1 Definition of risk

It would be useful before entering into the main subject to define more specifically what *risk* refers to. **Risk** can be defined as the combination of hazard and its consequences named as vulnerability where:

- **Hazard** refers to the probability a harmful/damaging event will occur at a specific time in a defined location with a given intensity. It is thus a source of potential harm.

- **Vulnerability** refers to any elements of a system or the surrounding environment such as people, infrastructures, nature and so on which may be directly or indirectly affected by the damage. Vulnerability defines thus more generally the consequences of the hazard.

Thereby, risk in its most generic definitions represents the combination of the consequences of an undesired event (Vulnerability) and its probability of occurrence (Hazard). Consequently, the risk doesn't exist if either hazard or vulnerability factor doesn't exist.
As an example, let's consider landslide as a harmful event. If a landslide occurs in a mountainous area where no people are living and no infrastructures, this landslide wouldn't constitute a risk because this hazard is not associated with any vulnerable element.

2.1.1.2 Definition of reliability

When the assumption that a system can potentially fail is made, the concept of reliability must be defined as well. According to ISO (International Organization for Standardization), reliability is defined as: "*The ability of an item to perform a required function, under given environmental and operational conditions and for a stated period of time*". This concept is particularly useful in risk analysis, environmental protection, engineering design, verification of quality/reliability of a product, and so on.
Mathematically, if we consider an item with a strength S and a load L applied on it, the reliability R is defined as the probability that the system doesn't fail, so the probability that the strength is strictly greater than the load:

$$R = P(S > L) \tag{2.1}$$

Both strength and Load are considered as a random variable and follow thus each a probability distribution function (pdf). The failure area represents thus the area in which the pdf of S is lower than the pdf of L as it is shown in Figure 2.1.

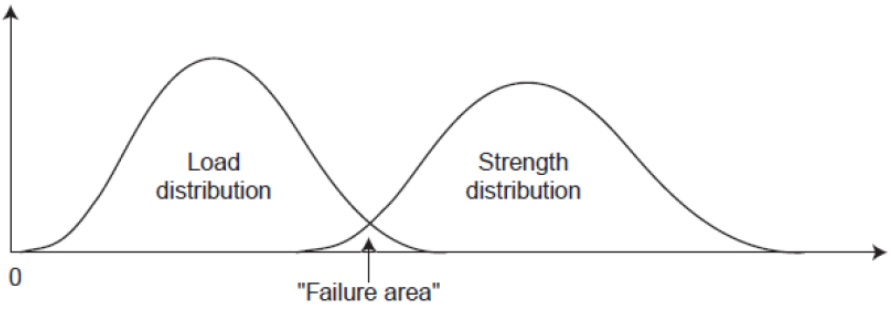

Figure 2.1: Probability distribution of strength and load

Furthermore, the concept of time is also important. Indeed, the strength of an item can decrease with time until the load becomes sufficiently greater than the strength to cause the failure of the system. This smallest time at which the system failed is defined as **time to failure** T and the reliability at time t is such as $R(t) = P(T > t)$. Most of the time, T is considered as a continuous random variable.

2.1.1.3 Definition of Fault Tree

A fault tree (FT) is a graphical representation that shows how the failure of a component can propagate thought the whole system and cause the failure of the complete system. More specifically, A FT represents a tree (mathematically, an acyclic graph) modeling how the individual components are related and interact with each other by the use of logic gates (AND, OR, ...). The FTs that will be considered in this work are standard/static FTs. However, it exists many extensions of the FT concept into for example dynamic FTs (the most common), extended FTs, repairable FTs, fuzzy FTs, and so on *(Ruijters et al. 2015)*. FIGURE 2.2 represents a typical structure of a classical fault tree.

2.1.1.4 History of Fault Tree Analysis

Historically, Fault Trees have been introduced around 1961 in Bell Labs by H. Watson for the analysis of launch control system for ballistic missiles. A few years later (in 1963), it has been accepted as an important system safety analysis tool by Dave Haasl working in the Boeing company. In the following years, FTA has been applied several times by Boeing company and started to be considered in the aerospace industry (aircraft and weapons). Then, in 1971-1980, FTA started to be applied in the Nuclear Industry as well and the Power industry improved the pre-existing codes and algorithms. The following decade (1981-1990), the use of FTA becomes international (especially in Nuclear Power Industry), more codes and algorithms are developed and the chemical industry starts adopting FTA as well. Finally, FTA continued to develop in more and more fields of studies, high-quality Fault Tree Commercial codes have been developed and a new extension of FTs concepts continues to emerge *(Ericson et al. 1999)*.

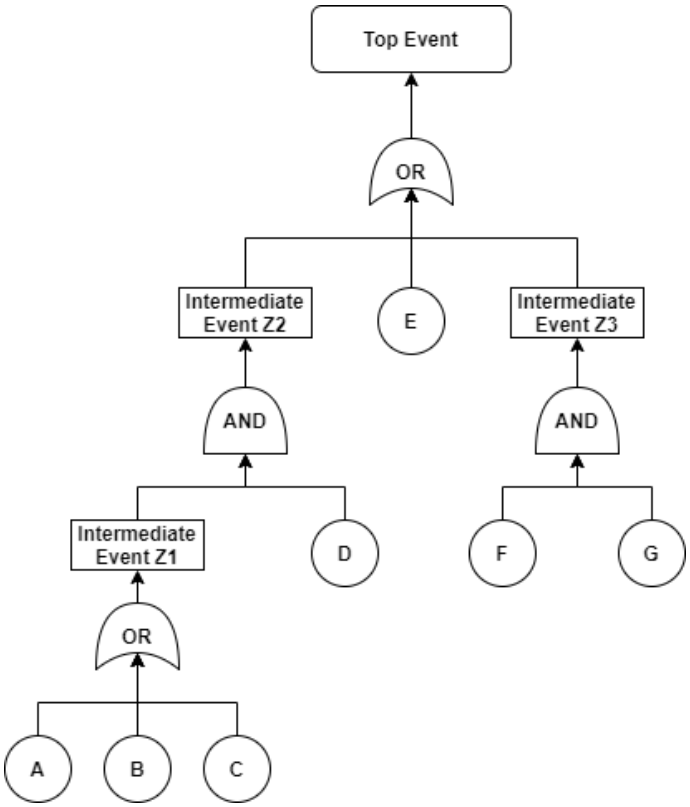

Figure 2.2: Example of a standard Fault Tree

2.1.1.5 Applications of FTA

FTA can be used for several purposes *(Ericson et al. 1999)*:

- **Root cause analysis:** it can be used to identify all the basic components/events and their parallel and/or sequential combination leading to the occurrence of an undesired event. It can thus be used as a **risk analysis tool**.
- **Risk assessment:** through quantitative analysis of the studied FT, it is possible to evaluate the probability that the undesired event occurs. With this analysis, it is also possible to identify the most safety-critical components of the system and thus perform measures to decrease the risk. It is consequently a good tool for **System evaluation**.
- **Design Safety Assessment:** by performing quantitative analysis, it is possible to detect where safety requirement is required by identifying the weakest components of the fault tree. FTA can thus be used as a **decision-making** tool by thinking about the new safe design of a pre-existing system.

2.1.2 Structure and construction of a fault tree

To move deeper into fault tree analysis, it is necessary to define the different components of a fault tree. As already mentioned, a fault tree is a directed acyclic graph consisting of nodes. These nodes can be of two types: **Events** and **Gates**. The different symbols representing distinct types of events or gates are found in Annex A.1.

Events:

The main event which is analyzed, the one that is not desired and for which we would like to evaluate the probability of occurrence is located at the top of the tree and is called **Top Event**. The individual components from which combined or not failures lead to the failure of the whole system (occurrence of the top event) are called **basic events** and are represented graphically by circles.
To understand better the connection between basic events and the Top event, **intermediate events** exist and are caused by at least one event. These types of events are represented by a rectangle.
It might also happen that some subsystems don't contain sufficiently information or are not considered to be enough relevant to be considered as basic events. These events are called **undeveloped events** and are represented by diamonds.
Finally, when the trees appear to be too complex, a triangle can be used to transfer events between multiple sub-fault-trees to build a large FT *(Ruijters et al. 2015)*.

Gates:

Gates are used to describing how basics events are combined to cause the failure of the whole system. There is one output by gate and at least one input. Let's describe the most common gates:

- **AND:** The output occurs when all the input events occur.
- **OR:** The output occurs when one of the input events occurs. However, in this thesis, we will consider that an **OR** gate that has 2 inputs can also generate output if the 2 inputs are true (inclusive). In the case where it is not accepted that the 2 inputs occur at the same time, we will call the gate **XOR** which refers to **OR exclusive**.
- **k/N (also called VOTING):** The output occurs when at least k of the N inputs occur.
- **INHIBIT:** The output occurs if the input events occurs and the conditional event occurs at the same time. This is equivalent to an AND gate.

Construction:

To build the fault tree, it is fundamental before starting to identify a specific Top event which is undesired. This one should not be too generic in order not to have too many causes related to it which would bring unnecessary complexity. Once it has been identified, it is necessary to think about which causes lead to the failure of the system and how these causes are connected with the use of the adequate gates. Then, for each cause, it is important to take time thinking about which sub-causes cause the failure of this intermediate event. If it is not possible to find any, it means that this event can be considered as a basic event directly. Otherwise, each intermediate event is developed into a combination of other basic events or intermediate events. Finally, it is preferable that each of these basic events can be quantified by a specific parameter measurement to perform quantitative analysis later on.

2.1.3 Qualitative analysis

When we talk about analysis methods of FTs, these can be distinguished between qualitative and quantitative techniques. This section aims to describe the qualitative aspects of FTs while the next one will focus on quantitative methods.

The qualitative analysis consists in investigating the insight structure of the tree to detect system vulnerabilities. The most commonly used qualitative techniques are minimal cut sets, minimal and critical path sets, and common cause failures *(Ruijters et al. 2015)*.

2.1.3.1 cut sets

Cut sets are very useful to identify the vulnerability of a system. Indeed, **cut sets (CS)** are defined as the combination of elements leading to the failure of the system. The whole system can be vulnerable for example if the existing cut sets contain too few elements (small combination leading to failure) or if one particular combination is too likely to happen. One way to increase the reliability of the system would be to decrease the probability of occurrence of these cut sets if it is possible.
Minimal cut sets (MCS) on the other hand are defined as sets that can't be reduced without losing its status as a cut set.

As an example, let's consider the FT in Figure 2.2, we have the following minimal cut-sets: {E}, {F,G}, {D,A}, {D,B}, and {D,C}. Indeed, each of these MCS can not lose one of their components without its status of CS.

Cut sets can be analyzed by 2 relevant methods: boolean manipulation and binary decision diagrams.

Boolean manipulation:

Let's consider mathematically the gates AND and OR represented respectively by $\cap$ and $\cup$. This method consists in writing as a boolean expression each intermediate event as a combination of other intermediate events (gates) and basic events. Starting from the Top event (Top-bottom method), it is possible to obtain a combination of basic events without any gates (intermediate events) leading to the failure of the system *(Ruijters et al. 2015)*.
Let's consider the example represented in the Figure2.2 and the intermediate events Z_1, Z_2 and Z_3, we get as an expression for the top event TE:

$$\begin{aligned} TE &= Z_2 \cup E \cup Z_3 \\ &= (Z_1 \cap D) \cup E \cup (F \cap G) \\ &= \Big((A \cup B \cup C) \cap D\Big) \cup E \cup (F \cap G) \\ &= (A \cap D) \cup (B \cap D) \cup (C \cap D) \cup (E) \cup (F \cap G) \end{aligned}$$

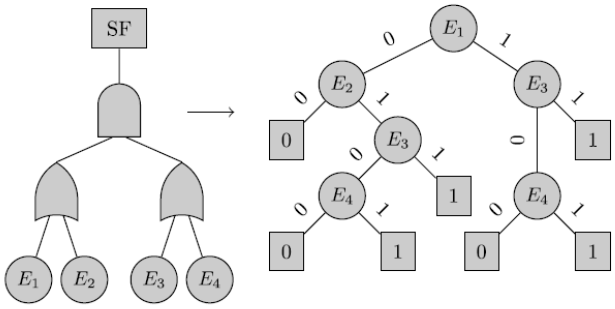

Figure 2.3: conversion of a fault tree into binary decision diagram

Through the expression obtained, all minimal cut sets are identified due to the substitution of all gates into its combination of basic events.

Binary Decision Diagrams:

The other efficient method to determine minimal cut sets is the conversion of Fault Trees into a binary decision diagram. As FTs, binary decision diagrams are also directed acyclic graph that represents a boolean function $f : \{x_1, x_2, ..., x_n\} \longrightarrow \{0, 1\}$ where the leaves take the value 1 or 0. The left child of each node represents the case in which $x_i = 0$ and means that the basic event x_i didn't fail and the right child represents the opposite (the case where $x_i = 1$, meaning the failure of the basic event) *(Ruijters et al. 2015)*.
To convert one fault tree into a binary decision diagram, one can use the Shannon formula to build the top node which is:

$$f(x_1, x_2, ..., x_n) = (x_1 \cap f(1, x_2, ..., x_n)) \cup (\neg x_1 \cap f(0, x_2, ..., x_n)) \tag{2.2}$$

where x_1 represents the top node, $f(1, x_2, ..., x_n)$ the right child and
$f(0, x_2, ..., x_n)$ the left child. As an example, FIGURE 2.3 shows well the conversion of a fault tree into a binary decision diagram.

The cut sets can be extracted from this diagram going up from 1-leaves to the top event root of the tree. In this particular example, it is seen from the binary decision diagram that the cut sets are: $\{E_4, E_2\}$, $\{E_3, E_2\}$, $\{E_4, E_1\}$, and $\{E_3, E_1\}$. The cut sets obtained might not necessarily be minimal according to which algorithm has been used to build the tree. Furthermore, the binary decision diagram built is not unique according to in which order the Basic events are analyzed. However, in practice, binary decision diagrams are more efficient than boolean manipulations *(Ruijters et al. 2015)*.

2.1.3.2 Path sets

Path sets have the opposite meaning of cut sets. It means that it represents the combination of elements of the tree which is such that if they don't fail, the overall system remains operational. Furthermore, as for cut sets, minimal path sets can be identified as well and constitute the minimal combination of components from

which their success ensures the functionality of the system.
As a consequence, while cut sets were an efficient way to assess the vulnerability of a system, path sets are on the other side useful to evaluate its reliability. Indeed, a path set with few elements will make the system more reliable by decreasing the probability that a cut set occurs.

2.1.3.3 Common Cause Failures

Finally, a last quality aspect that can be studied refer to **Common Cause Failure**. A common cause can be defined as an event or phenomenon (not listed in the tree) which, if it occurs, will induce the occurence of two or more fault tree elements (*Ruijters et al. 2015*).

2.1.4 Quantitative analysis

Unlike qualitative methods, the quantitative analysis aims to compute numerical values related to the fault tree. These measures can be distinguished from:

- **Importance measures:** these allow to measure how critical an element of the system can be.
- **Stochastic measures:** These are mostly related to the computation of failure probabilities. However, these measures are either related to single-time failure probabilities or continuous-time failure probabilities that take into account time (time to failure, ...). In this thesis, we will focus on a single-time analysis.

Furthermore, another important aspect is related to the **sensitivity** of the previous measures according to the variation of basic events probabilities *(Ruijters et al. 2015)*.

2.1.4.1 Stochastic measures

As mentioned in section 2.1, reliability can be defined as the probability that the failure of the system doesn't occur during a stated period of time. Mathematically, if we consider the fault tree F and the top event X_F taking the value 1 when it fails and 0 when it doesn't, we can define reliability by:

$$Re(F) = P(X_F = 0) = 1 - P(X_F = 1) \tag{2.3}$$

Reliability can thus be calculated from $P(X_F = 1)$. If we consider n independent basic events denoted by $e_1, e_2, ..., e_n$ and their corresponding binary values $b_1, b_2, ..., b_n$ ($\in \{0, 1\}$), one can write:

$$P(X_F = 1) = \sum_{b_1,b_2,...,b_n \in \{0,1\}} P(X_F = 1 \| X_{e_1} = b_1 \cap ... \cap X_{e_n} = b_n) \cdot P(X_{e_1} = b_1, \cap ... \cap X_{e_n} = b_n) \tag{2.4}$$

However, trying to compute the equation (2.4) straight away reveals to be complex. Several methods are thus considered to solve this issue *(Ruijters et al. 2015)*.

Bottom-up Analysis

In the case where gates don't share between each other common basic events, it is possible to evaluate the probabilities from bottom of the tree to the top by using standard probability laws. Indeed, if we consider the inputs $X_1, X_2, ..., X_n$ of a gate G, we can write if the logic gate is an AND:

$$\begin{aligned} P\Big(X_{AND}(X_1, ..., X_N) = 1\Big) &= P(X_1 = 1 \cap ... \cap X_N = 1) \\ &= P(X_1 = 1) \cdot ... \cdot P(X_N = 1) \end{aligned} \tag{2.5}$$

if it is an OR:

$$\begin{aligned} P\Big(X_{OR}(X_1, ..., X_N) = 1\Big) &= 1 - P(X_{OR}(X_1, ..., X_N) = 0) \\ &= 1 - P(X_1 = 0 \cap ... \cap X_N = 0) \\ &= 1 - \big(1 - P(X_1 = 1)\big) \cdot ... \cdot \big(1 - P(X_N = 1)\big) \end{aligned} \tag{2.6}$$

In this thesis, each fault tree will be composed of gates with only 2 inputs. As a consequence, we can write more specifically the 3 following equations:

$$P\Big(X_{AND}(X_1, X_2) = 1\Big) = P(X_1 = 1) \cdot P(X_2 = 1) \tag{2.7}$$

$$P\Big(X_{OR}(X_1, X_2) = 1\Big) = P(X_1 = 1) + P(X_2 = 1) - P(X_1 = 1) \cdot P(X_2 = 1) \tag{2.8}$$

$$P\Big(X_{XOR}(X_1, X_2) = 1\Big) = P(X_1 = 1) + P(X_2 = 1) - 2.P(X_1 = 1) \cdot P(X_2 = 1) \tag{2.9}$$

The inconvenience with this approach is that it doesn't work when basic events are shared by several gates *(Ruijters et al. 2015)*.

Binary Decision diagrams

When binary decision diagrams have already been built for the qualitative analysis, they can also be exploited to compute system reliability. Indeed, by considering an equation similar to Shannon formula (equation (2.2)), it is possible to write:

$$P\big(f(x_1, x_2, ..., x_n)\big) = P\big(x_1\big) \cdot P\big(f(1, x_2, ..., x_n))\big) + P\big(\neg x_1\big) \cdot P\big(f(0, x_2, ..., x_n)\big) \tag{2.10}$$

A mechanism in the algorithm allows then to store intermediate results to calculate the overall reliability. The complexity of this algorithm is linear in the size of the tree, which makes it efficient *(Ruijters et al. 2015)*.

Bayesian Network analysis

This method won't be studied in detail but it is relevant to know its existence. Indeed, this analysis is particularly relevant when basic events are statistically dependent. A Bayesian network is defined as: "sequence X_1, X_2, ... , X_n of stochastically dependent random variables, where X_i can only depend on X_j if $j < i$" because the failure distribution of an intermediate event is only dependant on its children *(Ruijters et al. 2015)*.

Monte Carlo Simulations

One other method to calculate system reliability is called Monte Carlo simulations besides the fact that most techniques are used in continuous-time FTA. For Single-Time FTA, the methods consist simply in assigning to each basic event a failure state according to its failure probability distribution and to compute the fault tree to determine if the undesired top event occurred or not. The simulation is then run several times and the proportion of simulations that don't lead to the failure of the system corresponds to its reliability *(Ruijters et al. 2015)*.

2.1.4.2 Importance measures

When performing quantitative analysis, other important inputs than reliability measures of a system that can be made are the importance measures. These refer to which parts of a system are the biggest contributors to the failure of the Top Event. Analyze these identified parts of the system is a good way to enhance system reliability *(Ruijters et al. 2015)*.
Different methods exist to quantify the relative importance of individual components of the Fault Tree to the Top event failure occurrence.

1) Risk Achievement (Worth) = RA(W)

This method is also known under the name *Top Increase sensitivity*. The concept is to identify which components lead to the highest risk achievement (probability of failure) of the system. Indeed, these constitute the most critical contributors that should be prevented in priority.

The Risk Achievement Worth (RAW) is calculated by quantifying again the top event failure by setting the probability of occurrence of the given event to 1.
Let us call $RA(i)$ the absolute risk achievement of the basic event i, P_T the top event probability and P_i the probability of failure of the basic event i, one can write:

$$RA(i) = P_T(P_i = 1) - P_T \tag{2.11}$$

In most of the cases, this number will be greater than 0 since that the top event failure probability considering $P_i = 1$ will be greater than in normal case because it dominates other basic event probabilities. However, when considering probabilities of basic events superior to 0.5 and the presence of XOR gates in the fault tree analysis, it is more likely to find negative values of $RA(i)$ due to the large contribution of

$-2 \cdot P(X_1) \cdot P(X_2)$ (from equation (2.9)) which will turn $P_T(P_i = 1)$ to be lower than P_T. Nevertheless, it doesn't constitute necessarily an issue as the main purpose of risk achievement measure is to range basic events from the most worth to contribute to the failure of the Top Event to the least worth.

Furthermore, the risk achievement worth (relative risk reduction) is considering the ratio of system unreliability when the basic event i is always in a failed state with the expected system unreliability:

$$RAW(i) = \frac{P_T(P_i = 1)}{P_T} \tag{2.12}$$

For the same reason than mentioned previously, this number is greater than 1 in most of cases.

Greater is Risk Achievement index, more important is this component regarding top event failure.

2) Risk Reduction (Worth) = RR(W)

On the other side, Risk Reduction also known under the name of *Top Decrease sensitivity* represents the opposite concept. Indeed, this index represents the decrease of top event occurrence related to the non-failure of a lower level basic event.

With the same notations than before, the absolute reduction of a basic event i is calculated with:

$$RR(i) = P_T - P_T(P_i = 0) \tag{2.13}$$

which is greater than 0 in most of the cases since $P_T(P_i = 0)$ would be lower than P_T in normal conditions. For the same reasons explained in the previous paragraph, it might happen it is not the case when considering high probability values and XOR gates.
Then, as for the Risk achievement, Risk Reduction Worth (relative risk reduction) is calculated as:

$$RRW(i) = \frac{P_T}{P_T(P_i = 0)} \tag{2.14}$$

which is greater than 1 for the same reasons as mentioned previously.

3) Birnbaum's Importance Measure (BM)

This index is similar to sensitivity analysis and has been introduced by Birnbaum *(Birnbaum 1968)*. It is obtained by subtracting the top event failure probability with the given basic event (i) probability set to 1 by the same top event failure probability with the same given basic event probability set to 0. As a consequence, we can write Birnbaum's Importance Measure (BM) as:

$$BM(i) = RA(i) + RR(i) \tag{2.15}$$

However, the equation (2.15) constitutes an approximation of BM because it is valid only if P_T is linear expression of the basic event probability considered.

The real index without approximation can also be obtained by partial differentiation of system top failure probability with respect to P_i such as:

$$BM(i) = \frac{\partial P_T}{\partial P_i} \tag{2.16}$$

The reason why this index is similar to classical sensitivity methods is that its meaning is the same. Indeed, a large BM translates the fact that a small change in the reliability of contributor i will induce a large change in overall reliability.

4) Fussell-Vesely (F-V) Importance

This last importance measure is also called the *Top Contribution Measure*. This index can be calculated not only for basic events but also for intermediate events at higher levels. This measurement allows giving a quantification of the importance of each causal factor.

More specifically, this index represents the probability that at least one minimal cut set that has component i is in failure state at time t given that the system is failed at time t. Let us call $Q_0 = P_T$ (probability of top event failure occurrence), m_i number of cut sets containing the element i and Q_j^i the probability that the minimal cut set j among those involving the element i is at failure state at time t, we can calculate:

$$FV(i) = \frac{1 - \prod_{j=1}^{m_i}(1 - Q_j^i)}{Q_0} \approx \frac{\sum_{j=1}^{m_i} Q_j^i}{Q_0} \tag{2.17}$$

2.1.4.3 Sensitivity analysis

Another aspect related to fault tree analysis is sensitivity. Indeed, even if reliability related to the top event can be evaluated, this value remains not so much useful if this value undergoes important variations when the basic event probabilities change. This is what we called sensitivity. However, if one particular component of the tree seems to play a role in the high sensitivity of the top event failure probability, improvement of this component can be performed *(Ruijters et al. 2015)*.

Rushdi 1985 describes a mathematical method used to evaluate the uncertainty related to the reliability with respect to a particular variable. Indeed, it is possible to obtain the variance of the unavailability of the system (the probability that the system failure occurs at a given time t) in function of central moments of mean values of basic events unavailabilities.
Another method consists in considering the BM index as mentioned in the previous section.

2.2 Monte Carlo Simulations

When talking about risk analysis in decision making and quantitative risk analysis, one widely used method to face uncertainties is called **Monte Carlo Simulation**. This method is used in many fields such as finance, energy, manufacturing, engineering, insurance, oil gas, transportation, and the environment. These simulations provide the user with plenty of different outcomes and their probabilities of occurrence *(Palisade 2020)*.

Indeed, let's describe the idea behind this methodology. Risk analysis through Monte Carlo Simulation is performed by building models of possible outcomes by considering probability distribution for each factor to which uncertainties are attached. The calculations are then performed repeatedly using different series of values extracted from the different probability distribution functions associated with each random variable considered. During each simulation, a set of values is thus randomly extracted from the input probability distributions and the resulting output of this specific sample is recorded. After all simulations are performed (the number is chosen by the user), statistics can be applied to all the different obtained outcomes such as their probabilistic distribution and so on. By doing so, Monte Carlo Simulation contributes to a much better physical understanding of the phenomenon. Indeed, more than revealing what is going to happen, the probabilistic distribution of the outcomes reveals how and how frequently it will happen *(Palisade 2020)*.
Working on probabilistic results instead of deterministic brings a couple of advantages such as the following *(Palisade 2020)*.

- Gives information about the frequency of occurrence of each outcome by analyzing their probability distributions.
- Easier to provide a graphical representation of the resulting outcomes.
- Can be applied as a sensitivity analysis tool. It is indeed easier to evaluate the impact of input parameters' changes considering probabilistic models than deterministic ones.
- Easier to implement scenario analysis due to the fact it is easier to consider different combinations of input values and their impact in probabilistic models than deterministic.

Chapter 3

FTA applied to permafrost environment

A large number of territories on Earth are characterized by permafrost environment. Climate change and anthropogenic activities tend to affect it by inducing the thawing of perennially cryotic ground. As a consequence, many environmental issues (including hydro(geo)logical fields) related to the ice thawing in cold environments exist and must be studied accurately.

In this section, the permafrost environment will be described as well as environmental concerns induced by ice thawing. One of these important issues connected to climate change is the formation of thermokarst lakes (accumulation of water in ponds due to the subsidence following the thawing of permafrost) and the thermal impact of these surface water bodies in the surroundings (talik formation).
The purpose of the following section is thus to apply Fault Tree Analysis to assess probabilities that such events happen.

3.1 Permafrost environment

3.1.1 Permafrost definition

First of all, to perform a study related to environmental issues in the permafrost environment, it is necessary to define and understand the meaning of the basic vocabulary.

Permafrost can be defined as ground that remains below 0°C for more than 2 consecutive years *(Harris et al. 2017)*. However, the definition turns to be more accurate and complex when considering ground thermal regimes, which means the evolution of the temperature with respect to the depth. Indeed, the intersection of the maximum and minimum ground temperature with the 0 °C isotherm defines the **perennially cryotic** ground which is equivalent to permafrost (no matter in which phase is the water). On the other hand, the intersection of these same curves with the freezing point depression isotherm (also called sub-zero temperature at which most of the water remains in solid-state) constitutes the **perennially frozen** ground and represents the area region where most of the soil water is frozen. The top of the permafrost layer is known as the **permafrost table** and is covered by **seasonally cryotic layer**. On the other side, the **Active layer** is defined as the top layer which overlays the perennially frozen ground and which is subject to seasonal freeze and thaws conditions. Finally, the perennially unfrozen ground also known under the name of **talik** is found under the frozen ground layer *(Woo 2012)*. All these features are visible in FIGURE 3.1.

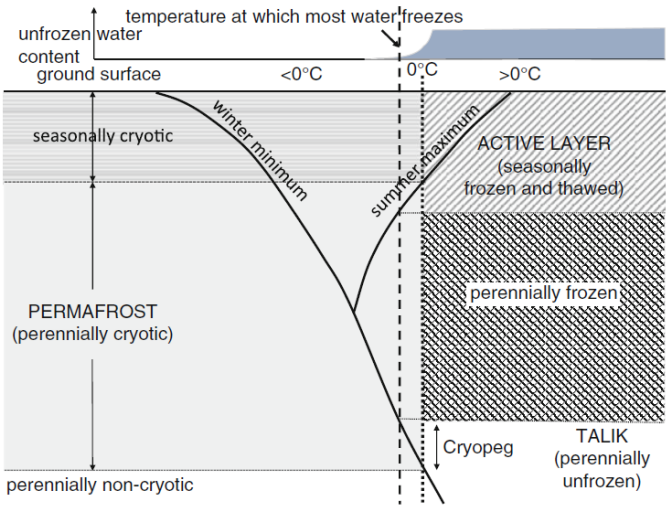

Figure 3.1: Definition of permafrost and its features with ground temperatures profile (from Woo 2012)

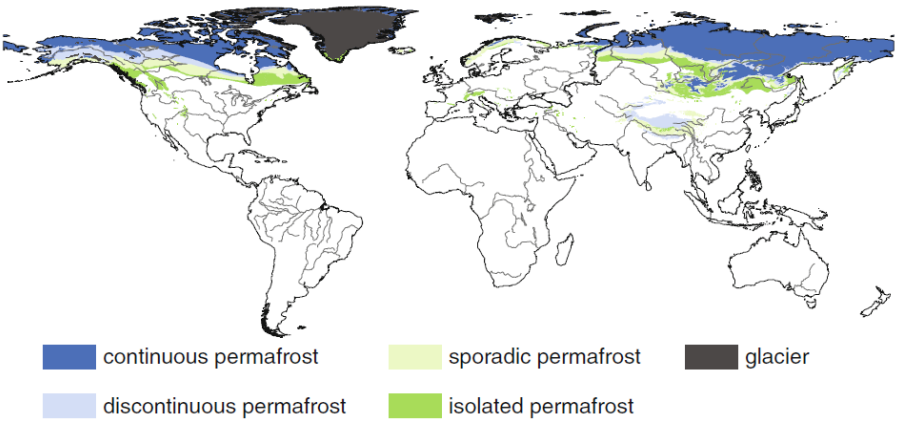

Figure 3.2: Permafrost distribution across the world (from Woo 2012)

3.1.2 Permafrost distribution in the world

Permafrost conditions appear only in the world's cold regions. To define a region as cold according to one measurable criterion, at least one of the following conditions must be respected *(Woo 2012)*:

- The average temperature of the coldest month is $< 0°C$
- The maximum observed snow depth on the ground is $> 0.3\ m$ (1 ft)
- The average duration of ice that prevents navigation exceeds 100 days per year
- the frost penetration exceeds $0.3\ m$ (1 ft) in at least 1 year of every 10

The cold regions that can be found in the northern hemisphere are mainly found at latitudes greater than 40° while the main cold region in the southern hemisphere is Antarctica *(Woo 2012)*.

Permafrost ground cover around 22% of the Earth's surface (excluding oceans) *(Brown et al. 1997)*. It constitutes consequently a non-negligible proportion of exposed land that can be studied. We can distinguish 2 types of permafrost regions:

1. Continuous permafrost: it defines regions where more than 90% of a geographical area covers permafrost.

2. Discontinuous permafrost: it occurs when some parts of the geographic regions are free of permafrost. In these regions, the circulation and recharge of the groundwater system above, within and under permafrost is not significantly disturbed.

As it can be seen in FIGURE 3.2, continuous permafrost is found in northern Canada and Siberia mostly while discontinuous permafrost is more likely to be found in the south of Canada, in the west part of Siberia and in the north of China.

3.1.3 Groundwater in the permafrost environment

Groundwater is an extremely important resource to study as it constitutes around 30% of freshwater available on Earth, the others 69% and 1% being respectively glaciers and surface water. It represents thus an important drinkable water supply that must be studied accurately. Indeed, groundwater has the advantages to underlie extended areas and to be less prompt to be polluted than surface water.
This groundwater is part of the hydrological cycle. Indeed, when droplets of water fall to the ground, some parts of them run-off but some others infiltrate the soil and recharge the aquifers, alimenting the groundwater flows in aquifers until reaching surface water bodies. Aquifers are geological formations that have enough porosity and permeability to store water and allow significant water movement through it.

In the permafrost environment, it is also necessary to develop groundwater studies as the water demand for freshwater also exists. Furthermore, groundwater problems can occur when mining, constructing buildings, highways, railways, pipelines and the whole is related to the extremes cold conditions.
Regarding permafrost, this last can be qualified as dry if it contains a few quantities of water or only ice. But permafrost can also be saturated by water, such as a case in which freezing point temperature is lower (e.g.: in the case of highly saline water). However, in most cases, water and ice co-exist in permafrost but when ice develops in the pores, it reduces considerably the permeability of the porous medium. This is the reason why permafrost layers are often considered as an aquiclude or aquitard. Groundwater is thus found in thawed zones of permafrost *(Woo 2012)*.
Groundwater flow can then occur in different configurations:

- **Suprapermafrost** (above permafrost): this circulation of water occurs mainly in the active layer which is subjected to seasonal changes. Consequently, water is stored as ice during the cold season but melt afterward during the thawing period. The recharge of groundwater in this zone is mostly done by snowmelt and rain. On the other hand, losses of groundwater in the active layer occur by evapotranspiration or by discharge either in intrapermafrost or to closer surface water bodies.

- **Intrapermafrost** (within permafrost): groundwater in this zone appears in taliks (perennially unfrozen ground) within permafrost and is constantly unfrozen. When open talik crosses the entire permafrost thickness, it creates a connection between supra and subpermafrost groundwater. The occurrence of these open taliks is facilitated by the existence of faults or permeable units which allow the flow of warmer water.

- **Subpermafrost** (under permafrost): Below permafrost, this water is under hydrostatic pressure with artesian conditions. In discontinuous permafrost area, recharge occurs through non-permafrost uplands or through supra or intra permafrost. On the other side, recharge in continuous permafrost conditions is much more restricted and occurs through fractures or solution conduits (e.g. sinkholes).

These different conditions are summarized in Figure 3.3.

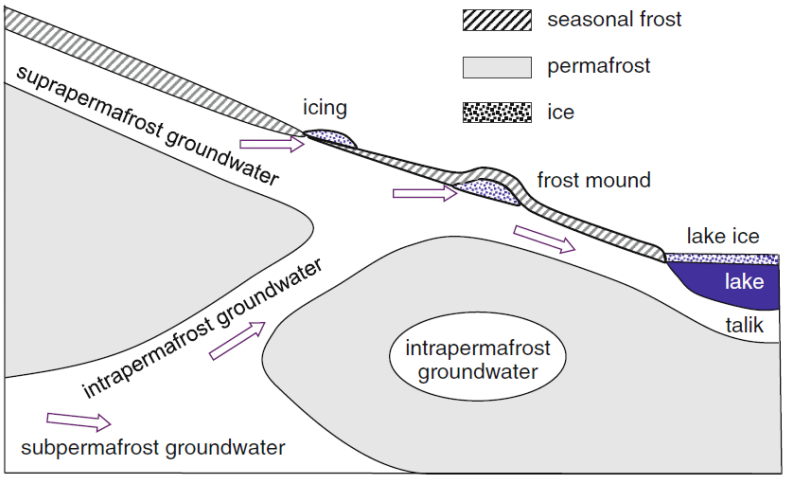

Figure 3.3: Sub, intra and supra permafrost groundwater conditions (from *Woo 2012*)

3.1.4 Impact of climate change on permafrost and thermokarst features

Many studies have demonstrated the existence of climate change and the impact it has on our environment. Concerning the cold environment, global warming significantly disturbs systems related to snow, ice, and permafrost. Indeed, cryosphere whose principal components are glaciers, frozen ground, mountains, floating ice shelves, seasonal snow cover on land, continental ice sheets, sea ice and lake, and river ice is extremely sensitive to effects of climate change *(Margesin 2008)*. Among the different observations, we could cite:

- Increase of glacial lake size
- Increase of frequency of Glacial lake outburst floods
- Reduction of mountain ice
- And so on

However, our attention will be focused on the degradation of the seasonally frozen ground and permafrost. Indeed, an increase of Active Layer thickness is observed. This deterioration results in the decline of mechanical strength of the ground, ground subsidence, and formation of a thermokarst environment *(Margesin 2008)*. The causes of the rapid thaw of very cold permafrost are the increase of mean summer air temperatures, the limited thermal buffering from overlaying organic layers, and vegetation and the presence of near-surface massive ice. The consequences of this permafrost degradation is a change in geomorphological configuration (formation of thermokarst basins *(Margesin 2008)*, piping of ice-wedges *(Seppälä 1997)*, ...), modification of the hydrological cycle, alteration of nutrients and carbon cycling, and damaging of overlaying infrastructures *(Farquharson et al. 2019)*.

Let's describe more into detail the thermokarst environment.
The processes related to excess ice degradation (usually by thawing) in permafrost areas are called thermokarst processes. This thawing of the permafrost layer induces 2 main consequences:

1. the change from frozen to unfrozen phase contributes to the reduction of soil strength.

2. the loss of excess ice causes a reduction of soil volume

Both aspects disturb the land surface morphology. It is understood that thermokarst processes began with disturbance of energy balance, which makes them good sensitive indicators of climate change *(Margesin 2008)*.

Among different thermokarst activities, the most common ones are:

- **Thermokarst subsidence**: Following excess ice ablation, the lowering of the ground surface occurs and is denoted as thermokarst subsidence. The degradation of ice is due to the melting induced by the heat conduction from the active layer deepening or surface water bodies (lakes, ponds, ...). However, the heat convection also occurs when the rain percolates into the ground or when the groundwater circulates. Consequently, when the unfrozen water goes away by drainage or evaporation, the soil consolidates inducing the subsidence of the land surface. This event is visible locally such as above intersecting ice wedges or where collapse pits occur at the floor of drained lakes.

- **Thermal erosion**: flowing water can have a thermal erosion effect due to heat conduction and heat convection processes. As a consequence, the exposed sediments after ice melting are mechanically eroded by the water. This phenomenon often occurs on hillslopes.

- **Surface ablation**: after erosion, remaining ice is exposed at the surface and can degrade by melting or sublimation.

- **Combinations**: these previous processes can occur successively or in proximity.

The reason to describe such a phenomenon is to introduce the environmental issue that will be treated by Fault Tree Analysis which is the generation of thermokarst lakes. Indeed, these surface water body features are deeply connected to thermokarst phenomena, especially thermokarst subsidence.

3.2 Thermokarst lakes

3.2.1 definition

Thermokarst lakes (also called thaw lakes) denote the surface water bodies that fill the closed pits that are generated by thermokarst subsidence following the thawing of ground ice. The occurrence of these lakes is most probable in ice-rich sediments throughout the permafrost zone. The geometry of these lakes, such as the lake circumference and bottom profile, is usually irregular. Furthermore, the lakes can enlarge laterally due to wave erosion of the shorelines inducing slumping of the banks. Most often, these lakes are initiated either by forest fires or global warming which ends up soil warming *(Christopher R Burn 1992)*.
To better understand the subject, the initiation, development, stabilization, and termination of thermokarst lakes will be described, based mostly on *Zhanju Lin et al. 2016* article. Furthermore, the scheme representing the different stages are visible in the appendix B.1.

Initiation

As already mentioned before, thermokarst features are good indicators of changes in temperature in cold regions. Nonetheless, anthropogenic activities became one of the primary factors of thermokarst lakes initiation, especially in Qinghai-Tibet-Plateau in China (QTP). As an example, the use of some heavy machinery degrade the vegetation and create small pits on the land surface that can be later filled with water and develop later on into lakes *(Zhanju Lin et al. 2016)*.

Some of the thermokarst lakes can be initiated by dams that outcome from the growing of ice-wedge polygons for example as it can be seen in Figure 3.4 *(Christopher R Burn 1992)*. However, most of these thaw lakes form when subsidence occurs due to local ground thawing. These local disturbances can be due to the degradation of surface vegetation or organic matter. As a consequence, this natural insulating layer no longer existing leads to an increase of heat absorption by solar radiation. Therefore, the ground temperature rises sufficiently to thaw the underlying permafrost. This thermokarst activity can also be due to rising summer air temperature, change in groundwater flow circulation, or precipitation. Finally, the small closed pits are filled either by water coming from precipitation and/or from surface runoff.

Figures A to C in Appendix B.1 represent the initiation stages. Figure A represents the undisturbed soil while B represents the disturbed surface. Finally, image C shows the initial pond due to water accumulation in the small depression as well as the rising of solar radiation.

Development

The development stages are represented in figures D to F in the Appendix B.1. While water accumulates in the depression area, the heat flux continues to warm the ground as long as the lake doesn't freeze to the bottom. As a consequence, the surrounding permafrost becomes warmer and this heat source boosts the thawing of

Figure 3.4: Thermokarst lakes related to ice-wedge polygon environment (*Streetly-Geog 2015 (accessed March 16, 2020)*)

the underlying ice-rich permafrost under the pond inducing a vertical development of the lake (section B in Figure D).

Furthermore, after the subsidence reaches a critical depth, the banks of the lakes can start to crack (section C in Figure E) and lake waves can erode the shoreline inducing slumping of the mass. Finally, while the shoreline backs off due to bank retrogression inducing the lateral expansion of the lake, the talik continues to develop vertically as long as the lake doesn't drain (Figure F).

Stabilization

The stabilization stage is represented by figure G in Appendix B.1. During this period, the lake growth stops, the lake doesn't drain yet and the heat exchange between the ground and the atmosphere is nearly at equilibrium.
This stabilization doesn't necessarily occur for all thermokarst lakes. Indeed, where the permafrost is thin, the lake can reach the drainage system before it gets time to stabilize because the whole permafrost layer is degraded too rapidly.

Termination

Finally, figures H to I in the Appendix B.1 represent the termination development. If talik develops through the entire permafrost thickness, the lake can then drain if the substrate is of high permeability which induces a lowering of lake level (Figure H). If the substrate is of low permeability, the lake can still reduce volume during periods of high evaporation and few precipitations.
Then, after having drained sufficiently, vegetation and permafrost develop again at the lake bottom and leave an empty depression pit on the land surface (Figure I).

3.2.2 consequences

As mentioned in the previous section, thermokarst lakes are disappearing after the stabilization stage. However, studies show that the frequency of thermokarst lakes is increasing with the warming of the local climate (Niu et al. 2011). The problem is that these warm thaw lakes constitute heat sources having consequences to the surrounding permafrost *(Zhanju Lin et al. 2011; Yang et al. 2016)*. Indeed, thermokarst lakes have consequences on the following aspects *(Wang et al. 2017)*:

1. **Local infrastructures**: this has been studied in particular by *Wen et al. 2018* and *Hu et al. 2018* who analyzed the effect of thermokarst lakes on a nearby embankment by numerical methods (their conceptual model is visible in FIGURE 3.5). They discovered indeed on the field that these thaw lakes can damage the nearby infrastructures due to thawing settlement for example. This can be explained by the continuous heat flow provided by the warm lake to the surrounding permafrost. Indeed, the effect of the lake can be divided into 2 stages. First, the temperature of permafrost underlying the structure rises due to the lateral thermal erosion induced by the lake. This decreases consequently the permafrost bearing capacity under the embankment. Secondly, a thawed layer can form under the structure due to the thermal effect of the engineering work in which the lake water can penetrate and degrade even more the permafrost. As a result, thaw subsidence occurs and can induce differential settlement under the structure affecting consequently the stability of the engineering work. This is the reason why a **critical safe distance** concept has been introduced. It is indeed advised to calculate a critical safe distance (in particular by the use of numerical methods), which is the minimum distance from the lake from which an engineering structure should be distant for a given service period (e.g. 50 years).

2. **Permafrost**: *Zhanju Lin et al. 2010* monitored a classical typical thermokarst lake of $2m$ deep in the Beiluhe Basin in Qinghai-Tibet-Plateau. They observed retrogression of the shoreline of the lake with a maximum rate of $1.8m/year$ between August 2007 and October 2008. Furthermore, they noticed that the thaw depth at the edge of the lake is $0.7m$ greater than in the surrounding terrains while the permafrost under the lake thawed entirely. The same effects have also been studied by *Niu et al. 2011*.

3. **Hydrological processes**: *Karlsson et al. 2012* confirmed that the increase in the area and number of thermokarst lakes induce by detecting a change in hydrological variables. Indeed, by performing a remote sensing study, they observed a decrease in intra-annual runoff variability and a decrease in water storage. These changes in water storage can be attributed to the permafrost degradation that alters water connectivity. For example, the generation of open taliks under thermokarst lakes influences the groundwater flow paths and alter consequently the quantity of water stored within a drainage basin.

4. **Contribution to climate change by releasing carbon preserved in the frozen ground**: *Walter et al. 2007* and *Jones et al. 2011* have demonstrated that organic carbon trapped in frozen sediments in the bottom of the lakes can be released after thermal degradation induced by the warm water.

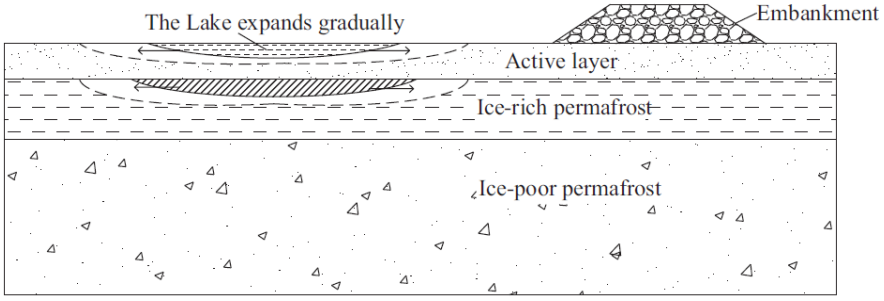

Figure 3.5: Lateral thermal erosion occurring around a lake in the proximity of an embankment (from *Wen et al. 2018*)

3.2.3 Cause factors

Let's now consider the factors that lead to the generation of thermokarst lakes. It is indeed necessary to study them to build the following Fault Tree. *Wang et al. 2017* performed a study evaluating the influence of specific factors on the generation of thermokarst lakes in the Beiluhe Basin in Qinghai Tibet Plateau. Indeed, they used spatial statistics tools (by remote sensing) to determine the frequency of lakes and their total cumulated areas found in zones where these different factors are involved. Finally, they performed a sensitivity analysis to identify which factors have the most influence on the thermokarst lakes generation. Many studies are indeed performed in Qinghai-Tibet Plateau due to the high ground temperatures and high ice content of permafrost which makes this region sensitive to global warming and human activities. More particularly, they studied the influence of six factors which are the permafrost type, the ground temperature, the vegetation, the soil, the hydrogeological categories, and the slope.

remark: Even if the factors differ from one region to another, this study helps to understand the basic factors that lead to thermokarst lakes generation.

- **Permafrost Types:** Different types of permafrost can be identified according to their ice-content:
  - ice-poor permafrost: ice-content $< 20\%$.
  - ice-rich permafrost: 20% <ice-content $< 50\%$
  - ice-saturated permafrost: 50% < ice-content

  This is an important factor as the ice-content constitutes the main water supply for thermokarst lakes after melting. This has been observed due to the high frequency of lakes found in regions with high ice-content.

- **Ground Temperatures:** Mean Annual Ground Temperatures (MAGT) has also been studied as a causal factor of thermokarst lake generation. Indeed, warm permafrost areas are more sensitive to surface disturbances such as thermokarst phenomena. It has also been observed due to the high frequency of lakes found in unstable to extremely unstable high-temperature zones.

- **Vegetation:** This factor is dependant on the study area cause all types of vegetation will differ according to the location of the studied zone. However, it is important to study it as the climate influences the permafrost condition by surface heat exchange. Consequently, it is is fundamental to study surface conditions such as vegetation types covering the land surface. In this specific area, they considered 4 types of vegetation covers which are meadows, desertification grassland, sparse desertification grassland, desertified steppe. However, the study of this factor is much more complex. Indeed, the highest frequency of lakes has been found in meadows but the highest cumulated lake areas (60% of total area) have been found in sparse desertification grassland. Consequently, the vegetation factor has not been considered in their sensitivity analysis.

- **Soil Type:** Water content of soil directly affects the ice content of permafrost. As a consequence, the generation of thermokarst lakes is also dependant on the nature of the soil. Five classes of soil have been considered: bedrock, gravel sand, silt and eolian sand, silty clay and eolian sand. 80% of the cumulated lakes area is found in gravel sand. It is indeed more likely to find thermokarst lakes in soils with great porosity such as gravel or sands which have higher water content and consequently, a higher ice-content as well.

- **Hydrogeological types:** It is not surprising to understand that groundwater also affects on the generation of thermokarst lakes. The study area has indeed been divided into four different hydrogeological classes according to what kind of soil and water is found above and below frozen layers. In this specific area, 70% of total lake areas are found in the hydrogeological class where the water above the frozen layer is tertiary sandstone fissure water while water below the frozen layer is tertiary sandstone-layered pore fissure water.

- **Slope:** Finally, an extremely important factor is related to terrain flatness. It has indeed been observed that no lakes are observed when the slope is greater than 15° and rarely observed when the slope is greater than 10°.

From all these factors, only 4 have been kept for the sensitivity analysis. The sensitivity coefficient for each factor translates the impact that this factor has on the generation of thermokarst lakes. A sensitivity coefficient greater than 1 means that the considered factor has a significant impact. Vegetation has not been considered cause the calculation of their sensitivity coefficient revealed to be more complex and less relevant than for other factors. Furthermore, the slope factor has the highest sensitivity coefficient and it has been showed that a slope lower than 10° is a requirement for thermokarst lake generation.
Consequently, the weight influence of the 4 remaining factors has been classified as followed: permafrost (0.4) > soil type (0.3) > ground temperature (0.2) > hydrogeological class (0.1).

Remark: The spatial statistics results related to this article are visible in Appendix B.2.

3.2.4 Fault Tree analysis

3.2.4.1 Construction of the tree

From section 3.2.3, we understand that 2 main conditions are required to have a thermokarst lake: a specific geometrical configuration and water accumulation.

1. **Geometrical configuration**: for this specific factor, 2 conditions are necessary : a flat terrain (slope $< 10°$) and a geometrical configuration which allows accumulation. This geometrical configuration is either due to subsidence of the ground or by dams induced by the growing of ice-wedges as already mentioned before *(Christopher R Burn 1992)*.

2. **Water accumulation**: as already mentioned several times before, lakes exist if water accumulates. A part of the water arises from the melting of permafrost as already mentioned by previous articles but another part also comes from precipitations *(Yang et al. 2016)*.

Knowing this, a fault tree related to thermokarst generation (Top event) has been built and is visible in FIGURE 3.6.

3.2.4.2 Qualitative analysis

Let's indicate the different basics events with alphabetic letters and let's consider P_χ with $\chi = \{A,B,C,D,E\}$, the probability that the basic event χ occurs. The events considered in the Fault Tree are the followings:

- P_A: the probability that it rains.
- P_B: the probability that permafrost thaws, providing water that can accumulate in a specific geometric configuration.
- P_C: the probability that the slope of the land surface is lower than $10°$.
- P_D: the probability that ice-wedge polygons grow, forming consequently natural dams where water can accumulate.
- P_E: the probability that the land surface undergoes settlement.

The first part of the analysis consists in analyzing the different cut sets leading to thermokarst lake generation. To do so, the fault tree represented in FIGURE 3.6 has been converted into a binary decision diagram as shown in FIGURE 3.7.

The diagram has been built starting from event A. Furthermore, the symmetry of this BDD is explained by the fact that the gate joining the event A and B is an OR and not a XOR, which allows thus both events A and B to occur. Consequently, 6 different cut sets (including 4 minimal) are identified: {B,C,D}, {B,C,E}, {A,C,D}, {A,C,E}, {A,B,C,D} and {A,B,C,E}.
Furthermore, one minimal path set can be identified which is {C}. Indeed, this event is part of all identified cut sets which induces that if this undesired basic event doesn't occur, thermokarst lakes won't be generated.

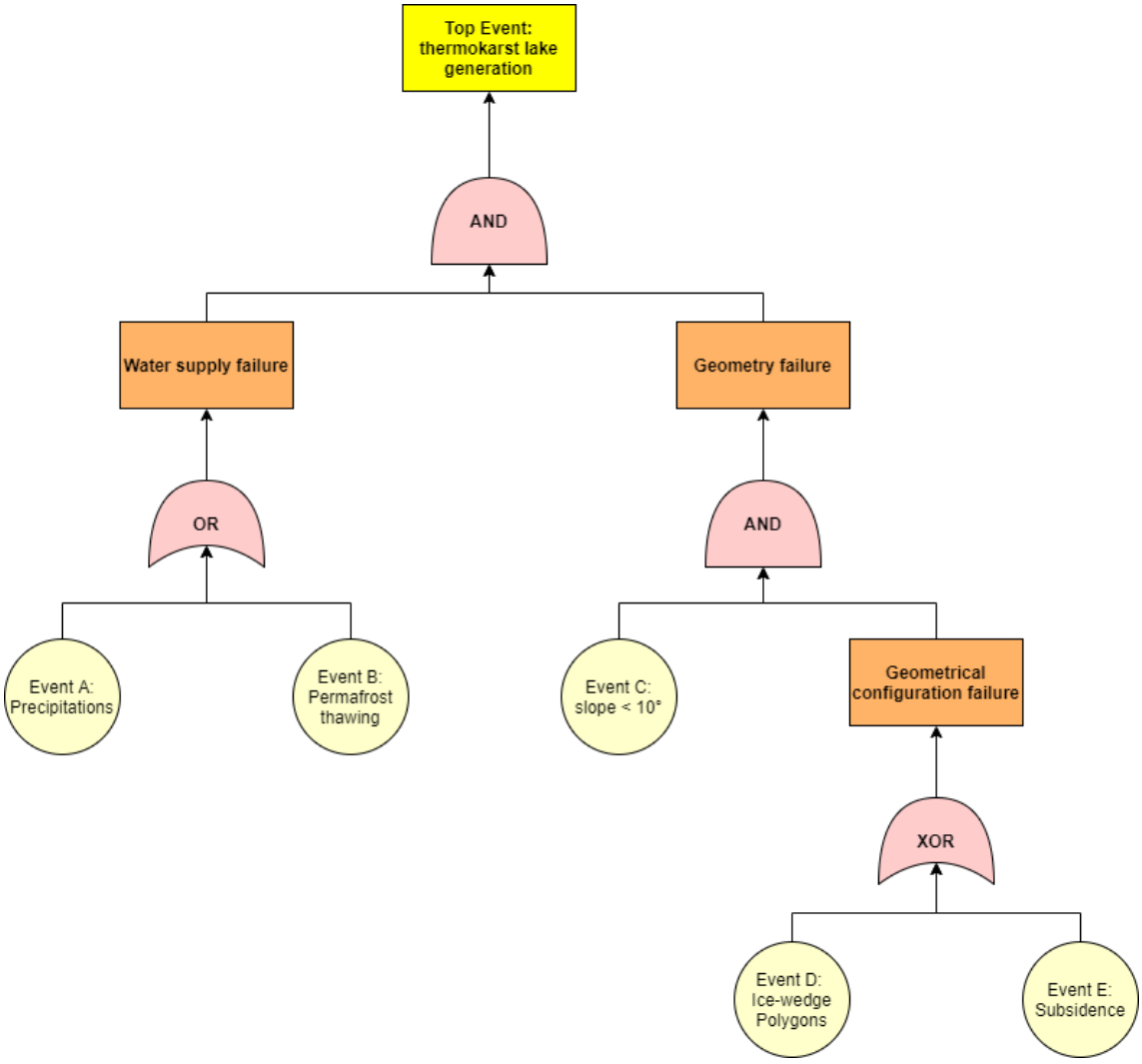

Figure 3.6: Fault Tree related to Thermokarst lake generation

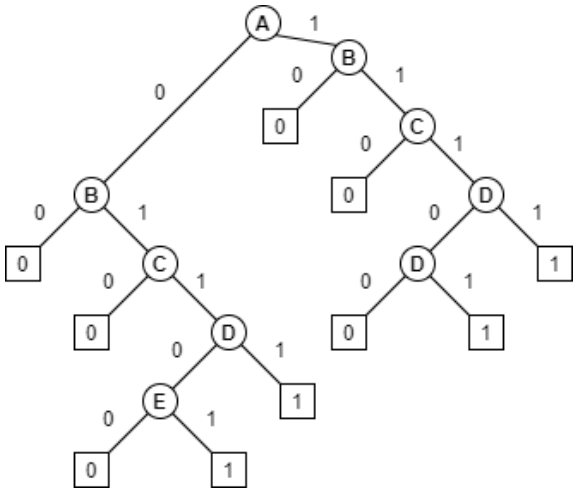

Figure 3.7: Fault tree related to thermokarst lake generation converted into a binary decision diagram

3.2.4.3 Quantitative analysis

Based on Boolean Manipulation already explain in the Chapter 2.1.3, it is possible to evaluate the probability that a thermokarst lake is generated (P_T). Considering the different logic gates involved in the Fault Tree, the probability that thermokarst lake generates is evaluated by: ,

$$\begin{aligned} P_T &= \Big(P_A + P_B - P_A \cdot P_B\Big) \cdot \Big(P_C \cdot \big(P_D + P_E - 2 \cdot P_D \cdot P_E\big)\Big) \\ &= P_A \cdot P_C \cdot P_D + P_A \cdot P_C \cdot P_E - 2 \cdot P_A \cdot P_C \cdot P_D \cdot P_E \\ &+ P_B \cdot P_C \cdot P_D + P_B \cdot P_C \cdot P_E - 2 \cdot P_B \cdot P_C \cdot P_D \cdot P_E \\ &- P_A \cdot P_B \cdot P_C \cdot P_D - P_A \cdot P_B \cdot P_C \cdot P_E \\ &+ 2 \cdot P_A \cdot P_B \cdot P_C \cdot P_D \cdot P_E \end{aligned}$$

Unfortunately, the previously created Fault Tree is very qualitative. Indeed, the top event considered is very generic and no articles mentioned quantitative measures related to basic events which would lead to the "Generation of a thermokarst lake". It is thus impossible to evaluate the probability that this environmental issue occurs. Another top event will thus be considered in the following section.

However, probabilities will be attributed to each basic event in an arbitrary manner (but still with coherent values) to apply quantitative analysis methods described in section 2.1.4 in a pedagogical purpose.
To do so, let's consider Beiluhe Basin in Qinghai-Tibet-Plateau as a specific geographical area that is sensitive to thermokarst lake generation.

1. P_A and P_B: *Yang et al. 2016* studied the hydrological contribution of permafrost in terms of water accumulation in thermokarst lakes. By using stable isotopes, he discovered that around 60% of the water in the studied lake (this lake is assumed to be representative of any thermokarst lakes in this area) comes from the thawing of permafrost while around 40% originates from precipitations. As a consequence, we will attribute the values $P_A = 0.4$ and $P_B = 0.6$. Once again, these values are extremely rough and arbitrary and are not considered to be representative of the real probabilities of occurrence.

2. P_C: *Wang et al. 2017* studied the influence of many factors in the Beiluhe basin leading to the generation of thermokarst lakes including the slope of the ground surface. By using GIS tools, they determined that 77% of the studied area has a slope lower than 10 °. As a consequence, we will consider $P_C = 0.77$.

3. P_D and P_E: Concerning these 2 basics events, it is harder to attribute coherent values of probabilities. Indeed, most of the articles related to thermokarst lakes cite subsidence as the main geometrical factor leading to a prompt shape to accumulate water while ice-wedge polygons have been mentioned only one time in *Christopher R Burn 1992*. Consequently, it has been decided to arbitrarily choose $P_D = 0.1$ and $P_E = 0.9$.

With these numbers, it is possible to evaluate the probability P_T by:

$$\begin{aligned} P_T &= \Big(0.4 + 0.6 - 0.4 \cdot 0.6\Big) \cdot \Big(0.77 \cdot \big(0.1 + 0.9 - 2 \cdot 0.1 \cdot 0.9\big)\Big) \\ &= 0.48 \end{aligned}$$

It is better not to interpret this number physically as it is based on extremely rough arbitrary attributions of probabilities. However, it is important to mention that a probability of occurrence of the undesired event close to 50% is extremely high value.

Importance measures

Let's now consider importance measures to determine the most important factors leading to thermokarst lake generation.

First of all, Birnbaum's importance measure will be considered:

$$\begin{aligned}
RA(A) &= P_T(P_A = 1) - P_T = 0.63 - 0.48 = 0.15 \\
RR(A) &= P_T - P_T(P_A = 0) = 0.48 - 0.38 = 0.1 \\
BM(A) &= RA(A) + RR(A) = 0.15 + 0.1 = 0.25 \\
\frac{\partial P_T}{\partial P_A} &= P_C \cdot P_D + P_C \cdot P_E - 2 \cdot P_C \cdot P_D \cdot P_E \\
&\quad - P_B \cdot P_C \cdot P_D - P_B \cdot P_C \cdot P_E \\
&\quad + 2 \cdot P_B \cdot P_C \cdot P_D \cdot P_E \\
&\quad = 0.25
\end{aligned}$$

$$\begin{aligned}
RA(B) &= P_T(P_B = 1) - P_T = 0.63 - 0.48 = 0.15 \\
RR(B) &= P_T - P_T(P_B = 0) = 0.48 - 0.25 = 0.23 \\
BM(B) &= RA(B) + RR(B) = 0.15 + 0.23 = 0.38 \\
\frac{\partial P_T}{\partial P_B} &= P_C \cdot P_D + P_C \cdot P_E - 2 \cdot P_C \cdot P_D \cdot P_E \\
&\quad - P_A \cdot P_C \cdot P_D - P_A \cdot P_C \cdot P_E \\
&\quad + 2 \cdot P_A \cdot P_C \cdot P_D \cdot P_E \\
&\quad = 0.38
\end{aligned}$$

$$\begin{aligned}
RA(C) &= P_T(P_C = 1) - P_T = 0.62 - 0.48 = 0.14 \\
RR(C) &= P_T - P_T(P_C = 0) = 0.48 - 0 = 0.48 \\
BM(C) &= RA(C) + RR(C) = 0.14 + 0.48 = 0.62 \\
\frac{\partial P_T}{\partial P_C} &= P_A \cdot P_D + P_A \cdot P_E - 2 \cdot P_A \cdot P_D \cdot P_E \\
&\quad + P_B \cdot P_D + P_B \cdot P_E - 2 \cdot P_B \cdot P_D \cdot P_E \\
&\quad - P_A \cdot P_B \cdot P_D - P_A \cdot P_B \cdot P_E \\
&\quad + 2 \cdot P_A \cdot P_B \cdot P_D \cdot P_E \\
&\quad = 0.62
\end{aligned}$$

$$
\begin{aligned}
RA(D) &= P_T(P_D = 1) - P_T = 0.06 - 0.48 = -0.42 \\
RR(D) &= P_T - P_T(P_D = 0) = 0.48 - 0.53 = -0.05 \\
BM(D) &= RA(D) + RR(D) = -0.42 - 0.05 = -0.47 \\
\frac{\partial P_T}{\partial P_D} &= P_A \cdot P_C - 2 \cdot P_A \cdot P_C \cdot P_E + P_B \cdot P_C \\
&\quad - 2 \cdot P_B \cdot P_C \cdot P_E - P_A \cdot P_B \cdot P_C \\
&\quad + 2 \cdot P_A \cdot P_B \cdot P_C \cdot P_E \\
&\quad = -0.47
\end{aligned}
$$

$$
\begin{aligned}
RA(E) &= P_T(P_E = 1) - P_T = 0.53 - 0.48 = 0.05 \\
RR(E) &= P_T - P_T(P_E = 0) = 0.48 - 0.06 = 0.42 \\
BM(E) &= RA(E) + RR(E) = 0.05 + 0.42 = 0.47 \\
\frac{\partial P_T}{\partial P_E} &= P_A \cdot P_C - 2 \cdot P_A \cdot P_C \cdot P_D + P_B \cdot P_C \\
&\quad - 2 \cdot P_B \cdot P_C \cdot P_D - P_A \cdot P_B \cdot P_C \\
&\quad + 2 \cdot P_A \cdot P_B \cdot P_C \cdot P_D \\
&\quad = 0.47
\end{aligned}
$$

From these equations, several things can be observed:

- First of all, there is the confirmation that $\frac{\partial P_T}{\partial P_i}$ permits also to calculate $BM(i)$ as it gives the same result than when considering Birnbaum's importance measure as the sum of risk achievement and risk reduction.

- Secondly, it is observed that event C (flat slope) constitutes the most important contributor to Top Event failure (generation of thermokarst lake). Indeed, its Birnbaum's importance measure is the greatest (0.64) translating a high sensitivity in contrast with all others BMs which are lower than 0.5. This means that a small change in P_C would induce a large change in P_T. That could have been expected even without performing any calculations. Indeed, it was already known than in equation describing P_T, P_C was multiplying every term of the equation. However, it is important to keep in mind the background behind it. Indeed, having a slope $< 10°$ doesn't mean a thermokarst lake will generate. It just means that in the context of permafrost conditions such as in the Beiluhe basin in Qinghai-Tibet-Plateau, lakes can generate only in flat ground surfaces.

- Finally, it is seen that BM(i) can also be negative, as it is the case for $BM(E) = -0.47$. The reason why negative values occur has already been explained in Chapter 2. Indeed, the high probability values assigned to which are added the presence of the XOR gate contribute to the negative values of importance measures.

Finally, Fussell Vesely (F-V) Importance will be calculated as well to have the confirmation that the basic event C is the most important contributor to Top Event Failure. To do so, let's consider the probabilities related to each different cut set occurrence:

$$\begin{aligned} P(\{A,C,D\}) &= P_A \cdot P_C \cdot P_D = 0.0308 \\ P(\{A,C,E\}) &= P_A \cdot P_C \cdot P_E = 0.2772 \\ P(\{B,C,D\}) &= P_B \cdot P_C \cdot P_D = 0.0462 \\ P(\{B,C,E\}) &= P_B \cdot P_C \cdot P_E = 0.4158 \\ P(\{A,B,C,D\}) &= P_A \cdot P_B \cdot P_C \cdot P_D = 0.01848 \\ P(\{A,B,C,E\}) &= P_A \cdot P_B \cdot P_C \cdot P_E = 0.16632 \end{aligned}$$

Considering the equation (2.17), it is possible to calculate FV index related to each basic event i. For example, let's evaluate FV coefficient related to event A:

$$\begin{aligned} FV(A) &= \frac{1 - \big(1 - 0.0308)\big)\big(1 - 0.2772)\big)\big(1 - 0.01848\big)\big(1 - 0.16632\big)}{P_T} \\ &= 0.8893 \end{aligned}$$

Considering the same method than previously, FV coefficient has been calculated for each basic event:

$$\begin{aligned} FV(B) &= 1.1338 \\ FV(C) &= 1.4183 \\ FV(D) &= 0.1931 \\ FV(E) &= 1.3503 \end{aligned}$$

$FV(C)$ being the greatest, this proves once again that event C is the greatest contributor to the top event failure.

Note: It is important to emphasize the fact that all these numbers are obtained from rough arbitrary choices of probabilities. Thus, this section doesn't pretend to provide an accurate estimate of the probability that a thermokarst lake generates but more to show that Fault Tree analysis can be applied to evaluate the risk related to an environmental issue.

3.3 Talik development under thermokarst lakes

3.3.1 Definition and consequences

As said previously, it is necessary to define a more specific environmental issue that can be described by quantitative variables. To do so, instead of considering how likely a thermokarst lake could generate, let's assume the lake already exists and define an environmental issue related to it. One of the problems which occur the most is the development of taliks (perennially unfrozen ground) beneath the lakes. Indeed, as already mentioned before, lakes in permafrost areas are the greatest sources of heat. Indeed, ground underneath lakes is usually warmer because the lake bottom temperature is greater than 0°. However, it is not necessarily the case when the water freezes until the bottom or under the terraces of the lakes which are more shallow *(Christopher R Burn 2002)*.

Typically, talik configuration can be visualized in the drawing made on the FIGURE 3.8. This shows a simplification of the real situation as the geological configuration is not as smooth as in the drawing and the distribution of the layers is always dependant on the geographical location of the lake. However, this allows representing better the parameters that influence the talik development such as the mean annual lake-bottom temperature (T_{lb}), the depths of the lake, of the floating ice, and of the water corresponding respectively to d_l, d_i, and d_w. These different parameters will be described later on.

Talik development under lakes is considered as an environmental issue due to its consequences which are the same as the ones related to thermokarst lakes, given both are deeply connected. As already explained, when a talik develops through the entire permafrost layer, it creates a pathway between suprapermafrost and subpermafrost water changing thus the hydrological variables and processes. Furthermore, one of the most damaging consequence is the fact that unfrozen ground (talik) is an anaerobic environment where bacteria can degrade organic matter contained in pre-existing permafrost. Consequently, taliks related to these thermokarst lakes constitute a serious source of atmospheric methane *(Roy-Leveillee et al. 2017)*.

3.3.2 Description of the phenomena

What governs the development of taliks is the heat transfer occurring from the warm lake bottom. Indeed, the evolution of talik boundaries is given by the evolution of the position of 0° isotherm lines. Indeed, many authors develop 2D heat transfer numerical models which allows visualizing the evolution of talik in time (*Ling et al. 2003, Ling et al. 2012, Ling et al. 2019 and Rowland et al. 2011*) by modeling the different isotherm lines under thermokarst lakes. For example, FIGURE developed by *Ling et al. 2019* in the appendix B.3 represents the development in time of the ground temperature distribution under a warm lake after several years for different lake bottom temperatures. The limit of the talik is seen in red and it can be seen that lake bottom temperature plays a huge role. Indeed, a warmer lake bottom temperature will induce a lowering of the talik boundary as well as further lateral expansion.

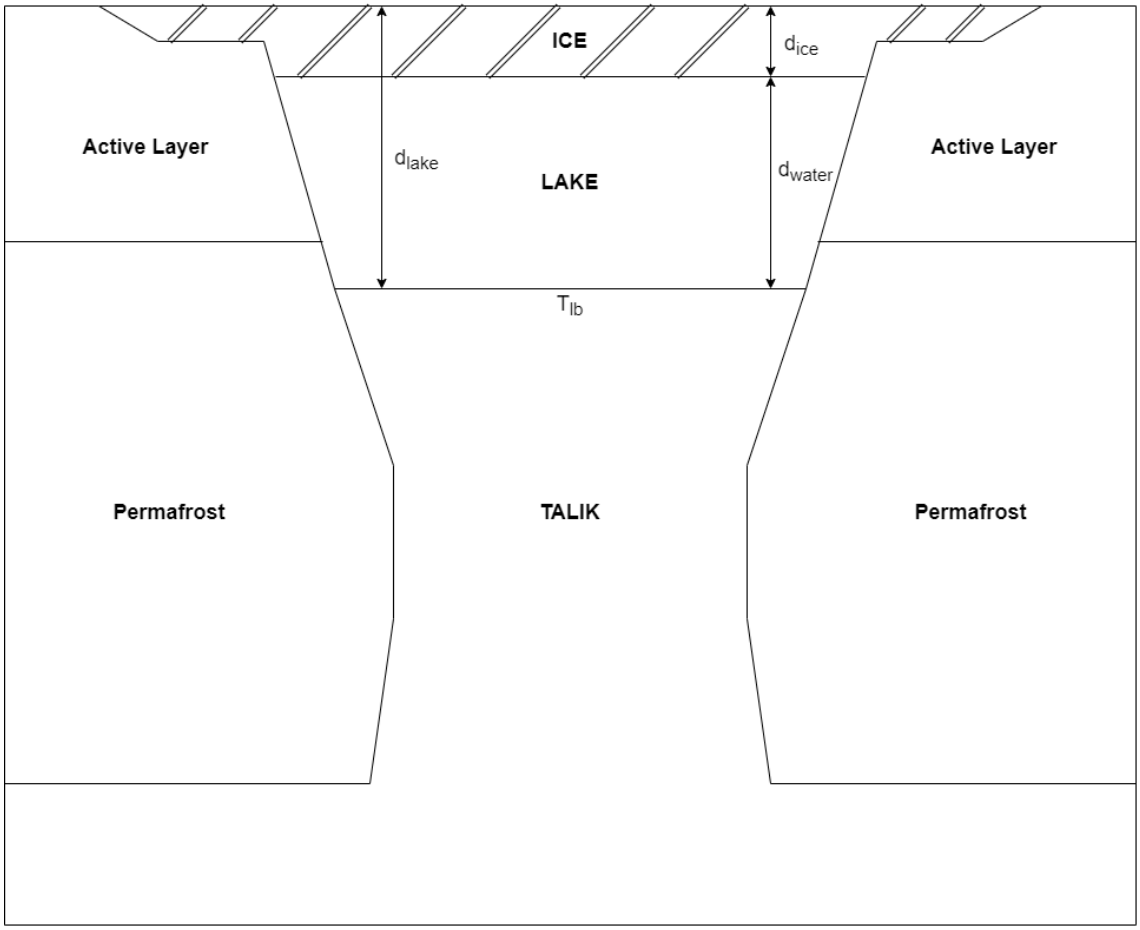

Figure 3.8: Scheme of talik configuration beneath thermokarst lake

remark: All these numerical models present the results in half of the domain as the lake is considered as symmetrical.

As it is understood, water plays a huge role in permafrost degradation as it transports heat. This is the reason why most developed models couple heat transport and groundwater flow processes while taking into account latent heat and modification of soil permeability due to water phase changes. Indeed, it has been shown that the thickness of durable permafrost thickness is 2 to 5 times greater in the absence of groundwater flow *(Rowland et al. 2011)*.
Indeed, previous simulations show that the permafrost thawing rates were about tens of meters over a huge period of time (centuries to millennia). However, these old simulations took into account only extremely cold regions (mean air temperature between -6 and -10° and mean near-surface ground temperature between -6 and -8 °) with really thick permafrost ($> 400m$). Furthermore, they made heat transfer simulations by considering conduction phenomena only, without considering advection induced by groundwater. However, in discontinuous permafrost areas, permafrost is much thinner (20 to 60 m) with warmer mean annual air temperature ($-2°$). When performing simulations that incorporate heat advection, the time to degrade frozen ground is much lower than when considering conduction only (nearly by half) *(Rowland et al. 2011)*.
The heat transfer equations used by *Ling et al. 2003, Ling et al. 2012 and Ling et al. 2019* to quantify temperature distribution under the lake are the following:

$$C\frac{\partial T}{\partial t} = \frac{\partial}{\partial r}\Big(k\frac{\partial T}{\partial r}\Big) + \frac{k}{r}\frac{\partial T}{\partial r} + \frac{\partial}{\partial z}\Big(k\frac{\partial T}{\partial z}\Big) \tag{3.1}$$

with ($0 < t < D$, $0 < z < Z$, $0 < r < R$). t is the time in seconds, z is the depth in meters, r the radial distance from the center of the lake in meters, D the total simulation period in seconds, Z and R the total depth and radius of the analyzed domain, T the temperature in $°C$. C and k are respectively the volumetric heat capacity in $J\ m^{-3}\ °C^{-1}$ and the thermal conductivity in $W\ m^{-1}\ °C^{-1}$ and are described by:

$$C = \begin{cases} C_f & \text{if } T < T_e - \Delta T \\ C_f + L_w\rho_b\dfrac{W - W_u}{\Delta T} & \text{if } T_e - \Delta T \leq T \leq T_e \\ k_u & \text{if } T > T_e \end{cases}$$

$$k = \begin{cases} k_f & \text{if } T < T_e - \Delta T \\ k_f + \dfrac{k_u - k_f}{\Delta T}[T - (T_e - \Delta T)] & \text{if } T_e - \Delta T \leq T \leq T_e \\ k_u & \text{if } T > T_e \end{cases}$$

where the subscripts u and f represent the unfrozen and frozen phases respectively. L_w is the mass-specific latent heat of water in $J\ kg^{-1}$, ρ_b is the dry bulk density of soil in $kg\ m^{-3}$, T_e the freezing or thawing temperature set to 0°C, ΔT the temperature interval where a phase change occurs (set to $1°C$).

remark: It is only in the article of *Ling et al. 2019* that the lateral expansion of the lake due to the erosion or slumping phenomena is taken into account by considering also $r(t) = r_0 + v_{he}t$ where v_{he} is the expansion rate in $m/year$.

3.3.3 Cause factors

The development of talik if deeply connected to lake parameters such as the mean lake bottom temperature, the lake thickness, the lake depth, or even the thermal conductivity of lake bottom sediments.

1. **Lake-Bottom temperature (T_{lb}):** what causes the non-sustainability of the permafrost beneath thermokarst lakes is the temperature of sediments underlying the water body which are warmer than the surrounding permafrost. When modeling talik development, it is commonly used to consider the long-term mean annual lake-bottom temperature (MALBT) to represent temperature conditions beneath the lake. Indeed, variations in thermal regime of sediments underlying the lake which affect talik development are captured by this value (*Roy-Leveillee et al. 2017, Chris R Burn 2005*). No talik development is observed with a MALBT which is $\leq 0\ °C$. Consequently, one necessary condition to have a talik development under thermokarst lake is to have a MALBT $> 0\ °C$ *(Ling et al. 2003)*. This defines the basic event A.

2. **lake ice-thickness (d_i):** It is commonly said that the lake bottom temperature is $> 0\ °C$ except in one case: when the lake's water freezes through the entire thickness (*Christopher R Burn 2002, Roy-Leveillee et al. 2017*). Consequently, another condition to have the development of thermokarst lake is to have ice-thickness lower than lake water depth: $d_i < d_l$. This constitutes the basic event B. However, this condition is problematic. Indeed, as already explained in the chapter related to Fault-Tree analysis, basic events leading to the top event failure must be independent. However, we understand that lake-bottom temperature is deeply dependant on lake-ice thickness. Yet, in a pedagogical purpose, it has been decided to continue the analysis as if the events are independent.

3. **The ratio of freezing degree-days to thawing degree-days at the lake bottom $\frac{FDD_{lb}}{TDD_{lb}}$**: indeed, it has been shown by *Roy-Leveillee et al. 2017* that talik can still develop when ice reach the bottom of the lake such as $d_i = d_l$ (Event C). In this situation, talik development is governed by the ratio of freezing degree-days to thawing degree-days at the lake bottom. FDD_{lb} and TDD_{lb} represent the "cumulative departures from $0°C$ in mean daily temperatures ($°C\ d$) during the freezing and thawing seasons, respectively" *(Roy-Leveillee et al. 2017)*. The permafrost becomes unstable and starts melting in these conditions when the ratio $\frac{FDD_{lb}}{TDD_{lb}} \approx \frac{\lambda_t}{\lambda_f}$ where λ_t and λ_f represent the thermal conductivity of underlying sediments in thawed and frozen state respectively. The ratio $\frac{FDD_{lb}}{TDD_{lb}}$ is expected to change over the years. Indeed, $\frac{FDD_{lb}}{TDD_{lb}}$ is expected to diminish with time with climate change which induces a longer warm season (increase of TDD) and shortening of the cold season (decrease of FDD). Consequently, when the ice reaches the bottom of the lake, talik development is initiated when $\frac{FDD_{lb}}{TDD_{lb}} \leq \frac{\lambda_t}{\lambda_f}$ (event D).

3.3.4 Fault Tree analysis

3.3.4.1 Fault-Tree construction

Based on section 3.3.3, a Fault Tree has been built and is visible in FIGURE 3.9 where it considers the talik development under thermokarst lakes as a Top Event.

Let's describe more in detail this fault tree. If we start from the top of the tree, we can see that one necessary condition to initiate the development of talik is to have a lake-bottom temperature $> 0°C$. On the other hand, the lake thickness also plays a role and this is the reason why an **AND** logical gate has been placed between **Event A** and **Ice-thickness failure**. Then, starting from Ice-thickness failure, we have 2 possibilities: either the lake-ice thickness is lower than the lake depth (**Event B**), either the ice reaches the bottom of the lake (**Shallow lake failure**). However, these events can't happen simultaneously and this is the reason why a **XOR** logical gate has been placed between Event B and Shallow Lake failure. Finally, in the case ice reaches the lake bottom (**Event C**), the talik development is observed only when $\frac{FDD_{lb}}{TDD_{lb}} \leq \frac{\lambda_t}{\lambda_f}$ (**Event D**) occurs. This is the motivation that pushes us to place an **AND** logical gate between event C and event D.

3.3.4.2 Qualitative analysis

As for thermokarst lake development, it is possible to identify cut-sets of this fault-tree by converting it in a binary decision diagram. FIGURE 3.10 is the representation of the fault tree.
From this scheme, 2 minimal cut-sets are identified: {A, B} representing the case in which thermokarst lakes are deep and {A, C, D} representing the opposite (shallow thermokarst lakes).
Furthermore, the minimal path set {A} can also be identified. This points out how important is the influence of lake-bottom temperature on talik development.

3.3.4.3 Quantitative analysis

Let's consider the following probabilities:

- P_A the probability that event A occurs: $T_{LB} > 0°C$.
- P_B the probability that event B occurs: $d_i < d_L$
- P_C the probability that event C occurs: $d_i = d_L$
- P_D the probability that event D occurs: $\frac{FDD_{lb}}{TDD_{lb}} \leq \frac{\lambda_t}{\lambda_f}$

If we design by P_T, the probability that talik develops under thermokarst lake, this one can be obtained from Boolean manipulation by:

$$\begin{aligned} P_T &= P_A \times \Big(P_B + \big(P_C \times P_D\big) - 2 \times P_B \times P_C \times P_D\Big) \\ &= P_A.P_B + P_A.P_C.P_D - 2.P_A.P_B.P_C.P_D \end{aligned} \tag{3.2}$$

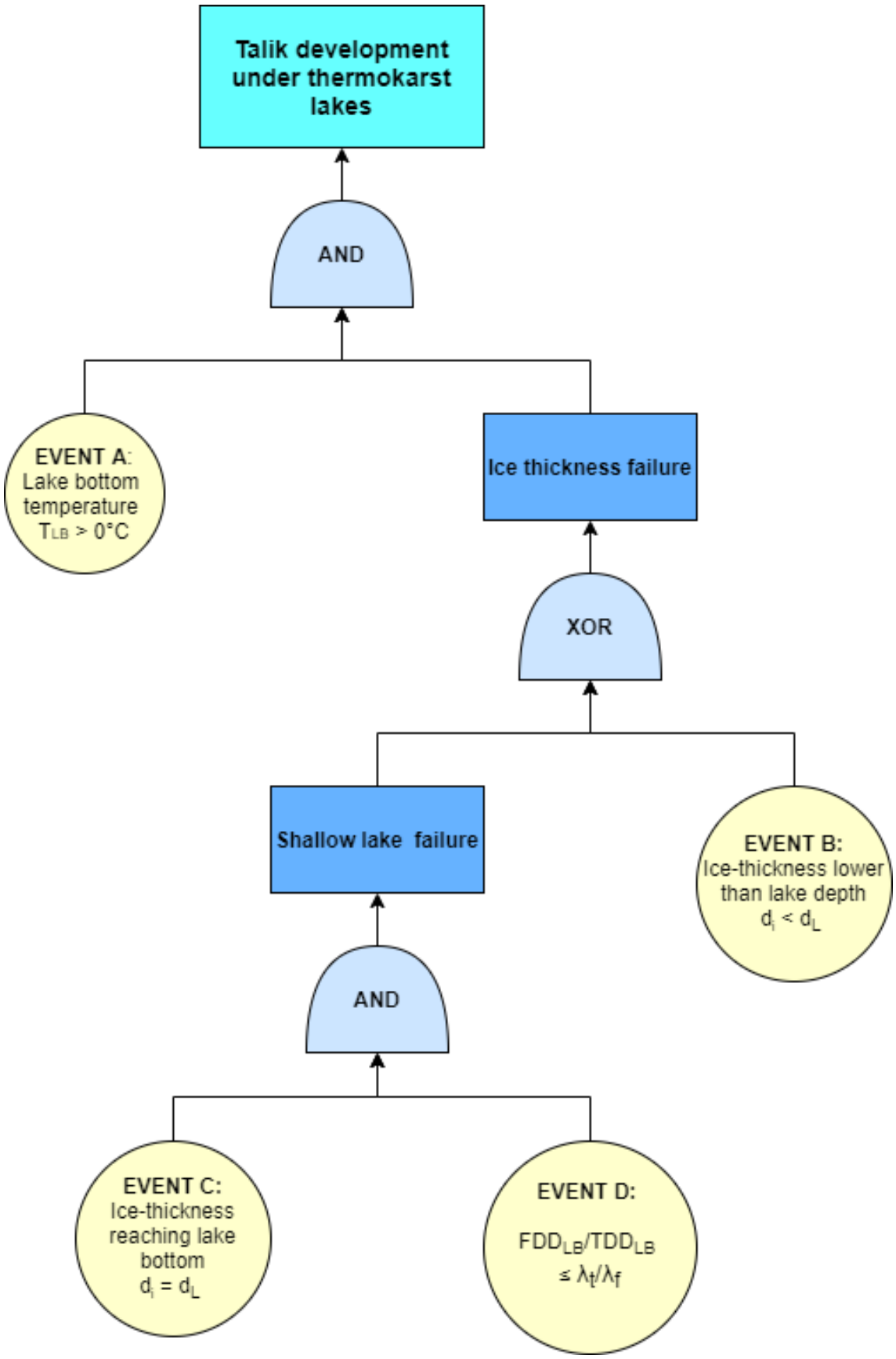

Figure 3.9: Fault Tree related to talik development under thermokarst lakes

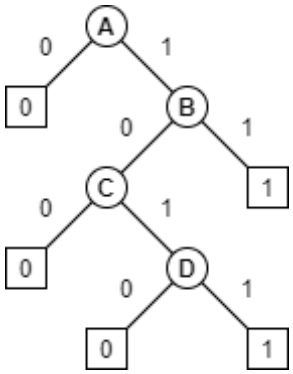

Figure 3.10: Binary decision diagram representation of fault tree related to talik development under thermokarst lakes

Evaluation of probabilities

The characteristics of lakes are dependent on climatic conditions such as mean air temperature, precipitations, wind conditions, and so on. Consequently, to evaluate probabilities, it is necessary to consider a location of the study. Indeed, calculating the proportion of lakes that freeze to the bottom in Coastal Arctic Plain in Canada won't be the same as in Siberia (Russia) or in Qinghai-Tibet-Plateau (China).

It has been decided to focus on Qinghai-Tibet-Plateau (QTP). Indeed, this geographical area is characterized by warmer ground temperatures and greater ice-content, making it thus more sensitive to climate change and anthropogenic activities *(Wang et al. 2017)*. As a result, more studies and articles are related to this geographical area.
More specifically, the Beiluhe basin (9250–9305E, 3442–3504N) will be considered. This zone is ranging between 4,500 and 5,200 meters of altitude inside of QTP (*Wang et al. 2017*). The following climatic characteristics are the following *(Zhanju Lin et al. 2016)*:

- mean annual air temperature: $-3.55°C$ (between 2005 and 2010).
- mean annual precipitations (including snow): 368 mm with most of it occurring between April and September. This induces few snow cover in winter so less insulating layer for the ground which also contributes to the wide thermokarst development in this basin.
- Mean annual evaporation: 1538 mm. Evaporation being much higher than precipitation, it weakens the buffering effect of the land surface (cause no snow) and the resistance of the soil to run-off.
- Continuous permafrost characterized by more than 20% of volumetric ice-content and a thickness ranging from 20 to 80 m.
- Mean annual ground temperature ranges from $-1.8°C$ to $-0.5°C$.
- Active layer thickness is ranging between 1.8 to 3 m.

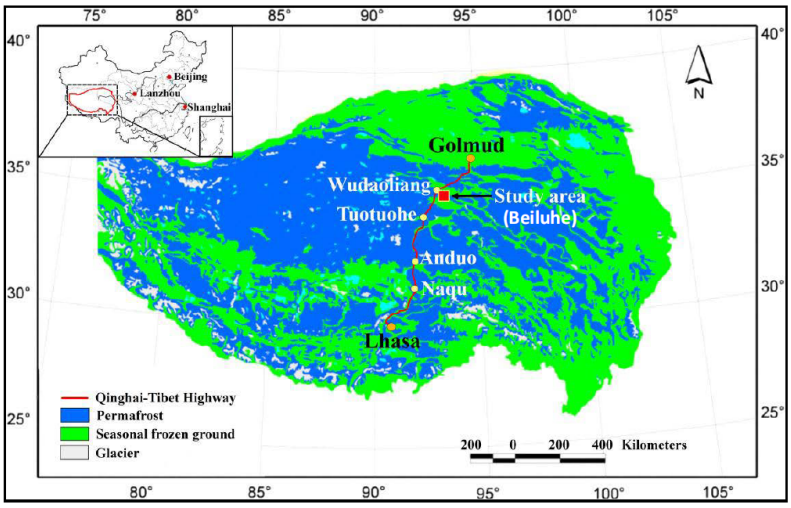

Figure 3.11: Location of Beiluhe Basin in QTP (from *Zhanju Lin et al. 2016*)

The location of the Beiluhe basin is visible in FIGURE 3.11.
Regarding thermokarst lakes, 600 have been identified in this study area covering a total area of 417.6 km^2.

Let's now try to find in the literature the probabilities of the different basic events related to the fault tree analysis to calculate the probability of talik development under thermokarst lakes (see Equation (3.2)).

Event A: $T_{lb} > 0°C$

As already mentioned before, T_{lb} represents an average temperature of the lake bottom temperature during the whole year ($MALBT$ = mean annual lake bottom temperature). Normally, the probability P_A should be the same as P_B as all authors mention that the MALBT is greater than $0°C$ when the ice doesn't reach the lake bottom. However, given that we need these events to be independent, it is necessary to determine P_A in another way.
Usually, in this specific climatic area, the freezing period starts from the end of October to March. *ZJ Lin et al. 2017* affirm after field investigation in 2009-2010 that more than 90% of the lakes have a lake-bottom temperature superior to $0°C$ in January. Even if this value doesn't represent a mean value over the year, we can assume that a temperature of lake bottom measured at half of the freezing period (January) would be a relevant indicator for talik development. Indeed, if the lake bottom temperature is already greater than $0°C$ at half of the freezing period, it can be assumed that it will also be the case for the MALBT. Knowing that the mean air temperature is increasing globally due to climate change, we can make the hypothesis that this proportion of lakes would be even higher. As a consequence, it has been decided to assign $P_A = 92.5\%$. However, it is important to highlight that this value is very subjective as it is hard to obtain quantitative data related to this subject.

Event B: $d_i < d_l$

To evaluate such a probability, it is necessary to find in the literature the proportion of lakes that stay unfrozen until the bottom during the winter season. As claimed by *Zhanju Lin et al. 2010*, three things can occur to the sediments underlying the lake:

1. The lake freezes to the bottom in early winter inducing a MALBT $< 0°C$. No taliks are observed in these conditions.
2. The lake freezes to the bottom at the end of the cold season. In this case, talik can develop but there are few chances that it penetrates permafrost.
3. The ice never reaches the bottom during the year and the talik can keep growing and degrading permafrost.

As a simplification, only the third case will be considered to evaluate the probability P_B. *Zhanju Lin et al. 2016* affirm that 80-85% of the lakes don't freeze to the bottom in winter in the Beiluhe basin due to their field observations. As a consequence, we will consider $P_B = 0.85$.

Event C: $d_i = d_l$

Considering the previous paragraph, the lakes satisfying the condition $d_i = d_l$ are the ones where the ice reaches the bottom in early winter or at the end of the cold season. According to field observations *(Zhanju Lin et al. 2010)*, around 20% of the lakes meet these criteria. As a consequence, we attribute $P_C = 0.2$.

Event D: $\dfrac{FDD_{lb}}{TDD_{lb}} \leq \dfrac{\lambda_t}{\lambda_f}$

As already mentioned, it is already hard to collect data on lake bottom temperature during a long time series. Consequently, it would be even more difficult to evaluate event D failure as it requires to have long time series of lake bottom temperature for many lakes as well as the thermal conductivity of lake bottom sediments in frozen and thawed state for each lake.

However, let's consider the following assumption. We know that the ratio $\dfrac{FDD_{lb}}{TDD_{lb}}$ is changing over time due to global warming. However, its change can be considered as small enough to consider this fraction as constant.
To determine its value quantitatively, the following approximation will be made:

$$\frac{FDD_{lb}}{TDD_{lb}} \approx \frac{t_{Freezing}}{t_{Non-Freezing}}$$

where $t_{Freezing}$ and $t_{Non-Freezing}$ represent respectively the freezing period of the lake water and the non-freezing period (ice-melting period + period preceding next freezing period). This constitutes the best approximation that can be made without having long time series temperatures data of lake bottom of several lakes. According to *ZJ Lin et al. 2017*, the total freezing period lasts 130 days inducing thus a non-freezing period of $365 - 130 = 235$ days. As a consequence, we obtain:

$$\frac{FDD_{lb}}{TDD_{lb}} \approx \frac{130}{235} = 0.5532$$

To obtain a rough estimation of P_D, the ratio $\frac{\lambda_t}{\lambda_f}$ will be calculated from all articles containing specific information about thermal conductivities of lake-bottom sediments and compared with 0.5532 value. Few articles mention this specific lake's information in permafrost conditions. However, from all the read articles about this specific field of studies, five of them mention numerical values of lake-bottom thermal conductivities and are visible in TABLE 3.1.

Articles	Types of sediments	λ_t	λ_f	$\frac{\lambda_t}{\lambda_f}$	> 0.5532 ?
Ling et al., 2019	Silty clay	1.18	2.28	0.5175	NO
Ling et al., 2012	Peaty Clay and Sand	1.36	2.12	0.6415	YES
Roy-Leveillee et al., 2017	Silty sand	1.12	2.2	0.5091	NO
J. C. Rowland et al., 2011	Silty sand	1.12	2.37	0.4726	NO
Zhi Wen et al., 2018	Silty clay	1.5	1.8	0.8333	YES

Table 3.1: Thermal conductivities of lake-bottom sediments mentioned by different articles

From this table, it can be seen that two articles from the five show a ratio $\frac{\lambda_t}{\lambda_f} > 0.5532$. Consequently, it will be considered that $P_D = 0.4$. Naturally, this constitutes an extremely rough estimation since this is based on only 5 articles. To be statistically representative, the ideal case would be to have values of conductivities of all lakes in Beiluhe Basin which is unfortunately not the case. However, the probability to have shallow lakes conditions being really low, a change in P_D would not have such a significant influence in the overall failure probability P_T. That will be shown in the next section related to importance measures.

Note: in *Rowland et al. 2011* article, only λ_f was mentioned so it has been decided to consider λ_t being the same as the value referred by *Roy-Leveillee et al. 2017* as the sediments constituting lake-bottom are the same.

Overall Top Event failure probability:

To sum up, the following probabilities will be considered:

- $P_A = 0.925$.
- $P_B = 0.85$.
- $P_C = 0.2$.
- $P_D = 0.4$.

Considering the equation (3.2), the probability that talik generates under a thermokarst lake in Beiluhe Basin is estimated by:

$$P_T = 0.925 \cdot 0.85 + 0.925 \cdot 0.2 \cdot 0.4 - 2 \cdot 0.925 \cdot 0.85 \cdot 0.2 \cdot 0.4 = 73.445\% \qquad (3.3)$$

Several comments can be made regarding this value.
First of all, knowing that talik development is an undesired event, such a high probability value is naturally unwanted. However, unlike electronic systems for example where it is possible to decrease the overall system failure by improving the reliability of specific components, it is impossible to change probabilities related to lake-bottom temperature or lake ice thickness due to the fact that these components of this system are not controlled by humans.
Secondly, we are fully aware that this value is a rough estimation of the real probability that taliks develop. However, this estimation is still useful to emphasize the impact of climate change on permafrost degradation phenomena. One better way to estimate this Top Event failure probability would be to use Monte Carlo Simulations. However, this analysis method requires to know the probability distribution of all random variables constituting our problem (T_{lb}, d_i, d_l, $\frac{\lambda_t}{\lambda_f}$), which is unfortunately not the case.

3.3.4.4 Importance measures

The exactly same methodology than in section 3.2.4.3 will be applied to quantify which factor is the most important regarding the generation of taliks under thermokarst lakes.

Birnbaum's importance measure

Firstly, Birnbaum's importance measure (BM) will be calculated based on the equation (3.2):

$$\begin{aligned} RA(A) &= P_T(P_A = 1) - P_T = 0.794 - 0.734 = 0.06 \\ RR(A) &= P_T - P_T(P_A = 0) = 0.734 - 0 = 0.734 \\ BM(A) &= RA(A) + RR(A) = 0.06 + 0.734 = 0.794 \\ \frac{\partial P_T}{\partial P_A} &= P_B + P_C \cdot P_D - 2 \cdot P_B \cdot P_C \cdot P_D = 0.794 \end{aligned}$$

$$\begin{aligned} RA(B) &= P_T(P_B = 1) - P_T = 0.851 - 0.734 = 0.117 \\ RR(B) &= P_T - P_T(P_B = 0) = 0.734 - 0.074 = 0.660 \\ BM(B) &= RA(B) + RR(B) = 0.117 + 0.660 = 0.777 \\ \frac{\partial P_T}{\partial P_B} &= P_A - 2 \cdot P_A \cdot P_C \cdot P_D = 0.777 \end{aligned}$$

$$
\begin{aligned}
RA(C) &= P_T(P_C = 1) - P_T = 0.527 - 0.734 = -0.207 \\
RR(C) &= P_T - P_T(P_C = 0) = 0.734 - 0.786 = -0.052 \\
BM(C) &= RA(C) + RR(C) = -0.207 - 0.052 = -0.259 \\
\frac{\partial P_T}{\partial P_C} &= P_A \cdot P_D - 2 \cdot P_A \cdot P_B \cdot P_D = -0.259
\end{aligned}
$$

$$
\begin{aligned}
RA(D) &= P_T(P_D = 1) - P_T = 0.657 - 0.734 = -0.077 \\
RR(D) &= P_T - P_T(P_D = 0) = 0.734 - 0.786 = -0.052 \\
BM(D) &= RA(D) + RR(D) = -0.129 \\
\frac{\partial P_T}{\partial P_D} &= P_A \cdot P_C - 2 \cdot P_A \cdot P_B \cdot P_C = -0.129
\end{aligned}
$$

From all Birnbaum's importance measures, the one translating the greatest importance is BM(A) = 0.794. Indeed, one necessary condition to observe talik development is to have a temperature greater than $0°C$. Without the achievement of this event, top event occurrence is not observed. However, it can be seen that event B, meaning the ice depth lower than the total lake depth has also great importance due to its great value of BM $(= 0.777)$.
Also, the events C and D are of lower importance due to their respective negative Birnbaum's importance measures. Consequently, this means that an error in the estimation of P_C and P_D would not affect so much the overall system failure P_T.

Fussel-Vesely (F-V)

Furthermore, let's compute Fussel-Vesely importance measures based on the following cut-sets probabilities:

- $P(\{A, B\}) = P_A \cdot P_B = 0.925 \cdot 0.85 = 0.78625$
- $P(\{A, C, D\}) = P_A \cdot P_C \cdot P_D = 0.074$

From these values, Fussel-Vesely coefficients are calculated for each basic event:

$$
\begin{aligned}
FV(A) &= \frac{1 - \big(1 - P(\{A, B\}\big) \cdot \big(1 - P(\{A, C, D\}\big)}{P_T} = 1.092 \\
FV(B) &= \frac{1 - \big(1 - P(\{A, B\}\big)}{P_T} = 1.071 \\
FV(C) &= FV(D)\frac{1 - \big(1 - P(\{A, C, D\}\big)}{P_T} = 1.008
\end{aligned}
$$

So the same conclusion emerges from these calculations: the event A constitutes the event having the most influence on Top event failure probability.

3.4 Conclusion

Through this chapter, we understand how important it is to focus our attention on the permafrost environment. Indeed, its degradation has significant consequences on our environment and it is therefore essential to study in detail the factors leading to this ecological disaster.
The first part of this chapter aimed to understand the concept behind the environments characterized by permafrost. We have understood that permafrost covers a significant part of the Earth's surface (excluding seas and oceans) where people can live. It is therefore fundamental to study the aspects linked to environmental concerns in this geographical part of the globe. Among these issues, the most recurrent are related to the thawing of permafrost causing thermokarst.
The first environmental problem studied was the generation of thermokarst lakes. These lakes are extremely unwanted in the sense that they constitute sources of heat that degrade consequently the permafrost in the surroundings. FTA was therefore used to firstly identify the factors driving the generation of these lakes and secondly, to highlight the relationship between these events that lead to this environmental problem. Then the application of the quantitative methods explained in the previous chapter was carried out, although we do not have data. This was done to show on the one hand how to apply these methods in practice and on the other hand, to prove that the FTA applies just as well to environmental problems as in other fields (electronics, nuclear, ...).
Finally, a more specific environmental issue still related to thermokarst lakes has been studied: the generation of taliks beneath them. This constitutes a major environmental concern in the sense that permafrost beneath thermokarst lakes contain methane that can be released following its thawing. Consequently, FTA techniques have been applied once again but with data. Although the estimates made are very imprecise, they show that the probability of these environmental problems occurring is very high. This is even worst when we realize that it is impossible to improve the reliabilities of the components of the fault tree due to the fact they are not human controlled.
The use of Fault Tree Analysis in the permafrost environment is a good way to prove quantitatively the impact of climate change and to urge the great powers to make a change in the current system in which we are living.

Chapter 4

Monte Carlo Simulations applied to seawater intrusion

Another very widespread environmental issue concerns seawater intrusion in coastal areas. These problems already occur naturally due to the difference in density between salt- and freshwater. Indeed, saltwater which is of higher density tends to infiltrate coastal aquifers and push freshwater inland. This leads in coastal aquifers to the existence of two distinct zones: one which contains only freshwater and the other containing both fresh- and saltwater, both separated by an interface called mixing or transition zone.
However, this particular issue is worsened by anthropogenic activities that trigger the extension of saltwater encroachment into the coastal areas. Indeed, the overexploitation of freshwater in coastal aquifers, the rising of sea-level induced by climate change, the diminution of the recharge, and so on provoke a movement of the saltwater wedge inland. The problem is that if the saltwater wedge intrudes too far, it can induce irreversible consequences such as the contamination of pumping wells, the degradation of the vegetation, and so on.

This chapter aims to describe first of all more into detail the problem of saltwater intrusion in coastal areas. Then, the second part of the chapter will be the application of Monte Carlo to saltwater intrusion after describing analytically the mathematical equations governing this physical phenomenon.

4.1 Saltwater intrusion

4.1.1 Introduction and cause factors

As already explained in the previous chapter, groundwater reserves are of considerable importance and must be managed properly. More particularly, fresh groundwater stored in coastal aquifers is particularly sensitive to deterioration due to its closeness with seawater. Knowing that higher population densities are found in coastal areas (around 70%), it is crucial to exploit coastal aquifer sustainably and optimally manner to control seawater intrusion *(Darnault 2008)*.

To understand better saltwater intrusion phenomena and control the phenomenon, it is necessary to explain the basics of coastal aquifer hydrodynamics to understand the connection between saltwater and freshwater. Indeed, in coastal aquifers, saline ($>$ 3% salt) and brackish ($<$ 3% salt) water can be found. What governs mainly saltwater intrusion are the following factors *(Darnault 2008)*:

- The initial natural saltwater presence.
- The intrinsic characteristics of the aquifer.
- Human activities.
- Tidal effects.
- Freshwater water table fluctuation.

Plenty of coastal aquifers are seriously impacted by saltwater intrusion. As an example, *Barlow and Reichard 2010* presents many instances of saltwater intrusion issues in North America while *Werner 2010* presented an overview of saltwater intrusion and coastal aquifer management in Australia. Furthermore, the Intergovernmental Panel On Climate Change estimates that the global mean sea-level could rise up to 50 *cm*. As a consequence, the process of saltwater intrusion would be accelerated *(Darnault 2008)*.

4.1.2 Hydrodynamics

Due to the work of *Ghijben* in 1888/1889 and of *Herzberg* in 1901, it has been discovered that saltwater manifestation in coastal aquifers occurs at a depth beneath sea-level (denoted by z) which is around 40 times the freshwater level above sea-level (denoted by h_f). Indeed, as already mentioned, coastal aquifers are characterized by the co-existence of 2 liquids with distinct densities which are freshwater and saltwater *(Darnault 2008)*. In equilibrium conditions, the pressure between the 2 liquids are balanced through the following equation :

$$\rho_s \cdot g \cdot z = \rho_f \cdot g \cdot (z + h_f) \tag{4.1}$$

with ρ_f and ρ_s representing respectively the freshwater and saltwater densities and g, the gravitational constant.
From this equation, it is possible to extract the depth of the saltwater interface beneath sea-level z:

$$z = \frac{\rho_f}{\rho_s - \rho_f} \cdot h_f \approx 40 h_f \tag{4.2}$$

In the case of confined aquifers, the water table can be replaced by the piezometric surface.
Equation (4.2) is very well known under the name of $Ghijben - Herzberg$'s principle or $Ghijben - Herzberg$'s assumption. The word "assumption" comes from the fact this equation is valid only if *(Darnault 2008)*:

1. The horizontal freshwater flow is horizontal. So it requires the Dupuits-Forchheimer assumption.

2. There is not a progressive movement of saline water. It considers thus the saltwater interface to be sharp without considering any mixing zone.

Furthermore, this equilibrium condition (4.2) between freshwater and saltwater requires the water table (or piezometric surface) to be above sea-level and with a slope directed towards the sea. Otherwise, saltwater would move inland naturally.
FIGURE 4.1 represents schematically the interface between freshwater and saltwater in equilibrium conditions.

The seawater intrusion (SWI) occurs when this equilibrium is disrupted, inducing a movement of the seawater towards the inland. Several causes are responsible for this disequilibrium initiation as already mentioned in section 4.1.1. However, the most frequent causes are related to overexploitation due to pumping and sea-level rise *(Werner 2017)*.

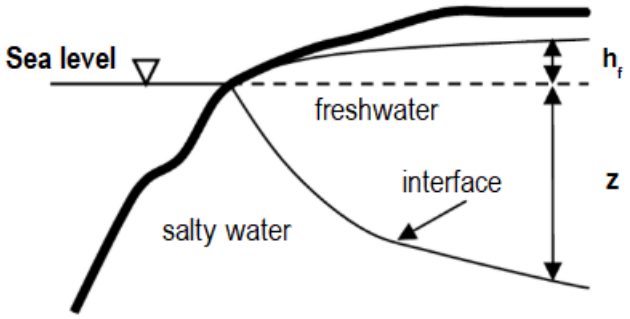

Figure 4.1: Sharp interface representation in a coastal aquifer (modified from *Darnault 2008*)

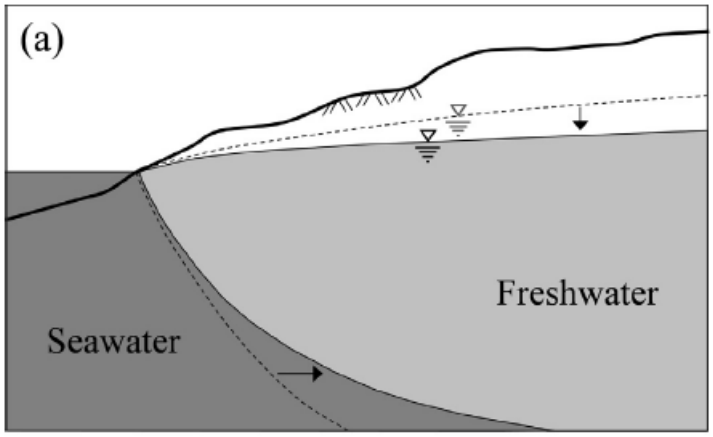

Figure 4.2: passive SWI in an unconfined aquifer (from *Werner 2017*)

4.1.3 Classification

We understood that the seawater intrusion occurs due to equilibrium disturbance. However, SWI can occur through different forms and *Werner 2017* explained in his paper how to make the differentiation between these different cases. Indeed, first of all, a distinction can be made between *passive SWI* and *active SWI*.

4.1.3.1 Passive SWI

This type of intrusion refers to the movement of seawater towards land in regions where fresh groundwater flows in the direction of the sea. FIGURE 4.2 shows schematically how passive SWI occurs in unconfined aquifers.

4.1.3.2 Active SWI

In this case, both freshwater and saltwater move landwards. However, two types of active SWI intrusions can be defined.

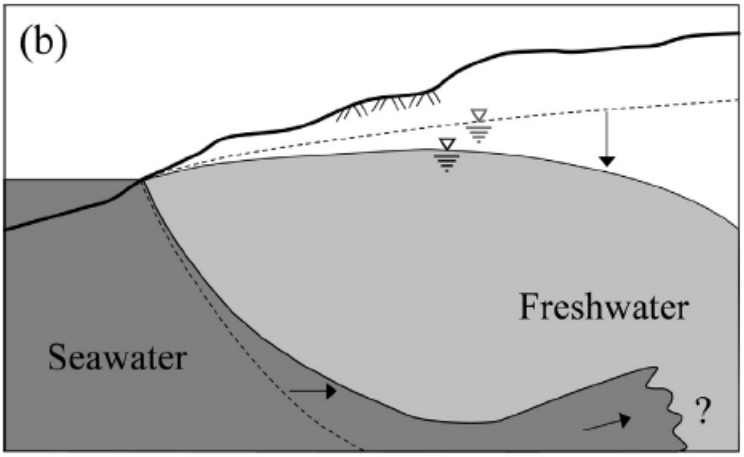

Figure 4.3: passive-active SWI in an unconfined aquifer (from *Werner 2017*)

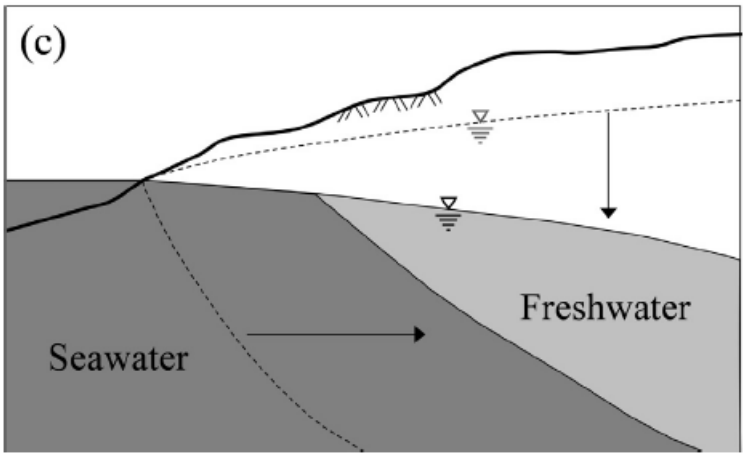

Figure 4.4: active SWI in an unconfined aquifer (from *Werner 2017*)

1) active-passive SWI

When the toe of the saltwater wedge reaches the fresh groundwater table peak, this type of intrusion occurs. In this case, we observe a movement of the freshwater towards the sea from the freshwater mound position to the sea (passive SWI) while both salt- and freshwater move landward in the landward side. For this reason, this type of configuration includes both passive and active intrusion according to the position of the peak of the freshwater water table. It is suggested that this specific type of intrusion occurs in unconfined aquifers.
FIGURE 4.3 represents this type of intrusion in unconfined aquifers.

2) active SWI

This type of intrusion constitutes the worst case as both fresh and saltwater move landwards. This is due to the non-existence of fresh groundwater mound and it is suggested to occur in confined aquifers. There is thus, in this case, cessation of freshwater discharge to the sea. This type of intrusion is illustrated for an unconfined aquifer in FIGURE 4.4.

4.1.3.3 Switching from one class of intrusion to another

Werner 2017 examined which combination of parameters would lead to one class from another. Consequently, by making use of the analytical methods developed by *Strack 1976* and by considering extremely simplified conditions such as "sharp interface" assumption, steady-state conditions, homogeneous aquifers, and so on, he developed a table defining the thresholds which allow predicting which types of intrusions are occurring for unconfined/confined cases considering uniform distributed recharge or not. This table and the associated nomenclature is visible in the annexes C.1.

4.1.4 Consequences

Once the saltwater wedge intrudes too further landwards, it might induce irreversible consequences among which we can cite:

1) Saltwater Up-Coning phenomena:

This denotes the rise of the saltwater interface beneath pumping wells. As a consequence, wells might get contaminated by saltwater. Indeed, this salinization of wells constitutes a widespread issue in plenty of coastal aquifers as it induces a shut down of the extraction wells and thus stops the supply from sources of freshwater for the population living nearby. And indeed, hundreds of wells have been shut down in several countries such as Cyprus, Mexico, Oman, Israel, Australia, and so on *(Felisa, Ciriello, and Di Federico 2013)*.
Jakovovic et al. 2016 studied the saltwater up-coning zone of influence (SUZI). They demonstrate that SUZI depends on well position, the pumping rate, the regional flow, ... which are the parameters governing seawater intrusion.

2) Degradation of coastal vegetation:

More than affecting the pumping wells, saltwater intrusion also has a deep ecological impact on the vegetation and soil quality along coastlines. As an example, that has been around 25 years that the coastal pine forest along the Ravenna coastline in Italy undergoes a lowering of vegetation density, uprooting, drying of pine plants, and modification in the diversity of plant species. These impacts are partly associated with shallow water tables and groundwater salinity which is connected to seawater intrusion.
This particular environmental issue has been studied in a probabilistic framework by *Felisa, Ciriello, and Di Federico 2013* who evaluate the probabilities that the saltwater wedge reaches the sensitive zones of vegetation areas.

3) Increase in the cost of coastal groundwater management: As long as freshwater is extracted in a coastal area, saltwater intrusion would occur for sure with different magnitudes. If the degree of intrusion is such that it implies any environmental risk, it is necessary to consider remediation measures to decrease the level of saltwater intrusion. These measures have an economical cost which is not negligible and constitutes thus another consequence of saltwater intrusion.

4.2 Case study in Cyprus

4.2.1 Description of the area

The coastal aquifer that will be studied is The **Akrotiri aquifer** in Cyprus. It has been decided to consider this unconfined aquifer for two main reasons:

1. First of all, the results regarding the toe position of the saltwater interface are available in the paper of *Koussis et al. 2012* for different parameters combination. As a consequence, the results of this paper have been reproduced to guarantee the reliability of the equations that will be used during Monte Carlo Simulations.

2. Secondly, several papers treated and studied this aquifer, allowing to get its different parameters such as the hydraulic conductivity, the recharge, the inland flow, the pumping rate, and so on.

This aquifer is located in the Akrotiri peninsula in Zakaki area in the south of Cyprus (see FIGURE 4.5). FIGURE 4.6 represents a cross-section of the aquifer, showing its different geometrical features.

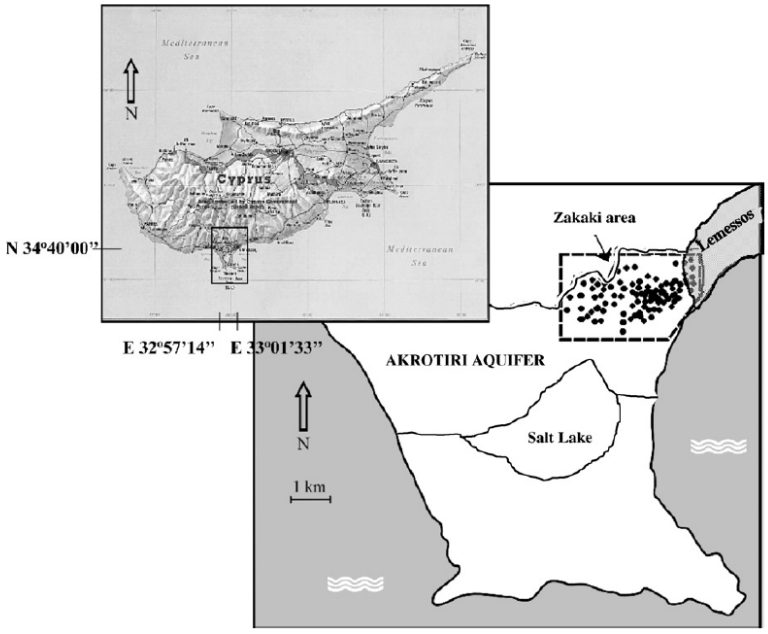

Figure 4.5: Location of Akrotiri aquifer in Cyprus (from *Koussis et al. 2012*)

As can be seen seen, the aquifer is inclined with a slope equal to $\sin\phi = 0.017$ (1 ° slope). The sea-level with respect to the base of the aquifer at the coast is equal to $H_{sea} = 50\ m$. The width of the Zakaki area is considered to be 4000 m (see FIGURE 4.5) while the aquifer inclined length where the recharge occurs is estimated to $L = 3000\ m$. Finally, the wells which are here assumed transformed into 2D-equivalent wells (horizontal well galleries) for not considering the lateral influence of pumping are located at an inclined distance of $l_w = 1000\ m$ from the coast *(Koussis et al. 2012)*.

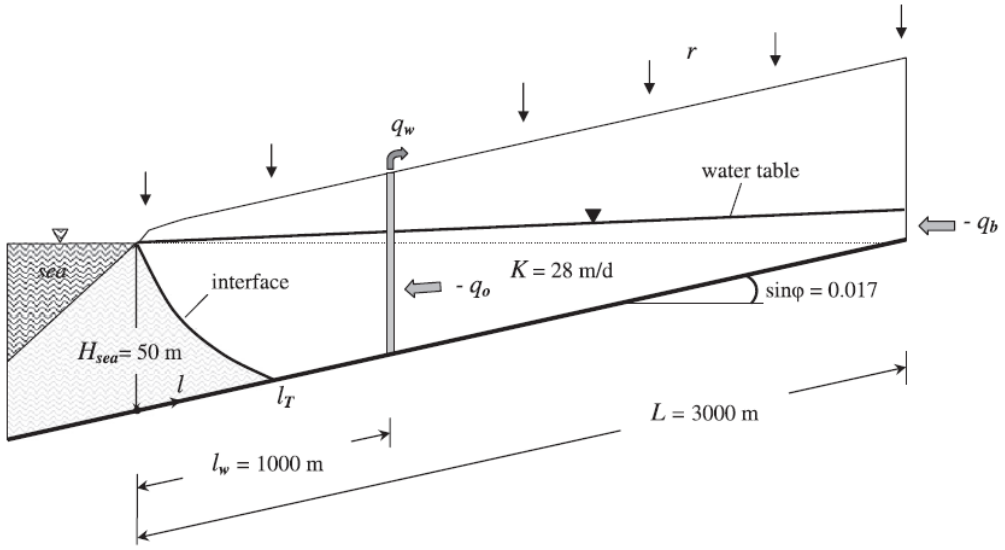

Figure 4.6: Cross section of Akrotiri aquifer (from *Koussis et al. 2012*)

Regarding other parameters, *Mazi et al. 2004* performed a precipitation-runoff model and applied it to the Akrotiri basin. He evaluated through his calibrated model in the period 1972-1992 a recharge of $r = 92\ mm/year$ and an inland boundary inflow per coast width of $q_b = -549\ m^3/m$. The average hydraulic conductivity has been evaluated by field studies and is estimated to be 28 m/day.
Finally, regarding pumping extraction rates, these withdrawal flowrates changed with time. Indeed, pumping was performed to supply the local population, provide water for irrigation purposes, and supply water to the city of Limassol. However, high salinity was observed in the wells ($\approx 1900\ ppm$, equivalent to 0.19%) in 1993. As a consequence, they reduced the extraction rates in 1997 by 25% to prevent a greater deterioration of fresh groundwater quality *(Koussis et al. 2012)*. They moved thus from withdrawals flowrates of $q_w = 2 \cdot 10^6\ m^3/year$ to $q_w = 1.5 \cdot 10^6\ m^3/year$. Transformed into 2D-equivalent wells, we get knowing that the coast width is 4000 m a flowrate $q_w = \dfrac{1.5 \cdot 10^6}{4000} = 375\ m^3/year/m$.

4.2.2 Analytical equation

In a risk an analysis purpose, the unwanted event corresponds here to the saltwater wedge toe reaching the pumping wells. Mathematically, if l_T denotes the inclined distance of the toe from the coast, there is a failure if:

$$l_T \geq l_w \tag{4.3}$$

where $l_w = 1000\ m$ refers to the inclined distance of the wells from the coast.

Many papers treated the analytical formulation of the sharp-interface position for unconfined and confined aquifers, the most known and often taken as a reference being the paper of *Strack 1976* who developed a Single-Potential solution for regional interface problems in coastal aquifers. However, few papers treated the case in which recharge is combined with pumping in coastal areas.

Fortunately, *Koussis et al. 2012* developed sharp-interface solutions related to seawater intrusion in sloping unconfined aquifer with pumping and recharge. As a consequence, the following analytical equations are extracted from this article.

Before considering the next developed equations, it is important to highlight the assumptions behind their analytical development.

1. First of all, sharp-interface theories are based on the Dupuits-Forchheimer's assumption. It means that the unconfined flow is simplified so that streamlines are considered horizontal (vertical components of flow neglected) and equipotential vertical. It is a strong assumption but due to the fact the wells are full-screened (cover the whole aquifer thickness) and that the aquifer is nearly flat (slight inclination), this assumption is considered reasonable. In reality, the separation between freshwater and saltwater is not narrow but more into the shape of a mixing/transition zone with brackish water. However, at a regional scale, it is reasonable to study this transition zone as a narrow sharp-interface.

2. Secondly, the Ghijben-Herzberg assumption and equation which have already been explained in section 4.1.2 will be considered as well.

3. Finally, the methodology used to obtain the saltwater interface equation is based on the one already developed by *Strack 1976*. However, it has been adapted to sloping aquifers to which recharge is applied.

The final equation describing the toe position of the interface is obtained through a step by step development that will be described shortly.

First of all, the groundwater discharge potential Φ (per unit width of the aquifer) equation is obtained based on Darcy's law and on the fact that the relationship between hydraulic head h and the saturated flow ϕ is linear ($h = \alpha\phi + \beta$):

$$\Phi = \frac{1}{2} K \alpha (\phi + \frac{\beta}{\alpha})^2 + const \tag{4.4}$$

Using the equation (4.2) from Ghijben-Herzberg relationship and considering that the aquifer is unconfined ($\alpha = 1$ and $\beta = 0$), the equation (4.4) becomes:

$$\Phi = \frac{1}{2} K \frac{\rho_s}{\rho_s - \rho_f} (\phi - H_{sea})^2 + const \tag{4.5}$$

where H_{sea} represents the sea-level from the base of the aquifer at the coast.
The constant *const* is determined such that Φ remains continuous across the salt- and freshwater boundary, which is the case at the interface's toe position. By doing so, the discharge potential becomes in the interface zone:

$$\Phi = \frac{1}{2} K \frac{\rho_s}{\rho_s - \rho_f} (\phi - H_{sea})^2 + \frac{1}{2} K \frac{\rho_s}{\rho_f} H_{sea}^2 \tag{4.6}$$

for $\phi \leq \frac{\rho_s}{\rho_f} H_{sea}$ (meaning that it is valid only in the interface zone).

The steps up to now were the same as the ones considered by *Strack 1976*. However, *Koussis et al. 2012* adapted the equation (4.6) to an inclined aquifer to which recharge is applied(FIGURE 4.7).

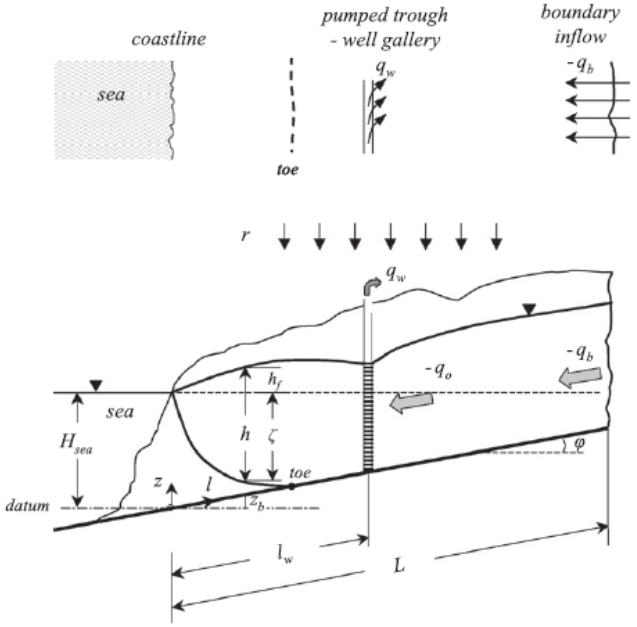

Figure 4.7: Inclined aquifer and nomenclature considered by *Koussis et al. 2012* (from *Koussis et al. 2012*)

If z_b represents the bed elevation above the datum and θ the aquifer angle inclination, one can write $\phi = z_b + h\cos\theta$. The equation (4.6) turns into the following discharge potential equation:

$$\Phi = \frac{1}{2}K\frac{\rho_s}{\rho_s - \rho_f}(\phi - H_{sea})^2 + \frac{1}{2}K\left(2h_0 z_{BT} + \frac{\rho_s}{\rho_f}(H_{sea} - z_{BT})^2\right) \tag{4.7}$$

where K represents the hydraulic conductivity, ρ_s ρ_f the salt- and freshwater densities respectively, ϕ the piezometric head, H_{sea} the sea-level above the datum, z_{BT} the bed elevation above the bottom.

Finally, an analysis of the equation (4.7) is performed by considering a well gallery located at an inclined distance l_w and a recharge r applied on the whole aquifer. One can write the equation governing the flow in the aquifer by substituting Darcy law into volume conservation equation such that:

$$\frac{d^2\Phi(l)}{dl^2} = -r\cos\theta \tag{4.8}$$

where l represents the inclined distance starting from the datum at the coast.

Integrating the equation (4.8) from the coast to the well gallery and from the well gallery to the land boundary yields respectively to:

$$\Phi_{sw}(0 \leq l \leq l_w) = -\frac{r}{2}l^2 + (rl^2 - q_b - q_w)l + \frac{1}{2}K\big(2h_0 z_{BT} + \frac{\rho_s}{\rho_f}(H_{sea} - z_{BT})^2\big) \tag{4.9}$$

$$\Phi_{wb}(l_w \leq l \leq L) = -\frac{r}{2}l^2 + (rl^2 - q_b)l - q_w l_w + \frac{1}{2}K\big(2h_0 z_{BT} + \frac{\rho_s}{\rho_f}(H_{sea} - z_{BT})^2\big) \tag{4.10}$$

where q_b represents the inland inflow and q_w the extraction rate of the wells per unit width of the aquifer. Furthermore, let's consider the inflow immediately upgradient the pumping well gallery q_0 so that the recharge above the withdrawal collector is considered, this later is written $-q_0 = -q_b + r(L - l_w)$ where q_b represents the flow from the land boundary. Equation (4.9) becomes:

$$\Phi_{sw}(0 \leq l \leq l_w) = -\frac{r}{2}l^2 + (rl^2 - q_0 - q_w)l + \frac{1}{2}K\big(2h_0 z_{BT} + \frac{\rho_s}{\rho_f}(H_{sea} - z_{BT})^2\big) \tag{4.11}$$

Finally, the location of the interface toe is obtained by matching equation (4.11) with the discharge potential $\Phi_T = \Phi(l_T)$ where l_T represents the position of the toe. By doing so, the equation governing the toe position is the following with $\delta = \dfrac{\rho_s - \rho_f}{\rho_f}$:

$$\Big(\delta(1+\delta)\sin^2\theta + \frac{r}{K}\Big)l_T^2 - 2\Big(\delta(1+\delta)sin\theta H_{sea} + \frac{rl_w}{K} - \frac{q_0}{K} - \frac{q_w}{K}\Big)l_T + \delta(1+\delta)H_{sea}^2 = 0 \tag{4.12}$$

It corresponds thus to a quadratic equation and the roots are given by $l_T = \dfrac{-b \pm \sqrt{b^2 - 4ac}}{2a}$ where a, b and c represent the coefficients of the quadratic equation. The physically coherent root is the one with $-\sqrt{b^2 - 4ac}$ since the toe position increases with H_{sea}, K, q_w and decreases with r and q_b.

In conclusion, the unwanted event corresponds to the following inequality:

$$\boxed{\frac{-b - \sqrt{b^2 - 4ac}}{2a} \geq l_w} \tag{4.13}$$

with:

$$\begin{aligned} a =& \delta(1+\delta)\sin^2\theta + \frac{r}{K} \\ b =& -2\Big(\delta(1+\delta)sin\theta H_{sea} + \frac{rl_w}{K} - \frac{q_0}{K} - \frac{q_w}{K}\Big) \\ c =& \delta(1+\delta)H_{sea}^2 \end{aligned}$$

Note: in the performed Monte Carlo simulation, the combinations of the parameters might be such that the discriminant $b^2 - 4ac < 0$ leading thus to complex solutions. In such a case, the results are not considered to evaluate the overall failure probability because the solutions are not physically meaningful.

4.2.3 Qualitative Fault Tree

Even if FTA won't be analyzed as deep as in CHAPTER 3, it would be interesting to develop a fault tree to identify more clearly the factors leading to seawater intrusion. Consequently, the following Fault tree as been obtained (FIGURE 4.8).

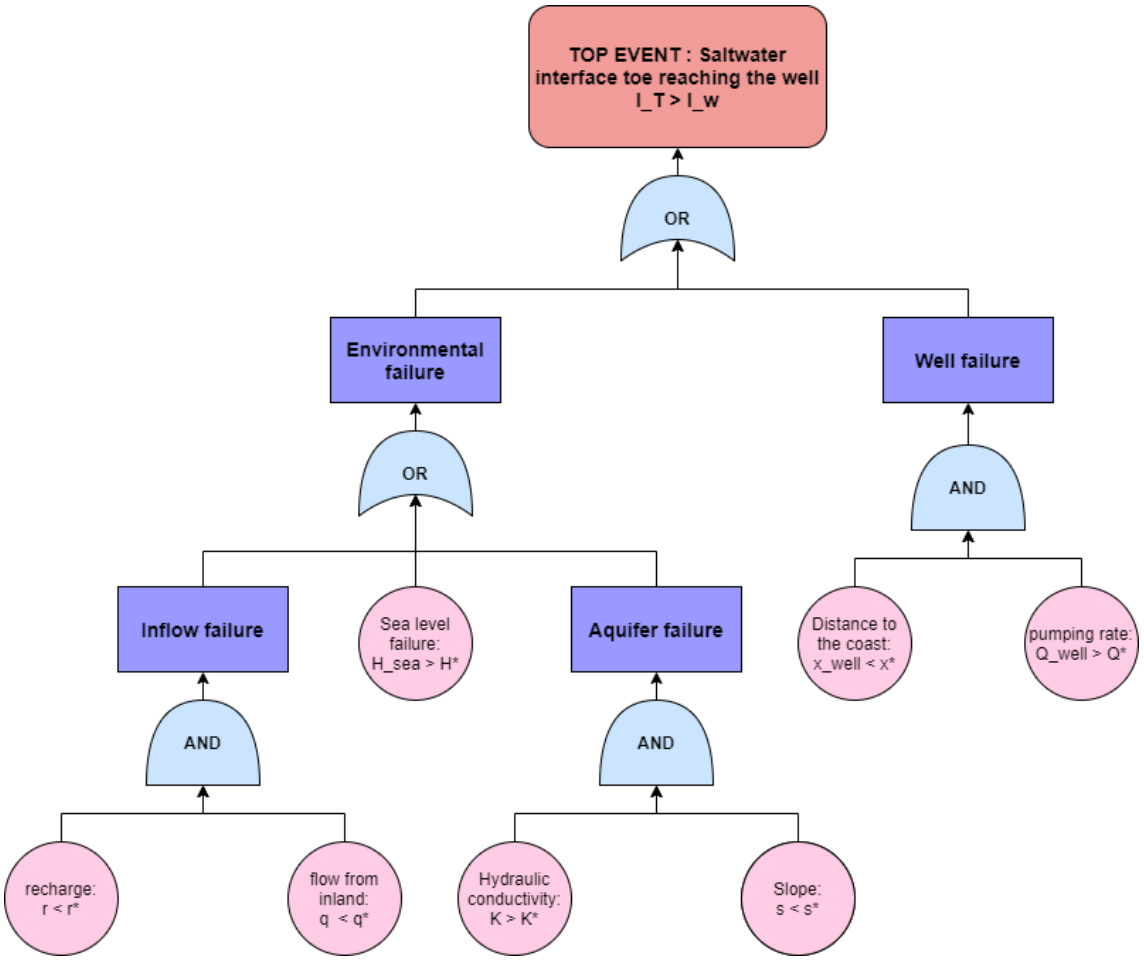

Figure 4.8: Fault Tree related to seawater intrusion reaching pumping wells in a coastal aquifer

The reason why Fault Tree analysis can't be performed is that all parameters constituting the basic events of this tree (K, r, H_{sea}, ...) are all inter-dependant through EQUATION (4.13). This is also why the choice of logic gates is also not perfectly relevant in the sense that there exist plenty of different combinations of all these parameters that could induce $l_T \geq l_w$. As a consequence, it is not possible to define real threshold r^*, q^*, and so on since these laters would be dependant on other parameter values.

However, this fault tree has the advantage to highlight better the cause factors that would promote the top event to occur (saltwater interface's toe reaching the well).

Well failure:

First of all, a failure associated with the well is considered. Indeed, if the well is located too close to the coast ($x_{well} < x^*$), the wells are more prompts to be contaminated due to its closeness with the saltwater interface's toe. Furthermore, pumping water with a high extraction rate ($Q_{well} > Q^*$) would decrease the quantity and pressure of freshwater in the coastal aquifer, inducing a movement of the saltwater interface landwards.

Aquifer failure:

Furthermore, failure related to the intrinsic properties of the aquifer is identified. First of all, It will be shown in the future results that the inclination of the aquifer helps to protect the wells from seawater intrusion. Indeed, a flat aquifer ($s < s^*$) is less protected from seawater intrusion than an inclined aquifer. Furthermore, it is understood through EQUATION (4.13) that great values of hydraulic conductivity ($K > K^*$) would promote the intrusion of the saltwater wedge landwards.

Inflow failure:

Also, one can understand physically that the inflows of freshwater entering the coastal aquifer such as the recharge or the flow from inland are beneficial for its protection by pushing the interface seawards. Consequently, a failure could be observed if the inflows are not sufficient enough ($r < r^*$ and $q_b < q_b^*$).

sea-level failure:

Finally, if the sea-level rises too much in the long-term future ($H_{sea} > H^*$), the greater saltwater pressure-induced would displace the interface landwards, promoting thus contamination of the wells.

4.2.4 Methodology and considered scenarii

The analytical equation (4.13) developed in the section 4.2.2 groups different parameters to which uncertainty might be attached. Consequently, one can distinguish deterministic from probabilistic parameters.

Deterministic parameters: Uncertainty will always be connected to any measurements. However, some measurements are more reliable than others because they are not affected by too many external factors. This is especially the case for geometrical measurements or for parameters set by men in a system. As a consequence, the following parameters are considered deterministic:

- The fresh- and saltwater densities denoted both by ρ_f and ρ_s respectively. As a consequence, the parameter $\delta = \dfrac{\rho_s - \rho_f}{\rho_f}$ is considered deterministic and fixed.
- The aquifer inclination $\sin\theta$ is considered to be well known as well.
- The land boundary position from the coast: L.
- The well position from the coast: l_w.
- The sea-level from the datum at the coast: H_{sea}.
- The pumping rate set by the workers: q_w.

Probabilistic parameters: On the other hand, some parameters are less well known than the deterministic ones mentioned previously. In particular, 3 parameters will be considered as random variables with an associated probabilistic distribution:

- The hydraulic conductivity K: when a deterministic groundwater situation is studied, the value of K refers to an average value in the aquifer. However, the reality is such that the hydraulic conductivity is space-dependant. The variability of K depends thus on the intrinsic heterogeneity of the studied aquifer. Furthermore, hydraulic conductivity can't be negative. As a consequence, it has been decided to consider that K follows a Log-normal probabilistic distribution (*Prieto, Kotronarou, and Destouni 2006*; *Dagan et al. 2003*). This latter will be obtained by transforming the Normal distribution into its equivalent log-normal.
- The recharge r and the inland flow q_b: while K varies with space, the recharge r and the inland flow q_b are time-dependant. Indeed, the deterministic values considered for the study are obtained by averaging the annual recharge and the annual inland flow over a period of time (1972-1992). Consequently, there is uncertainty related to time. Furthermore, it has been decided to associate to r and q_b a Normal distribution (*Prieto, Kotronarou, and Destouni 2006*).
- The sea-level from the datum at the coast H_{sea}: in a long-term perspective the sea-level will rise over time due to climate change impact according to IPCC (Intergovernmental Panel on Climate Change). However, there is uncertainty regarding the magnitude of this rise, which makes us decide to associate a uniform distribution for H_{sea} ranging from the most optimistic to the most pessimistic scenario.

Because of the uncertainty attached to these parameters, it has been decided to apply Monte Carlo simulation methods to evaluate the probability that the inequation (4.13) is true, meaning the probability that the toe of the saltwater interface reaches the well.
To do so, the following Monte Carlo methodology will be applied:

1. Step 1 : Decide the number of simulations that will be performed. It has been decided to choose a large value $N_{sim} = 20000$ for more accuracy.

2. Step 2 : For each simulation, values of random variables K, r, q_b and H_{sea} are extracted from the probabilistic distributions associated with each probabilistic parameters.

3. Step 3: Knowing all the parameters, the toe position l_t is calculated for each simulation and is compared with the position of the well $l_w = 1000$. If $l_t \geq l_W$, the number of failures N_{fail} initiated to 0 before running the simulations is incremented by 1.

4. Step 4: Once the simulations are over, the probability that the toe of the saltwater interface reaches the wells is obtained by: $P_{failure} = \dfrac{N_{fail}}{N_{simul} - N_{compl}}$ where N_{compl} represents the number of complex solutions identified.

To perform a relevant study, different scenarii will be considered to identify the influence of each parameter on the toe position while being compared with a reference. For each scenario, the same parameters than for the reference will be considered but with a modification applied to one (or more) parameters. The following scenarii are considered.

Reference scenario:

As already mentioned in section 4.2.1, some deterministic parameters such as geometrical ones or the pumping extraction rates are already known. They correspond to:

- the saltwater and freshwater densities denoted both respectively by: $\rho_s = 1024$ and $\rho_w = 998\ kg/m^3$ such that $\delta = \dfrac{\rho_s - \rho_f}{\rho_f} = 0.0261$.
- $L = 3000\ m$ and $l_w = 1000\ m$.
- $H_{sea} = 50\ m$.
- $\sin\theta = 0.017$
- $q_w = 375\ m^3/year/m$.

Furthermore, the parameters K, q_b, and r are considered as random variables and have already been treated by *Prieto, Kotronarou, and Destouni 2006* who studied in their papers the influence of temporal hydrological randomness on seawater intrusion in coastal aquifers by considering the case study in Cyprus (and 2 other ones in Israel and on the island of Rhodes in Greece).

First of all, a log-normal distribution will be attributed to the parameter K as already mentioned previously. The log-normal law is defined by:

$$f(x;\mu',\sigma') = \frac{1}{x\sigma'\sqrt{2\pi}} \exp -\frac{(\ln x - \mu')^2}{2\sigma'^2} \tag{4.14}$$

If the mean μ and the variance σ^2 of K following a normal law is known, the parameters μ' and σ' according to MATLAB HELP can be obtained through:

$$\mu' = \ln \frac{\mu^2}{\sqrt{\sigma^2+\mu^2}} \tag{4.15}$$

$$\sigma' = \sqrt{\ln \frac{\sigma^2}{\mu^2+1}} \tag{4.16}$$

For the reference scenario, a small level of heterogeneity will be considered by assigning a coefficient of variation $CV = 0.5$ such that:

$$\begin{aligned}\mu_K &= 28 \cdot 365 = 10220 \ \ m/year \\ \sigma_K &= 0.5 \cdot \mu_K = 5110 \ \ m/year\end{aligned}$$

Secondly, a normal distribution has been attributed to the parameter r with $CV = 0.3$ such that:

$$\begin{aligned}\mu_r &= 92/1000 = 0.092 \ \ m/year \\ \sigma_r &= 0.3 \cdot \mu_r = 0.0276 \ \ m/year\end{aligned}$$

Finally, a normal distribution has also been attributed to the parameter q_b but with the same coefficient of variation than for the recharge $CV = 0.3$ such that:

$$\begin{aligned}\mu_{q_b} &= 549 \ \ m^3/year/m \\ \sigma_{q_b} &= 0.3 \cdot \mu_K = 164.7 \ \ m^3/year/m\end{aligned}$$

FIGURE 4.9 shows the typical distribution of K, r, and q_b after running all the simulations, highlighting the log-normal distribution for K and the normal distribution for r and q_b.

Scenario 1: flat aquifer

The first scenario that will be considered would be to consider the aquifer as flat such that $\sin\theta = 0$. This would not happen in reality but it would allow understanding if flat aquifers are more or less prompt to seawater intrusion.

Scenario 2: high pumping rate

The second scenario aims to highlight the effect of the pumping flowrate's magnitude on seawater intrusion. To do so, the previous extraction rate before 1997 of 500 $m^3/year/m$ will be considered.

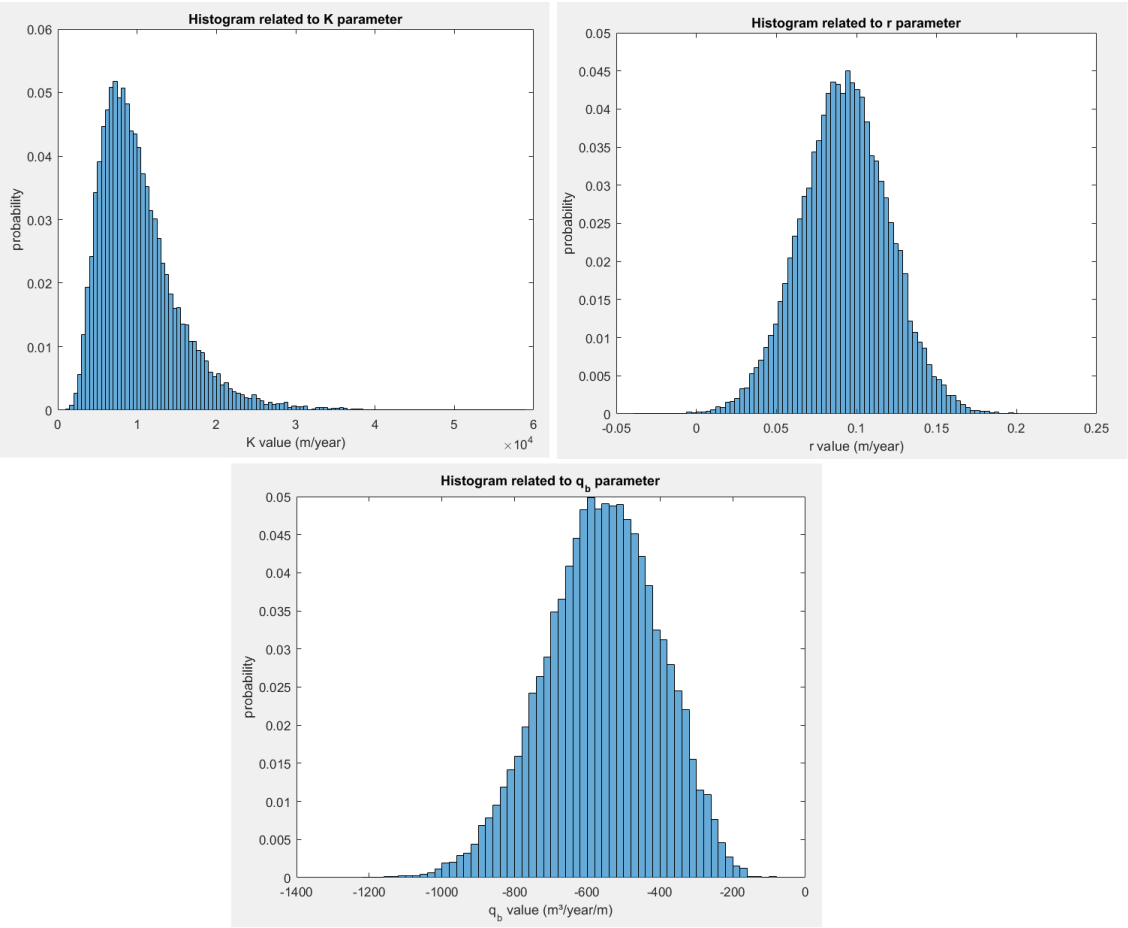

Figure 4.9: Probabilistic distributions of parameters K, r and q_b

Scenario 3: dry and wet weather

This third scenario aims to show the effect of the rainfall on seawater intrusion. To do so, two sub scenarii are considered: dry weather scenario and wet weather scenario. For the dry weather scenario, a mean recharge of 75 $mm/year$ is considered. For the wet weather, a mean recharge of 120 $mm/year$ is taken.

Scenario 4: low- and high-level of heterogeneity

The fourth scenario aims to study the impact of heterogeneity's level of the aquifer. To do so, coefficients of variation $CV_{K_{low}} = 0.1$ and $CV_{K_{high}} = 0.9$ are used to represent respectively low- and high-level heterogeneity inside the aquifer.

Scenario 5: sea-level rise

The fifth scenario consists in evaluating the effect of the sea-level rise in the long-term period. Indeed, The Intergovernmental Panel on Climate Change (*Oppenheimer et al. 2019*) published their last report last year and evaluated the sea-level rise in the following decades. This future rise of global mean sea-level is induced by the melting of glaciers, ice sheets, and land water storage changes due to global climate change. However, there are uncertainties regarding the magnitude of the global mean sea-level rise. According to their most optimistic and pessimistic scenario (RCP2.6 and RCP8.5 respectively), the rise of the global mean sea would range between 0.43 and 0.84 m (FIGURE 4.10) in 2100. As can be understood, the sea-level rise is not spatially heterogeneous and can vary at regional scale. However, APPENDIX C.2 shows that in the Adriatic sea, the rise seems to follow the global sea-level rise. Consequently, it has been decided to attribute a uniform distribution for H_{sea} varying between 50.43 and 50.84 m to observe the effect of sea-level rise by 2100.

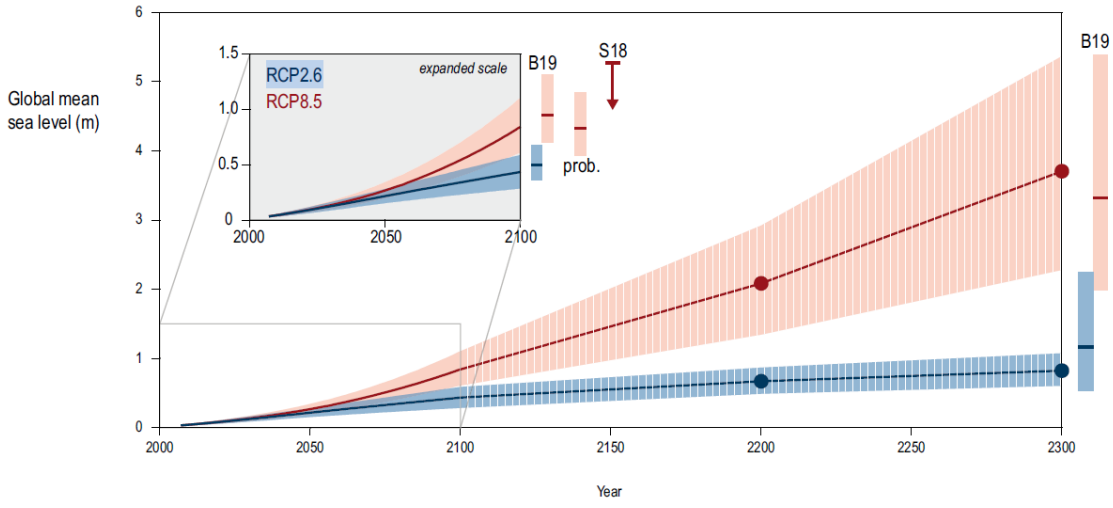

Figure 4.10: Projected sea-level rise until 2300 (from *Oppenheimer et al. 2019*)

Scenario 6: climate change scenario

This scenario aims to study roughly the impact on climate change on seawater intrusion. As already explained in scenario 5, IPCC already mentioned the effect of climate change on sea-level rise. However, another negative aspect of climate change is the diminution of recharge and groundwater flows in the coming decades, which is especially more highlighted in the southern part of Europe such as in Cyprus. Consequently, the same uniform distribution of H_{sea} than for scenario 5 will be attributed. Added to this is a reduction of the mean values of r and q_b which correspond respectively to $\mu_r = 0.075\ m/year$ and $\mu_{q_b} = 314\ m^3/year/m$ (both coefficients of variation related to r and q_b remaining equal to 0.3).

4.2.5 Results and discussions

The results will be presented as followed: for each scenario, a histogram of the results (position of the toe for each simulation excluding complex solutions) will be compared with the reference scenario in terms of displacement of the histogram and in terms of overall failure probability. Furthermore, a log-normal fit will be applied to the histogram of the results. Finally, a summary of the different statistical parameters and the probability of failures will be presented in a table. The red dashed line represents the position of the well ($l_w = 1000\ m$).

Note: for scenarii 3 and 4, both sub-scenarii will be compared in the same FIGURE. As a consequence, histograms won't be represented graphically for the sake of visibility and clarity.

4.2.5.1 Reference scenario

First of all, the reference scenario introduced in SECTION 4.2.4 will be analyzed. FIGURE 4.11 represents the histogram related to the interface toe position's results of the reference scenario with a log-normal fit over the histogram (blue line). Theoretically, if we had an infinite number of results, the probabilistic distribution function $f_{l_T}(x)$ would be known and the probability of failure would correspond to:

$$P_{failure} = \int_{l_w=1000}^{+\infty} f_{l_T}(x)dx \tag{4.17}$$

This corresponds to the area between the horizontal axis and the log-normal fit (the blue curve) after the position of the well (red dashed line).
However, as mentioned earlier, the number of results is discrete and the probability of failure is thus given by $P_{failure} = \dfrac{N_{fail}}{N_{simul} - N_{compl}}$.

The histogram informs us that most of the results are positive, meaning that the toe position is lower than 1000 m, the position of the well gallery. However, some results are located at a distance greater than l_w and a probability of failure $P_{failure} = 7.04\%$ is obtained. The histogram takes a log-normal shape since the parameter K influencing the toe position is also following a log-normal distribution.

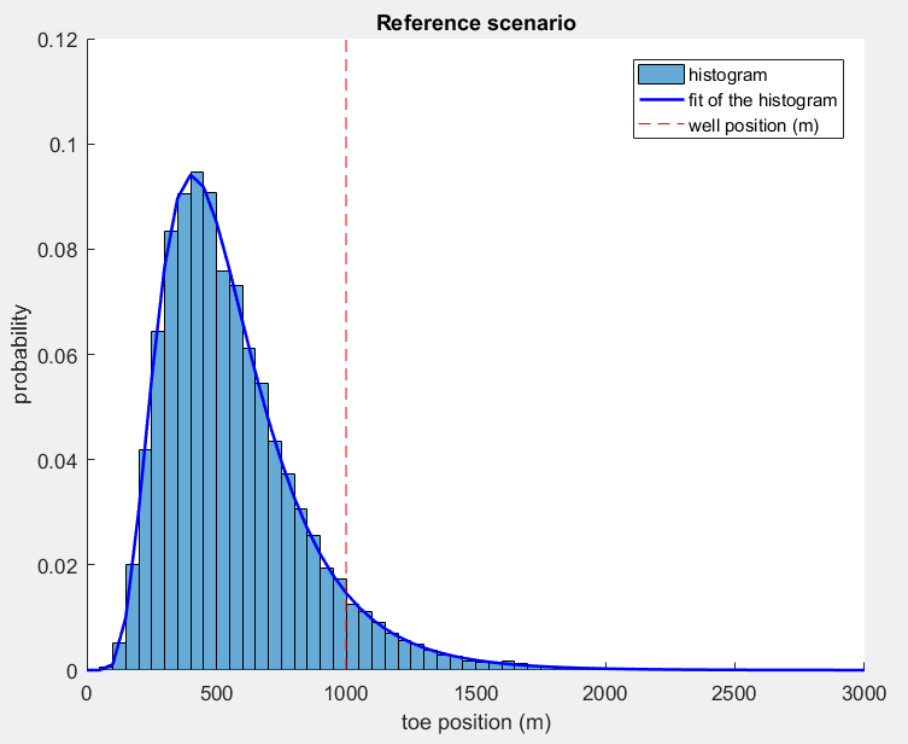

Figure 4.11: Reference scenario

4.2.5.2 Scenario 1: flat aquifer

One can wonder if a flat aquifer would be less or more protected than an inclined one. This corresponds to scenario 1 in which the slope $\sin\theta$ of the aquifer is imposed to 0. The results of such a change are visible in FIGURE 4.12. As can be seen, a much higher probability of failure ($P_{failure} = 28.4\%$) is observed for flat aquifers due to a greater area below the fitted log-normal curve after $l_w = 1000\ m$. As a consequence, inclined aquifers are thus better protected to saltwater intrusion as it was already noticed by *Koussis et al. 2012*. However, the slope is not a parameter that would vary in a human time scale so this parameter would not change for this Cyprus aquifer.

4.2.5.3 Scenario 2: high pumping rates

Then, scenario 2 aims to visualize the change of failure probability when considering the same pumping rates than before 1997 ($Q_{well} = 500\ m^3/year/m$). It can be seen in FIGURE 4.13 that an increase in the extraction rate would induce an increase in failure probability due to a greater number of results superior to $l_w = 1000\ m$. We have thus a failure of probability $P_{failure} = 16.1\%$ which is greater than the one observed in the reference scenario. That makes sense physically in the sense that a greater pumping rate would induce a reduction of pressure in the freshwater zone, allowing thus the saltwater wedge to penetrate more easily landward.

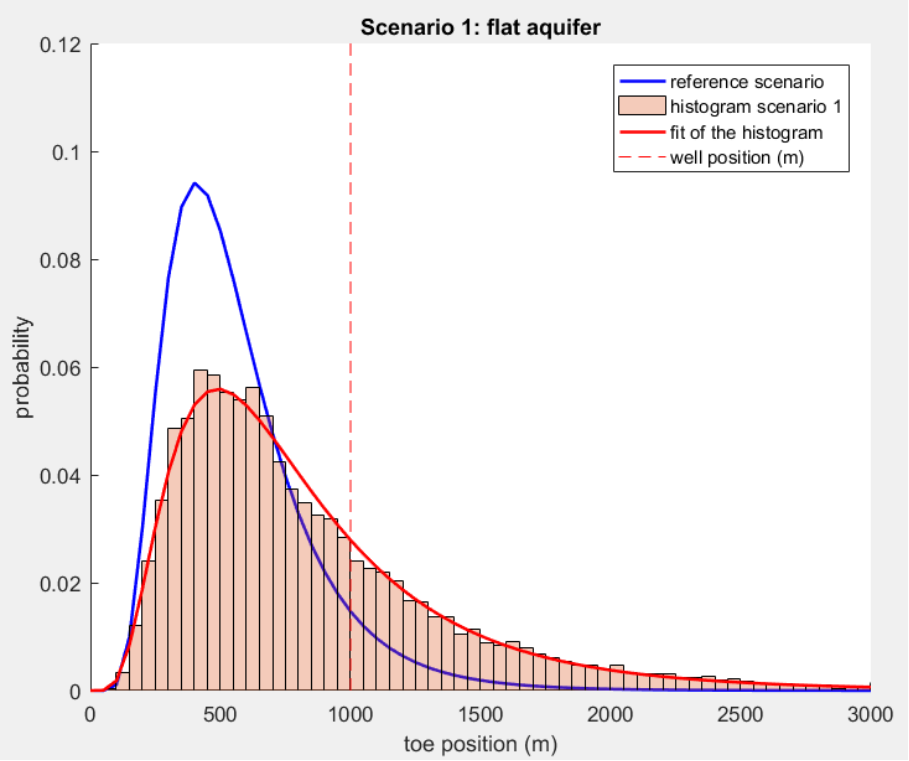

Figure 4.12: Scenario 1 compared to reference scenario

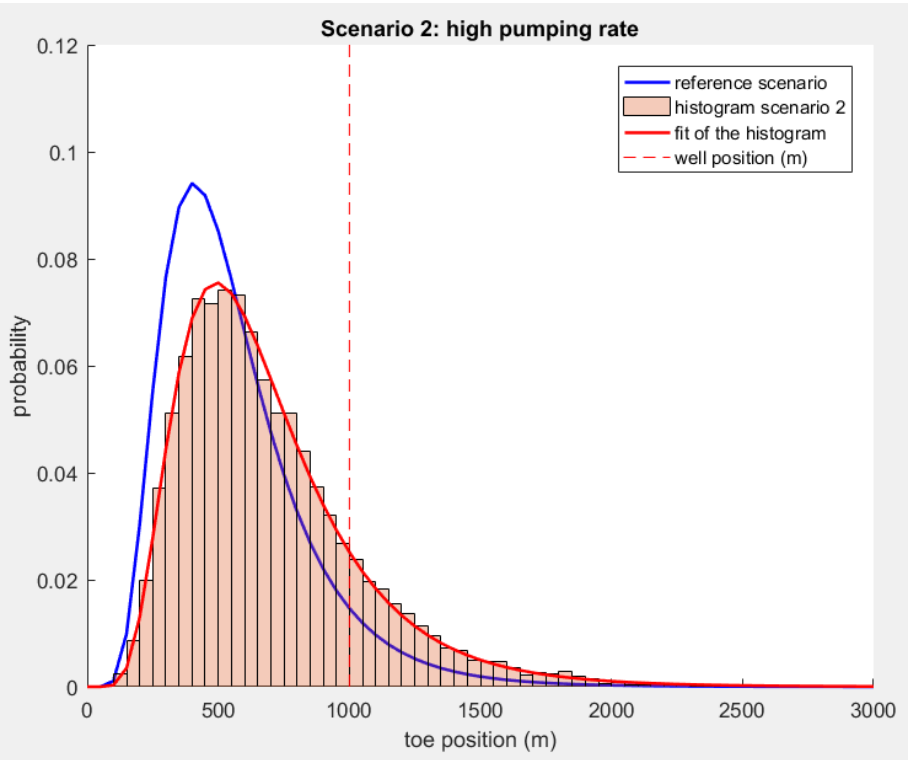

Figure 4.13: Scenario 2 compared to the reference scenario

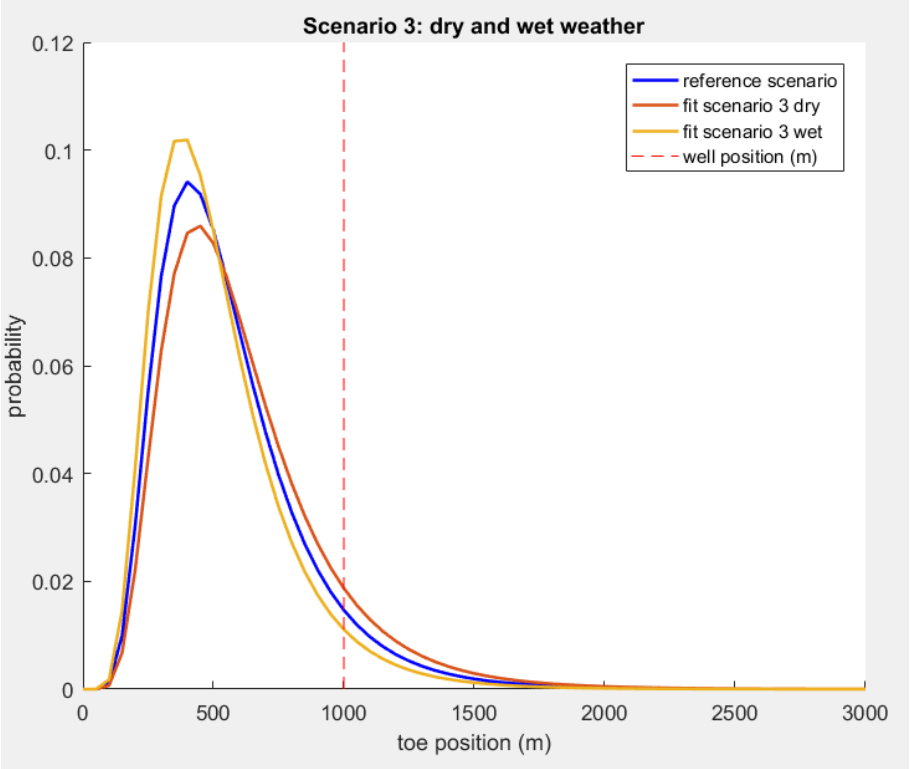

Figure 4.14: Scenario 3 compared to the reference scenario

4.2.5.4 Scenario 3: dry and wet weathers

Scenario 3 aims to study what would be the impact on saltwater wedge displacement when the recharge varies. Two sub-scenarii have thus been considered representing respectively a dry ($r = 75\ mm/year$) and a wet weather ($r = 120\ mm/year$). FIGURE 4.14 shows the influence of the recharge variation with respect to the reference scenario. As expected, dry weather would induce a greater probability of failure ($P_{failure} = 10.14\ \%$) due to the fact there would be less inflow into the aquifer that could "push" the saltwater wedge, which is in coherence with the previously built Fault tree. On the other side, an increase in recharge induced by wet weather would increase the aquifer inflow, "push" the saltwater wedge and reduce consequently the probability of failure ($P_{failure} = 4.67\ \%$).

4.2.5.5 Scenario 4: low and high levels of heterogeneity

This scenario aims to see how would the probability of failure varies if the aquifer is more or less heterogeneous. FIGURE 4.15 indicates the change of the toe position results when considering a lower and higher coefficient of variation associated with the hydraulic conductivity (low and high heterogeneity respectively). A shift to the left is observed for the yellow curve when considering a higher level of heterogeneity but with a greater associated failure probability ($P_{failure} = 9.43\ \%$). On the other hand, a shift to the right is observed for the red curve when considering a lower level of heterogeneity but with a lower associated failure probability ($P_{failure} = 5.04\ \%$). Furthermore, it can be seen that this latter is less widespread than when considering a highly heterogeneous aquifer due to its lower coefficient of variation.

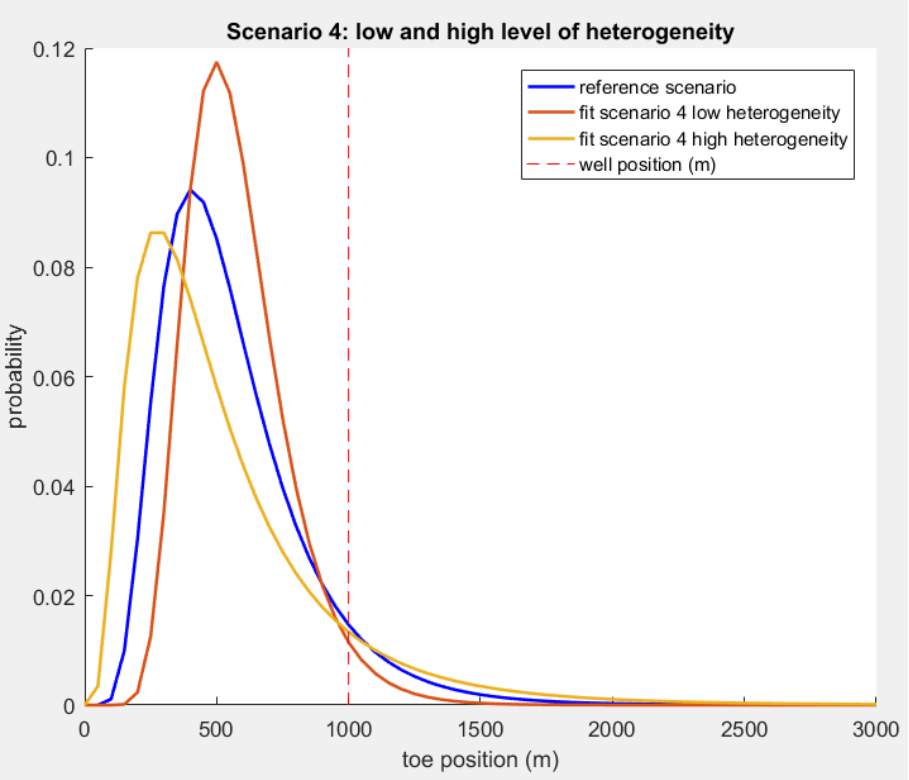

Figure 4.15: Scenario 4 compared to the reference scenario

The higher probability of failure observed when considering a greater level of heterogeneity is explained by the fact that if a higher coefficient of variation is considered, there is a higher probability to observe great values of K, promoting thus the displacement of saltwater wedge inland.

4.2.5.6 Scenario 5: sea-level rise

Scenario 5 consists in evaluating the change in failure probability when the sea-level rises in the next decades. FIGURE 4.16 shows that an increase in sea-level would slightly increase the probability of failure ($P_{failure} = 7.66$ %). This increase is explained by the fact that a greater sea-level would induce a greater pressure of the saltwater that would displace the saltwater interface further inland. Even if this increase in failure probability might not seem significant, if the sea-level rise is combined with other unwanted scenarii (decrease of recharge, greater pumping rate, and so on), it would contribute to the saltwater intrusion.

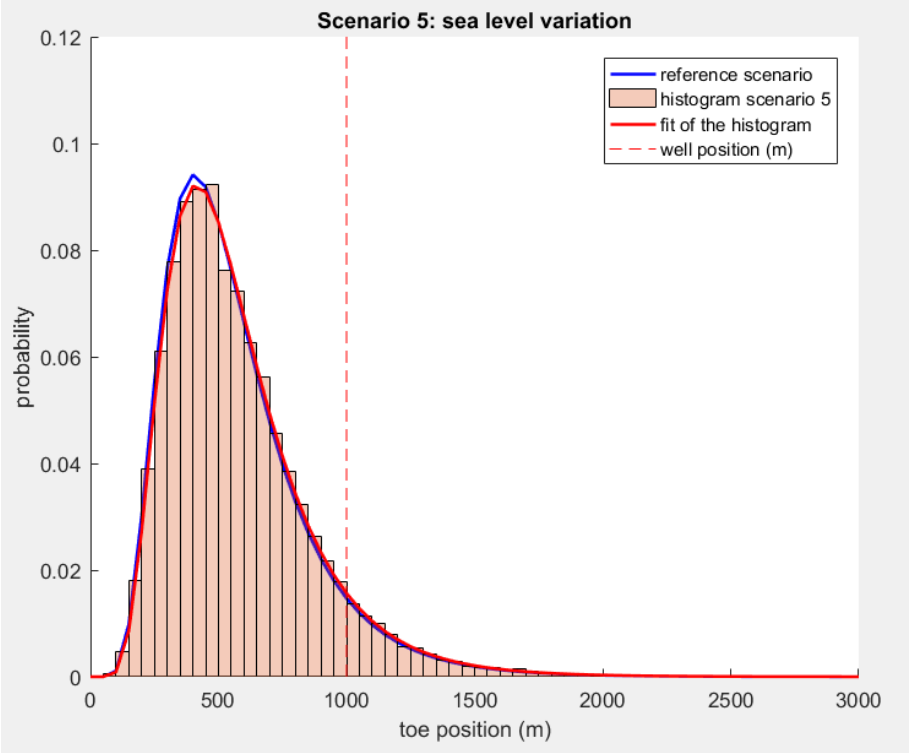

Figure 4.16: Scenario 5 compared to the reference scenario

4.2.5.7 Scenario 6: climate change

Finally, the last scenario aims to evaluate the impact of climate change in the increase of probability that the saltwater wedge's toe reaches the well galleries. FIGURE 4.17 shows that the simultaneous decrease in both recharge/groundwater inflow and the increase in sea-level induce a considerable increase in the failure probability ($P_{failure}$ = 42.93 %). Indeed, the simultaneous increase in saltwater pressure induced by sea-level rise combined with a decrease in freshwater pressure due to the decrease of freshwater inflows has the effect to significantly displace saltwater interface landwards. This is visible graphically by the displacement of the histogram to the right with a greater number of simulations results located further than well position.

4.2.6 Summary of results

Finally, FIGURE 4.18 represents a table summarizing all relevant statistical parameters for each scenario as well as the probability of failure. Furthermore, the relative failure's variability represents how much the failure's probability varies with respect to the reference scenario ($Variability = \frac{\mid P_{failure} - P_{failure_{ref}} \mid}{P_{failure_{ref}}}$).

The greatest probability of failure ($P_{failure}$ = 42.93%) is associated with the climate change scenario, in which a simultaneous sea-level rise and decrease in aquifer replenishment occur. This is also the scenario in which the greatest mean and median of toe's position are observed. A failure's probability of around 43% is not acceptable, and this climate change scenario doesn't even consider a greater pump-

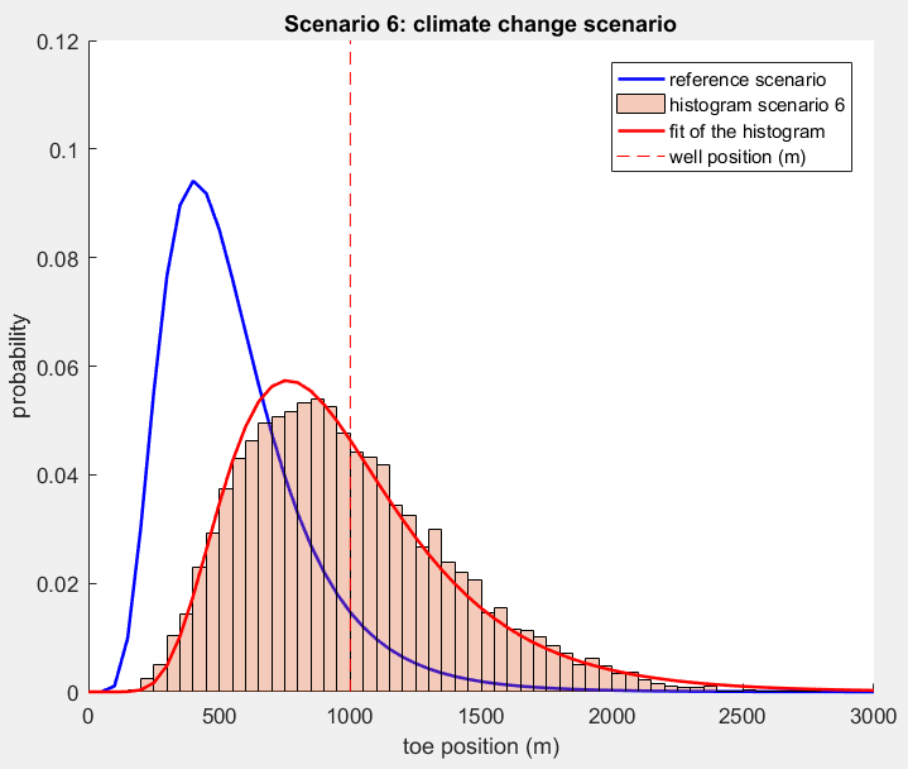

Figure 4.17: Scenario 6 compared to the reference scenario

ing rate that could be necessary due to an increase in water demand induced by the growing population in coastal areas. These results and the extremely high failure's variability (510%) with respect to reference scenario highlights the devastating effect of climate change on seawater intrusion.

One can also see that the second greatest probability of failure ($P_{failure}$ = 28.4 %) is attributed to scenario 1, which assumes the aquifer to be flat. This is also in the same scenario that the greatest standard deviation of the toe position is observed. Furthermore, a great failure variability is observed with a difference of 303% with respect to the reference scenario. However, the slope of the aquifer not being assumed to change, our interest will turn more into comparing scenarii 2 to 5 between each other.

Regarding the other scenarii, we can see that the increases in failure probabilities in descending order are associated to scenario 2 (pumping scenario), scenario 3 dry, scenario 4 high heterogeneity and scenario 5 (sea-level rise) with respective corresponding failure probabilities of 16.1%, 10.14%, 9.43%, and 7.66%. However, a decrease in failure probabilities is also observed for scenario 3 wet and scenario 4 low heterogeneity with respective corresponding failure probabilities of 4.67% and 5.04%. It seems that the parameters having the most influence on seawater intrusion are in descending order: pumping rate, the freshwater recharge, the level of heterogeneity, and the sea-level rise.

From these results, one can conclude that the parameters that contribute to the saltwater interface movement landwards are an increase in flowrate, a decrease in

the recharge (and of the inland flow) and sea-level rise.

Toe position (m)	mean	stdv	median	mode	max	min	P_failure (%)	Variability failure (%)
scenario reference	562.42	272.19	505.03	76.54	2499.76	76.54	7.04	0
scenario 1: flat	854.74	830.93	692.08	80.71	79413.78	80.71	28.40	303
scenario 2: pumping	691.80	336.99	619.57	92.54	2540.75	92.54	16.10	129
scenario 3 dry	611.36	300.34	550.22	79.45	2818.25	79.45	10.14	44
scenaro 3 wet	517.92	249.48	468.13	70.88	2327.79	70.88	4.67	34
scenario 4: low heterogeneity	584.00	220.41	529.04	230.74	2239.40	230.74	5.04	28
scenario 4: high heterogeneity	525.62	334.79	449.86	22.45	2387.83	22.45	9.43	34
scenario 5: sea level	574.62	277.09	516.29	78.13	2426.64	78.13	7.66	9
scenario 6: climate change	985.62	396.86	927.46	145.11	2778.73	145.11	42.93	510

Figure 4.18: Table presenting statistical results related to toe position (m) for each scenario

4.3 Recommendations

From SECTION 4.2.6, it seems that the most influential parameters regarding seawater intrusion in descending order are:

$$\textit{geometrical configuration} > \textit{pumping rates} > \textit{boundary conditions} > \textit{intrinsic properties}$$

To prevent seawater intrusion, one should modify these parameters in such a way it would decrease the probability of seawater intrusion. However, some of them are not alterable such as the geometrical configuration of the aquifer (such as its slope) or its intrinsic properties (such as its hydraulic conductivity). Nevertheless, it is possible to modify the pumping rates and the boundary conditions of the system.

pumping rates: decreasing pumping rates is one way to decrease the occurrence of saltwater intrusion. However, it is difficult to perform in terms of socio-economical point of view in the sense that the demand in freshwater in a coastal area will get greater and greater with the population increase. One suggestion for public authorities would be that cities develop landward instead of along the coast so that the population living further from the sea is dependant from freshwater extracted further from the coast than the freshwater extracted from previously existing well along the coast. It is also necessary to install wells far away from the coast, but this situation is not possible when the wells are already existing, as it is the case in Akrotiri aquifer.

boundary conditions: regarding boundary conditions, meaning the freshwater inflow into the aquifer (from the recharge and land inflow), it is possible to reduce saltwater intrusion by considering natural or artificial recharge. *Abd-Elhamid et al. 2018* listed in their paper a series of methods to control saltwater intrusion. Regarding **natural recharge**, it consists in collecting surface water by use of dams and weirs to let runoff water infiltrate into the aquifer instead of being discharged to the sea as can be seen in FIGURE 4.19. Furthermore, **artificial recharge** can be combined with saline abstraction wells that would extract saline water to discharge it into the sea (see FIGURE 4.20). The effect of the recharge (natural or artificial) is to increase the fresh groundwater pressure while the saline abstraction wells would diminish the saline groundwater pressure. Finally, a more costly but more efficient

method consists in desalinating the withdrawn brackish water (from abstraction wells) before injecting it into the fresh groundwater as shown in FIGURE 4.21. This method is called ADR and refers to abstraction, desalination, and recharge.

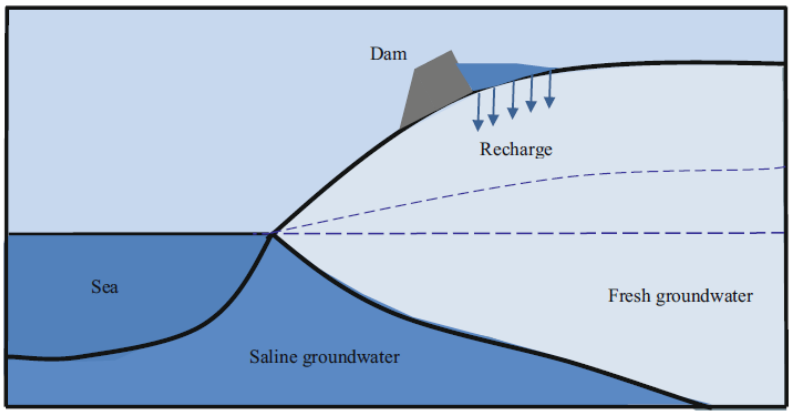

Figure 4.19: Simplified scheme of natural recharge (from *Abd-Elhamid et al. 2018*)

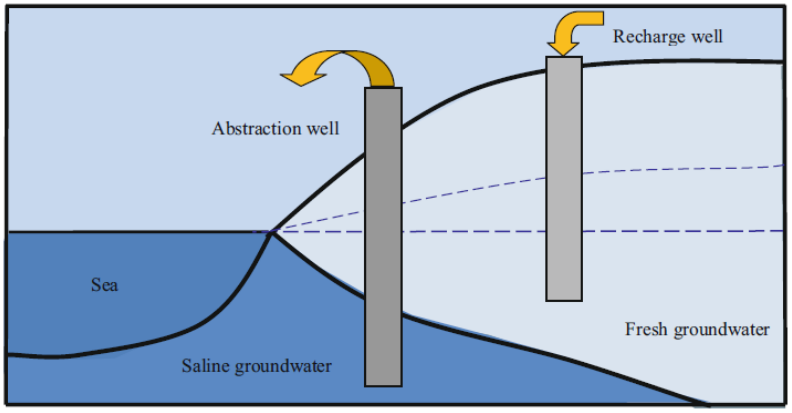

Figure 4.20: Simplified scheme of artificial recharge and abstraction wells (from *Abd-Elhamid et al. 2018*)

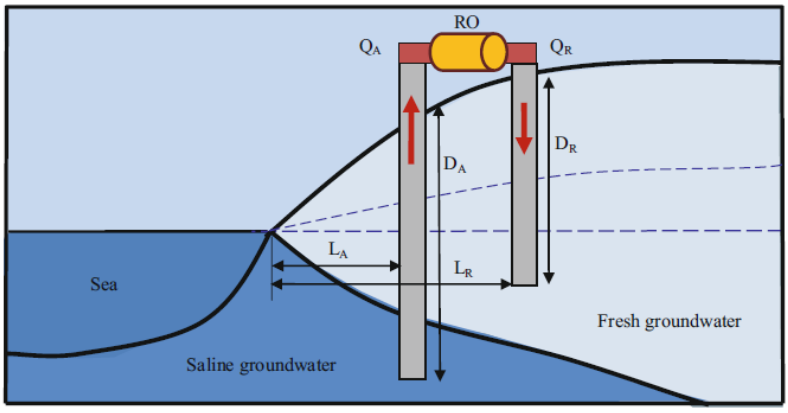

Figure 4.21: Simplified scheme of ADR (from *Abd-Elhamid et al. 2018*)

4.4 Conclusion

Through this chapter, another very frequent groundwater-related issue has been studied and corresponds to seawater intrusion. It is fundamental to study this environmental aspect since there is a growth of the global population, inducing a greater demand in freshwater. Consequently, for the population living in the coastal areas, it is necessary to pump freshwater to satisfy all types of water demand (drinking water, irrigation, and so on). The greater pumping rates associated with growing demand in coastal areas combined with climate change effect (sea-level rise, decrease in recharge, ...) considerably increases the risk of saltwater contamination in the coastal areas, explaining thus the reason why it is crucial to study this issue.
The first part of this chapter aimed to understand better groundwater coastal environment, its hydrodynamics, the classification of coastal aquifers, and so on. Furthermore, it introduced the causal factors leading to saltwater intrusion (anthropogenic but also natural factors) and its consequences.
The second part consisted in applying Monte Carlo simulation to evaluate the risk of saltwater intrusion in a real case study in Cyprus (Akrotiri aquifer). After describing the geographical area and the geometrical configuration of the aquifer, the analytical equation describing the position of the toe has been developed and was considered to apply Monte Carlo simulation. After performing Monte Carlo simulation to each developed scenario, the associated probabilities that the saltwater intrusion reaches the well galleries have been obtained. The influence of each parameter governing the toe position was in adequacy with the previously built Fault Tree. It has been shown that the most influential parameters regarding seawater intrusion in descending order are the geometrical configuration of the aquifer (its slope), the extraction rate of the well galleries, the boundary conditions (freshwater inflows) and the intrinsic properties of the aquifer (hydraulic conductivity). Furthermore, it has been shown that climate change has a serious impact on the increase in the risk of saltwater intrusion. Indeed, the combined increase of sea-level and decrease of freshwater recharge induced by global warming considerably increases the probability of failure (up to six-time the reference failure probability). This must motivate public authorities to take measures to slow down global warming and to take measures in coastal areas to prevent saltwater intrusion.

Chapter 5

Conclusion

This whole thesis aimed to demonstrate the applicability of two techniques in uncertainty analysis to groundwater-related environmental issues. The first technique refers to Fault Tree Analysis while the other one is called Monte Carlo Simulation.

The paper started with an introduction which explained the major impact of human on the whole planet, leading to the birth of a new geological epoch called Anthropocene. More specifically, global warming was addressed as well as its consequences being defined in detail in the different reports produced by the Intergovernmental Panel on Climate Change. It has been decided to perform uncertainty analysis to the two following groundwater environmental issues: permafrost's thawing related concerns, meaning the generation of thermokarst lakes and the talik development under these latter as well as the saltwater intrusion in a coastal area.

Two risk analysis methods have been considered and described in the second chapter: Fault Tree Analysis and Monte Carlo simulation. The present paper intended to apply Fault Tree Analysis to environmental concerns to prove its applicability out of the industry sector. This uncertainty analysis displays plenty of advantages such as the identification of causal factors and their interconnection through logical gates, its use in risk assessment by evaluating failure's probability of the studied environmental system and its utility regarding design safety assessment by identifying the components of the systems which are the most prompt to lead to the failure of the system. However, FTA presents also disadvantages due to its events' independence assumption. Consequently, it was necessary to introduce Monte Carlo Simulation to workaround the Independence problem occurring in the saltwater intrusion issue.

Fault Tree Analysis was applied to permafrost related concerns.
The first environmental issue studied was the generation of thermokarst lakes due to the degradation of permafrost. They cause problems in the sense that they constitute sources of heat that degrade consequently the permafrost in the surroundings. FTA was therefore used to firstly identify the factors driving the generation of these lakes and secondly, to highlight the relationship between these events that lead to this environmental problem. Then the application of the quantitative methods was carried out, although data were not available. A rough estimation of top event probability of 48% has been obtained and importance measure analysis highlighted

the fact that having a flat geometrical configuration (slope inferior to 10°) in unstable ground temperature zone is the factor that is the most prompt to lead to the generation of thermokarst lakes. This use of FTA was done to show on one hand how to apply these methods in practice and on the other hand, to prove that the FTA applies just as well to environmental problems. This first application of FTA highlights the fact that it is necessary to have plenty of data related to each basic event responsible to the system failure to obtain a more accurate estimation of the failure's probability of the undesired event.
The second environmental concern which is still related to thermokarst lakes is related to the thawing of permafrost under these latter. The use of FTA allowed obtaining a probability of failure of 73.445%. Although this value still constitutes an estimation due to the fact the probabilistic distribution of the parameters is not known, this great value informs us of the disastrous effect of climate change on permafrost environment. Indeed, through importance's measures analysis, the factor which is the most prompt to lead to top event failure is the lake bottom temperature. This is even more problematic when we realize that it is impossible to improve the reliabilities of the components of the fault tree due to the fact they are not human controlled.
The use of Fault Tree Analysis in the permafrost environment is a good way to prove quantitatively the impact of climate change and to urge the great powers to make a change in the current system in which we are living.
It is recommended to keep studying in the future the evolution in time of the different parameters related to these environmental concerns. Indeed, a database regarding these parameters would allow getting a probabilistic distribution for all the random variables involved in the physical process, permitting thus to evaluate more accurately the failure's probability of these environmental systems.

The second groundwater environmental risk studied was the intrusion of saltwater into well galleries in coastal aquifers in Cyprus (Akrotiri aquifer). The study of the hydrodynamics governing saltwater intrusion highlighted the non-applicability of standard fault tree analysis due to the non-independence of all parameters governing the saltwater wedge toe position. However, it was possible to build a fault tree for identifying the factors leading to the salt water intrusion among which are the recharge, the inland groundwater flow, the sea-level, the hydraulic conductivity, the slope of the aquifer and the pumping rate.
To obtain quantitative results, Monte Carlo simulation (20000 simulations) has been applied for different scenarios to study the influence of different parameters on seawater intrusion and more important, the increase of failure probability associated with a climate change scenario. Indeed, a probability of contamination of the wells of 42.93% has been obtained when considering the sea-level rise occurring in 2100 and the decrease of freshwater replenishment of the aquifer while the probability of failure related to the reference scenario is 7.04%. Furthermore, the study of the results associated with the different scenarios revealed that the most influential parameters regarding sea water intrusion are in descending order: geometrical configuration, pumping rates, boundary conditions, and intrinsic properties.
It is recommended to think about a new manner to develop coastal cities and to distribute freshwater into them in such a way that the increasing water demand is not accompanied by increasing pumping rates in the coast. Furthermore, for each

risky exploitation of freshwater in a coastal aquifer, it is necessary to study with details possible remediation/protection measures such as natural/artificial recharge, abstraction wells, or combination of them.

Through this master thesis, the applicability of Fault Tree Analysis and Monte Carlo simulation to groundwater environmental risks has been demonstrated. It revealed how powerful it can be to prove to public authorities that it is necessary to act now to slow down climate change which is largely responsible for the occurrence of these environmental concerns. However, it is necessary for the future to study accurately the different parameters related to these undesired events, so that more accurate probabilities of failures can be evaluated. While Fault Tree Analysis is a powerful tool to evaluate top event failure when the factors are independent, Monte Carlos reveals to be useful to quantify the same probability when events are dependent. These are thus uncertainty analysis tools that are pretty relevant and complementary to evaluate environmental risks.

Appendix A

Fault Tree Analysis (FTA)

A.1 Symbolism in Fault Trees

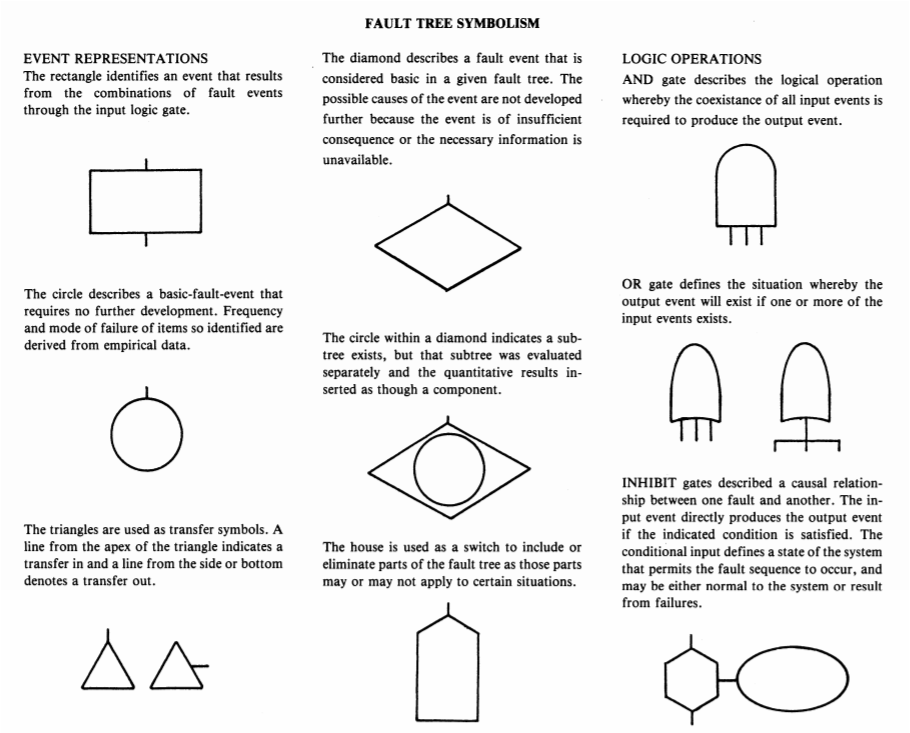

Figure A.1: Symbolism used for representing events and gates in Fault Trees (from *Lee et al. 1985*)

Appendix B

FTA applied to permafrost environment

B.1 Thermokarst lake development

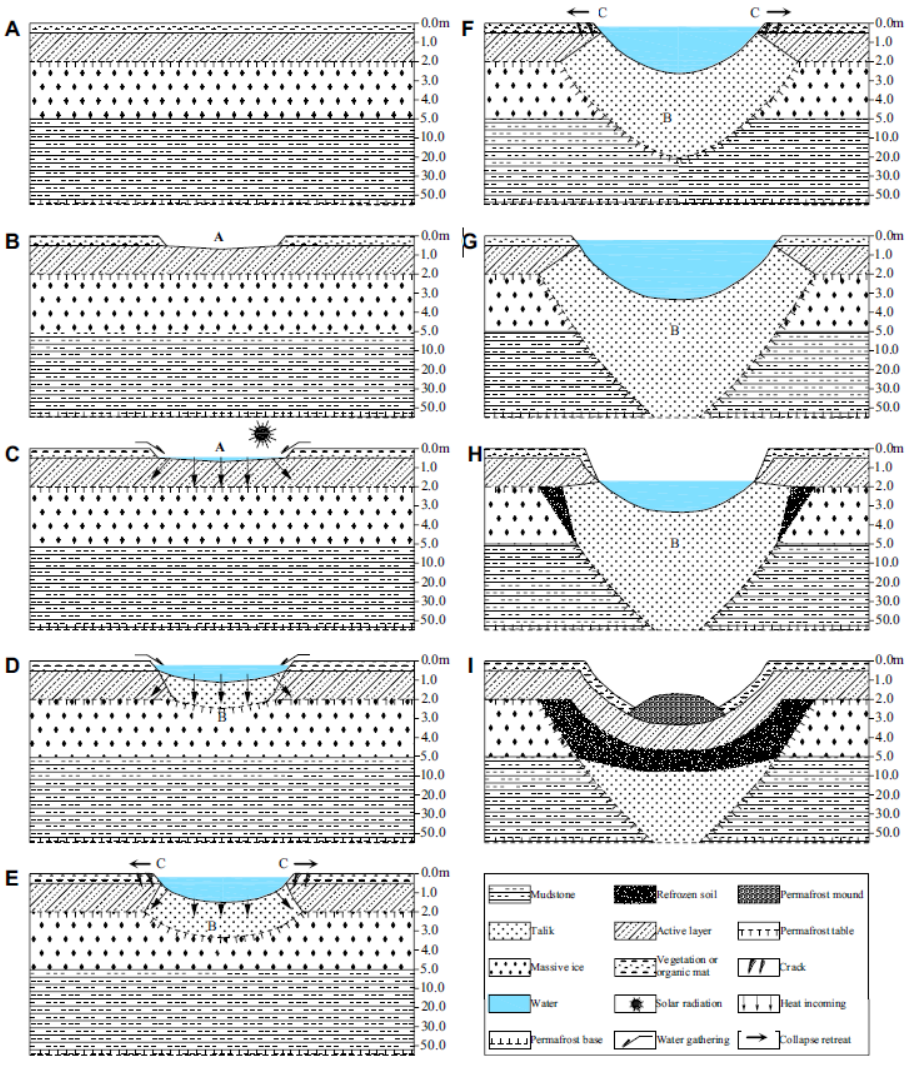

Figure B.1: Initiations (A-C), Development (D-F), Stabilization (G) and termination (H-I) stages of thermokarst lakes (from *Zhanju Lin et al. 2016*)

B.2 Spatial statistics related to *Wang et al. 2017* article

Table 4 Statistical analyses of thermokarst lakes

Type	Type area (km^2)	Number of thermokarst lakes	Percentage of total lakes (%)	Dot density (points/km^2)	Thermokarst lake area (m^2)	Percentage of total lake area (%)	Surface density
Permafrost							
Ice-saturated	53.4	132	22	2.47	987311.62	18.39	0.0185
Ice-rich	210.59	372	62	1.77	4199603.02	78.24	0.0199
Ice-poor	130.01	65	10.83	0.5	87684.88	1.63	0.0007
River taliks	23.6	31	5.17	1.31	93631.56	1.74	0.004
Ground temperature							
TCP-0	31.19	37	6.16	1.19	1440378.67	26.83	0.0462
TCP-1	79.26	106	17.67	1.34	1182034.6	22.02	0.0149
TCP-2	118.88	241	40.17	2.03	2371627.11	44.18	0.02
TCP-3	105.99	153	25.5	1.44	333786.1	6.22	0.0031
TCP-4	82.27	63	10.5	0.77	40404.6	0.75	0.0005
Vegetation type							
Meadow	235.87	357	59.5	1.51	993275.5	18.5	0.0042
Desertification grasslands	75.28	97	16.17	1.29	1025783.57	19.11	0.0136
Desertified steppe	7.24	28	4.66	3.86	128106.64	2.39	0.0177
Sparse desertification grasslands	99.2	118	19.67	1.19	3221065.37	60	0.0325
Soil type							
Bedrock	117.72	20	3.33	0.17	145006.36	2.7	0.0012
River valley	16.62	6	1	0.36	8212.54	0.15	0.0005
Gravelly sand	166.89	276	46	1.65	4279791.81	79.72	0.0256
Silty clay	62.26	168	28	2.7	210724.32	3.93	0.0034
Silt and eolian sand	54.09	130	21.67	5.07	724496.06	13.5	0.02
Hydrogeological type							
D1	23.01	14	2.33	0.61	532947.58	9.93	0.0232
D2	69.57	30	5	0.43	250751.6	4.67	0.0036
D3	179.89	307	51.17	1.71	3785770.12	70.52	0.021
D4	145.13	249	41.5	1.72	798761.79	14.88	0.0055
Slope							
0°–5°	183.54	426	71	2.32	2969544.19	55.31	0.0162
5°–10°	136.87	151	25.17	1.10	2316748.7	43.15	0.0169
10°–15°	58.77	14	2.33	0.24	58526.49	1.1	0.001
≥ 15°	38.12	9	1.5	0.24	23410.60	0.44	0.0006

Figure B.2:

B.3 Talik development under warm lake

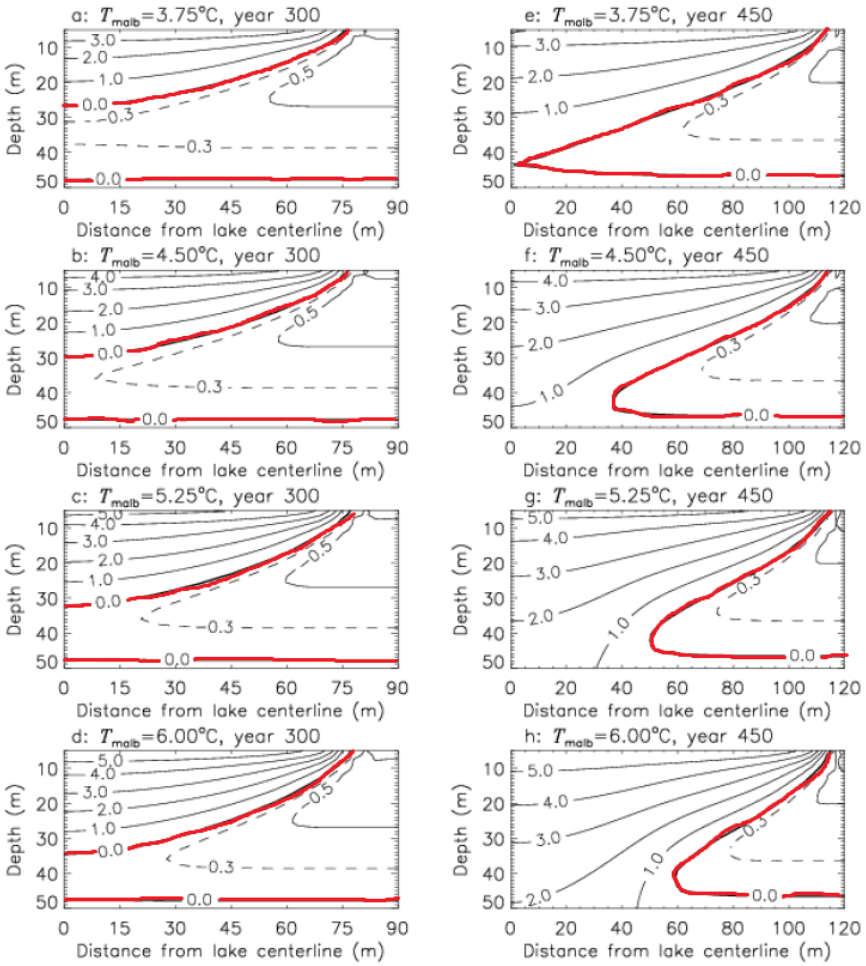

Figure B.3: Ground temperature distribution under thermokarst lake with talik boundary represented in red (modified from *Ling et al. 2019*)

Appendix C

FTA applied to seawater intrusion

C.1 Threshold table for predicting classes of SWI

.

Nomenclature

D^*	Smith's (2004) dispersion parameter	S_y	specific yield
D_m	molecular diffusion	V^*	Smith's (2004) mixed convection ratio
FGDS	fresh groundwater discharge to the sea	W_{net}	distributed net recharge
h	freshwater thickness	x	inland distance from the shoreline
h_0	confined aquifer thickness	x_b	x at the inland boundary
h_b	h_f at the inland boundary	x_n	x at the groundwater mound peak
h_f	freshwater head above sea level	x_T	x at the seawater wedge toe
h_n	h_f at the peak of a groundwater mound	z	depth of the interface below sea level
K	hydraulic conductivity	z_0	depth of the aquifer base below sea level
K_z	vertical hydraulic conductivity	α_L	longitudinal dispersivity
n	porosity	α_T	transverse dispersivity
q_b	freshwater inflow at the inland boundary	δ	dimensionless density difference
q_0	FGDS	δ^*	modified δ to account for dispersion
S_s	specific storage	ρ_f	freshwater density
SWI	seawater intrusion	ρ_s	seawater density

Figure C.1: Nomenclature used by *Werner 2017*

Coastal aquifer setting	Threshold condition	Formulae for threshold condition
Unconfined aquifer, no recharge	Passive to active SWI	$q_0 = 0$ $h_f = 0\ (x \geqslant 0)$
Unconfined aquifer, with recharge	Passive to passive-active SWI	$q_0 = \sqrt{W_{net}K\delta(1+\delta)}z_0$ $h_n = \delta z_0$ $x_n = q_0/W_{net}$ $h_b = \sqrt{\left(\frac{\delta}{\delta+1}\right)\frac{2q_0x_b - W_{net}x_b^2}{K}}\ (x_b \leqslant x_n)$ $h_b = \sqrt{\frac{2q_0x_b - W_{net}x_n^2}{K} + (\delta+1)z_0^2} - z_0\ (x_b \geqslant x_n)$
	Passive-active to active SWI	$q_0 = 0$ $^a h_b = \sqrt{(\delta+1)z_0^2 - \frac{W_{net}x_b^2}{K}} - z_0$
Confined aquifer, no recharge	Passive to active SWI	$q_0 = 0$ $h_f = \delta(z_0 - h_0)\ (x \geqslant 0)$
Confined aquifer, with recharge	Passive to passive-active SWI	$q_0 = \sqrt{W_{net}K\delta h_0}$ $h_n = \delta z_0$ $x_n = q_0/W_{net}$ $h_b = \sqrt{(2q_0x_b - W_{net}x_b^2)\frac{\delta}{K}} + \delta(z_0 - h_0)\ (x_b \leqslant x_n)$ $h_b = \frac{2q_0x_b - W_{net}x_n^2}{2Kh_0} + \delta(z_0 - \frac{h_0}{2})\ (x_b \geqslant x_n)$
	Passive-active to active SWI	$q_0 = 0$ $^a h_b = \delta\left(z_0 - \frac{h_0}{2}\right) - \frac{W_{net}x_b^2}{2Kh_0}$

Figure C.2: Table to define classes of intrusion made by *Werner 2017*

C.2 Regional sea level rise

.

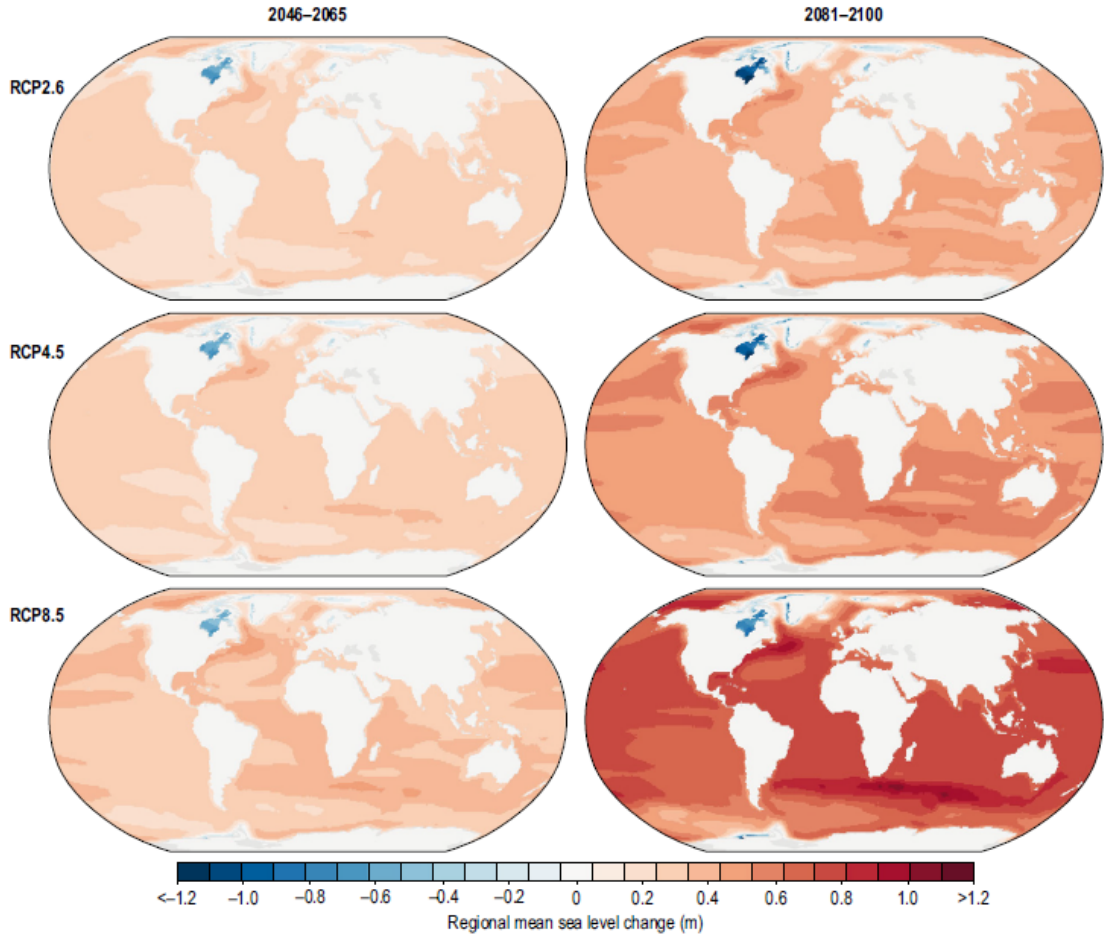

Figure C.3: Regional sea level rise for scenarios RPC2.6, RPC4.5 and RPC8.5 until 2100

Bibliography

Abd-Elhamid, Hany F et al. (2018). "Control of Saltwater Intrusion in Coastal Aquifers". In: *Groundwater in the Nile Delta*. Springer, pp. 355–384.

Barlow, Paul M and Eric G Reichard (2010). "Saltwater intrusion in coastal regions of North America". In: *Hydrogeology Journal* 18.1, pp. 247–260.

Birnbaum, Zygmund William (1968). *On the importance of different components in a multicomponent system*. Tech. rep. Washington Univ Seattle Lab of Statistical Research.

Brown, Jerry et al. (1997). *Circum-Arctic map of permafrost and ground-ice conditions*. US Geological Survey Reston, VA.

Burn, Chris R (2005). "Lake-bottom thermal regimes, western Arctic coast, Canada". In: *Permafrost and Periglacial Processes* 16.4, pp. 355–367.

Burn, Christopher R (1992). "Thermokarst lakes". In: *Canadian Geographer/Le Géographe canadien* 36.1, pp. 81–85.

— (2002). "Tundra lakes and permafrost, Richards Island, western Arctic coast, Canada". In: *Canadian Journal of Earth Sciences* 39.8, pp. 1281–1298.

Dagan, G et al. (2003). "Flow and transport in highly heterogeneous formations: 1. Conceptual framework and validity of first-order approximations". In: *Water Resources Research* 39.9.

Darnault, Christophe JG (2008). *Overexploitation and Contamination of Shared Groundwater Resources: Management,(Bio) Technological, and Political Approaches to Avoid Conflicts*. Springer Science & Business Media.

Ericson, Clifton A et al. (1999). "Fault tree analysis". In: *System Safety Conference, Orlando, Florida*. Vol. 1, pp. 1–9.

Farquharson, Louise M et al. (2019). "Climate change drives widespread and rapid thermokarst development in very cold permafrost in the Canadian High Arctic". In: *Geophysical Research Letters* 46.12, pp. 6681–6689.

Felisa, Giada, Valentina Ciriello, and Vittorio Di Federico (2013). "Saltwater Intrusion in Coastal Aquifers: A primary case study along the Adriatic coast investigated within a probabilistic framework". In: *Water* 5.4, pp. 1830–1847.

Harris, Stuart A et al. (2017). *Geocryology: Characteristics and Use of Frozen Ground and Permafrost Landforms*. CRC press.

Hu, Xiaoying et al. (2018). "Effect of Thermokarst Lake on Foundation Under Embankment in Permafrost Regions". In: Springer, pp. 1364–1367.

Jakovovic, Danica et al. (2016). "Saltwater upconing zone of influence". In: *Advances in Water Resources* 94, pp. 75–86.

Jones, Benjamin M et al. (2011). "Modern thermokarst lake dynamics in the continuous permafrost zone, northern Seward Peninsula, Alaska". In: *Journal of Geophysical Research: Biogeosciences* 116.G2.

Karlsson, Johanna Mård et al. (2012). "Thermokarst lake, hydrological flow and water balance indicators of permafrost change in Western Siberia". In: *Journal of Hydrology* 464, pp. 459–466.

Koussis, Antonis D et al. (2012). "Analytical single-potential, sharp-interface solutions for regional seawater intrusion in sloping unconfined coastal aquifers, with pumping and recharge". In: *Journal of Hydrology* 416, pp. 1–11.

Lee, Wen-Shing et al. (1985). "Fault Tree Analysis, Methods, and Applications A Review". In: *IEEE transactions on reliability* 34.3, pp. 194–203.

Lewis, Simon L et al. (2015). "Defining the anthropocene". In: *Nature* 519.7542, pp. 171–180.

Lin, Zhanju et al. (2010). "Thermal regime of a thermokarst lake and its influence on permafrost, Beiluhe Basin, Qinghai-Tibet Plateau". In: *Permafrost and Periglacial Processes* 21.4, pp. 315–324.

— (2011). "Hydrothermal processes of alpine tundra lakes, Beiluhe basin, Qinghai-Tibet Plateau". In: *Cold Regions Science and Technology* 65.3, pp. 446–455.

— (2016). "Development of a thermokarst lake and its thermal effects on permafrost over nearly 10 yr in the Beiluhe Basin, Qinghai-Tibet Plateau". In: *Geosphere* 12.2, pp. 632–643.

Lin, ZJ et al. (2017). "Interannual variations in the hydrothermal regime around a thermokarst lake in Beiluhe, Qinghai-Tibet Plateau". In: *Geomorphology* 276, pp. 16–26.

Ling, Feng et al. (2003). "Numerical simulation of permafrost thermal regime and talik development under shallow thaw lakes on the Alaskan Arctic Coastal Plain". In: *Journal of Geophysical Research: Atmospheres* 108.D16.

— (2012). "Modelling open-talik formation and permafrost lateral thaw under a thermokarst lake, Beiluhe Basin, Qinghai-Tibet Plateau". In: *Permafrost and Periglacial Processes* 23.4, pp. 312–321.

— (2019). "Quantifying Impacts of Mean Annual Lake Bottom Temperature on Talik Development and Permafrost Degradation below Expanding Thermokarst Lakes on the Qinghai–Tibet Plateau". In: *Water* 11.4, p. 706.

Margesin, Rosa (2008). *Permafrost soils*. Vol. 16. Springer Science & Business Media.

Mazi, K et al. (2004). "A groundwater-based, objective-heuristic parameter optimisation method for a precipitation-runoff model and its application to a semi-arid basin". In: *Journal of Hydrology* 290.3-4, pp. 243–258.

Niu, Fujun et al. (2011). "Characteristics of thermokarst lakes and their influence on permafrost in Qinghai–Tibet Plateau". In: *Geomorphology* 132.3-4, pp. 222–233.

Oppenheimer, Michael et al. (2019). "Sea level rise and implications for low lying Islands, coasts and communities". In:

Palisade (2020). *Monte Carlo Simulation*. `https://www.palisade.com/risk/monte_carlo_simulation.asp`.

Prieto, Carmen, Anastasia Kotronarou, and Georgia Destouni (2006). "The influence of temporal hydrological randomness on seawater intrusion in coastal aquifers". In: *Journal of Hydrology* 330.1-2, pp. 285–300.

Rowland, J C et al. (2011). "The role of advective heat transport in talik development beneath lakes and ponds in discontinuous permafrost". In: *Geophysical Research Letters* 38.17.

Roy-Leveillee, Pascale et al. (2017). "Near-shore talik development beneath shallow water in expanding thermokarst lakes, Old Crow Flats, Yukon". In: *Journal of Geophysical Research: Earth Surface* 122.5, pp. 1070–1089.

Ruijters, Enno et al. (2015). "Fault tree analysis: A survey of the state-of-the-art in modeling, analysis and tools". In: *Computer science review* 15, pp. 29–62.

Rushdi, Ali M (1985). "Uncertainty analysis of fault-tree outputs". In: *IEEE transactions on reliability* 34.5, pp. 458–462.

Seppälä, Matti (1997). "Piping causing thermokarst in permafrost, Ungava Peninsula, Quebec, Canada". In: *Geomorphology* 20.3-4, pp. 313–319.

Steffen, Will et al. (2018). "Trajectories of the Earth System in the Anthropocene". In: *Proceedings of the National Academy of Sciences* 115.33, pp. 8252–8259.

Strack, ODL (1976). "A single-potential solution for regional interface problems in coastal aquifers". In: *Water Resources Research* 12.6, pp. 1165–1174.

StreetlyGeog (2015 (accessed March 16, 2020)). *Ice Wedge Polygons*. `https://audioboom.com/posts/3075169-ice-wedge-polygons`.

Walter, K M et al. (2007). "Thermokarst lakes as a source of atmospheric CH4 during the last deglaciation". In: *science* 318.5850, pp. 633–636.

Wang, Huini et al. (2017). "Factors influencing thermokarst lake development in Beiluhe basin, the Qinghai–Tibet Plateau". In: *Environmental earth sciences* 76.24, p. 816.

Wen, Zhi et al. (2018). "Thermal interaction between a thermokarst lake and a nearby embankment in permafrost regions". In: *Cold Regions Science and Technology* 155, pp. 214–224.

Werner, Adrian D (2010). "A review of seawater intrusion and its management in Australia". In: *Hydrogeology journal* 18.1, pp. 281–285.

— (2017). "On the classification of seawater intrusion". In: *Journal of Hydrology* 551, pp. 619–631.

Woo, Ming-ko (2012). *Permafrost hydrology*. Springer Science & Business Media.

Yang, Yuzhong et al. (2016). "Evaluation of the hydrological contributions of permafrost to the thermokarst lakes on the Qinghai–Tibet Plateau using stable isotopes". In: *Global and planetary change* 140, pp. 1–8.